TÉCNICO LISBOA

Studying the Application of Additive Manufacturing to Large Parts

Leonor Machado Santos Carvalho Neto

Thesis to obtain the Master of Science Degree in

Mechanical Engineering

Supervisors: Prof. Eurico Gonçalves Assunção

Prof.ª Maria Luísa Coutinho Gomes de Almeida

Examination Committee

Chairperson: Prof. Rui Manuel dos Santos Oliveira Baptista

Supervisor: Prof. Eurico Gonçalves Assunção

Members of the Committee: Dr. Filomeno Martina

Prof.ª Inês da Fonseca Pestana Ascenso Pires

May 2017

Dedicated to

Alexandre Augusto Figueiredo de Carvalho Neto

“When eating an elephant take one bite at a time”

Creighton Abrams

Acknowledgments

First, I would like to thank Professor Luísa Coutinho and Dr. Eurico Assunção for offering me the unique opportunity to develop this project. Also for all the guidance, support and availability throughout this incredible challenge.

My sincere thanks to Professor Stewart Williams and Dr. Filomeno Martina for receiving me at Cranfield University and sharing the expertise of the Additive Manufacturing technology. The valuable advices and comments, guided me through many challenges and steered me in the right direction.

I would like to thank all my Cranfield colleagues, that I now consider great friends. Clément, Flemming, Gianrocco, Gonçalo, Kuladeep, Kwasi, Jialou, Michaelle Angelo, Nisar, Paul, Sérgio, Sónia, Supryo, Xiang Fang, Yash, thank you for making me feel part of the amazing family that you are. A special thank you to Júlio, for the initial guidance and friendship. To Florent and Jan, for the unbelievable patience, know-how and motivation. To Pawel and Zsolt, for the funniest moments and uplifting spirit. To Armando for being my good good friend. To Eloïse for not only tutoring and guiding me through this process but also being a great friend. Last but not least, a gigantic thank you to Wojciech for the incredible support, patience, kindness and friendship, particularly in this last months.

I would also like to thank my childhood friends, Ana Catarina, Maria, Margarida and Sara for always being there. To my university friends, with whom I faced the best and the worst, thank you for the joy and motivation to carry on, as well as, the tears and the sleepovers at University. Special thank you to Daniel, Diogo, João, Mário, Miguel, Pedro, Tiago, Zé, and to my girls, Daniela, Joana, Paula and Soraia. I could not have done this journey without you all by my side.

Most of all, I would like to thank my family, specially my parents and sister. My mother for encouraging my curiosity and appetite for learning with extreme patience and kindness. My father for introducing me to my passion, guiding me through it and simultaneously teaching me how to enjoy life. My sister for expanding my horizons and making me want to always seek out for more. You are my role models and I will never forget the unconditional love and support you gave me every day.

Abstract

The full intake of Wire+Arc Additive Manufacturing (WAAM) for large aluminium aircraft components is hampered by the absence of deposition algorithms and variable mechanical properties of as-deposited aluminium. In this study, different intersection strategies were investigated. Single bead and multi-bead thick walls with various intersections were manufactured using AA4043 and AA2319 wires with Cold Metal Transfer processes. For thick wall intersections, two approaches were used, combination of parallel-oscillated deposition and combination of crossings with parallel deposition. The parallel-oscillated strategy was ultimately selected to manufacture the final part (6-metre long demonstrator). Two strengthening mechanism by cold work, side rolling and machine hammer peening (MHP), were investigated. A depth of porosity free zone, which varied from 0.6 to 1.85 mm depending on the material and peening density, was obtained in MHP samples. Side rolled samples exhibited a reduction of porosity only in narrow regions below the edges of the flat roller. After solution treatment and natural aging, a decrease in porosity was obtained, but after artificial aging gas pores reappeared. By applying heat treatment to AA2319 peened samples resulted in the abnormal grain growth. An increase of surface hardness by 50-70% was achieved by peening and 20% increase was achieved by side rolling with 150 kN load, as compared to as-deposited condition. The strength increased for peened and as-deposited and heat treated samples. The elongation considerably increased for peened and heat treated conditions. It has been shown that WAAM process is capable of manufacturing large aerospace components in aluminium alloys.

Keywords: Wire + Arc Additive Manufacturing (WAAM), aluminium alloy, intersections and cross-overs, cold work, machine hammer peening, side rolling

Resumo

A implementação de "Wire+Arc Additive Manufacturing" (WAAM) para componentes aeroespaciais encontra-se limitada pela ausência de algoritmos de deposição e pela variação das propriedades mecânicas do alumínio depositado. Neste estudo, são investigadas diferentes estratégias de interseções de cordões simples e paredes com elevada espessura, utilizando fios de AA4043 e AA2319 e processos "Cold Metal Transfer". Para interseções de paredes espessas, os melhores resultados foram obtidos aplicando as estratégias: combinação de deposição paralela-oscilada e combinação de cruzamentos com deposição paralela. Foi selecionada a primeira opção para o fabrico da estrutura final, componente com 6 metros de comprimento. Dois mecanismos de endurecimento de trabalho a frio, rolamento lateral e martelagem, foram investigados. A profundidade de zona livre de porosidade variou de 0.6 a 1.85 mm e depende do material e da densidade de martelagem. Amostras de rolamento lateral apresentaram uma redução de porosidade muito localizada, mas com profundidade significativa, na superfície abaixo do bordo do cilindro. Após tratamento e envelhecimento natural a porosidade reduziu, tendo reaparecido depois de envelhecimento artificial. Em amostras marteladas, sujeitas a tratamento térmico, foi obtida uma microestrutura irregular e conseguiu-se um acréscimo superficial de dureza correspondente a 50-70%. Recorrendo a rolamento lateral utilizando uma carga de 150 kN, obteve-se um incremento de apenas 20%. A resistência melhorou para amostras marteladas e amostras depositadas com tratamento térmico. O alongamento aumentou consideravelmente para condições de martelagem e tratamento térmico. Foi demonstrado que o processo WAAM permite fabricar, com qualidade, componentes aeroespaciais de grandes dimensões, em ligas de alumínio.

Palavras-chave: Wire + Arc Additive Manufacturing (WAAM), ligas de aluminio, intersecções e cruzamentos, trabalho frio, martelagem, rolamento lateral

Contents

List of Figures

List of Tables

Abbreviations

AM	Additive Manufacturing
WAAM	Wire plus Arc Additive Manufacturing
AA 2XXX/4XXX/6XXX	Aluminium Alloys
CAD	Computer Aided Design
CAM	Computer Aided Manufacturing
CNC	Computer Numeric Control
EWW	Effective Wall Width
TWW	Total Wall Width
SW	Surface Waviness
CMT	Cold Metal Transfer
CMT-P	Cold Metal Transfer Pulsed
CMT-ADV	Cold Metal Transfer Advanced
CMT-PADV	Cold Metal Transfer Advanced Pulse
MHP	Machine Hammer Peening
CTWD	Contact Tip to Work Distance
D	Diameter
t	Distance
s	Line pitch
d	Displacement
TS	Travel Speed
p	Pressure
F	Frequency
N	Number of repetitions
WFS	Wire Feed Speed
T	Temperature
R	Radius
Ov.	Overlap
P	Peened material without heat treatment
P+ST+NA	Peened, solution treated and natural aged material
P+ST+NA+AA	Peened, solution treated, natural aged and artificial aged material
P+ST+AA	Peened, solution treated and artificial aged material
AGG	Abnormal Grain Growth
HT	Heat treatment
HV	Vickers Hardness
AD	As-deposited
AD_{HT}	Heat treated as-deposited material
P_{HT}	Heat treated peened material

Ver	Vertical
Hor	Horizontal

1. Introduction

1.1. Background

With an ever-growing industrial competition, the need to reduce costs and optimize processes is in constant demand. Conventional processes, such as machining and forging, consist of time consuming tasks and often lead to a high material waste. Additive manufacturing (AM) processes have proven to be a suitable solution. By manufacturing near-net shapes a reduction of material wastage is obtained and lead times of manufacturing are highly reduced [1,2].

AM processes can be defined by the feedstock used, as powder-fed/bed and wire-feed processes. Powder-fed processes are used for high accuracy deposition, which leads to higher manufacturing time. Also, the powder supplies can be more expensive and not all fed material is utilised in deposition. In contrast, wire-feed processes have generally lower accuracy and the feature resolution is limited. However, the high deposition rates and nearly total usage of cheaper wire feedstock make this process more competitive for deposition of medium to large parts with medium complexity [3].

As arc-based AM processes are also associated with high deposition rates and large working envelops, the combination of an arc as heat source and wire as the feedstock is the most suitable option for large component manufacturing. This option was named Wire plus Arc Additive Manufacturing (WAAM) by Cranfield University, one of the most active research institutes in AM technologies [1,4].

The capability of WAAM for high deposition has been demonstrated for several materials [1,5]. The initial research on AM was mainly focused on titanium and nickel alloys due to their high value and large waste in conventional manufacturing. However, after the discovery of precipitation hardened aluminium alloys, the aerospace industry showed a high interest in applying AM technology to aerospace parts. Aluminium alloys present a suitable compromise between weight and strength and, therefore, are used to replace other more expensive materials or where weight reduction is important. To satisfy the demands of the industry, the capability of WAAM to deposit aluminium alloys has to be further developed and features, such has crossings and complex intersections established [5].

In applications of aluminium deposition, control of defects and material properties are the key to ensure good integrity of the part. The most common defect is porosity, which is caused by hydrogen entrapment in the deposited material. Hydrogen contamination is hard to control, since its main sources comes from the ambient environment and is stored in the feedstock material, which is directly fed into the weld pool, and the substrate in which the material is deposited [8]. It was found that low heat input decreases the likelihood of porosity and, for this reason, new cold MIG processes, like Fronius CMT, started being a better option for aluminium [6].

To further reduce or even eliminate porosity, different options of cold work were studied. Cold work when applied in the form of inter-layer rolling (every layer deposited) has proven to be an effective way of eliminating porosity in aluminium alloys [9,10]. This process although effective is not an efficient process. Since it needs to be applied in every layer, the process becomes time consuming and flattens the beads shape of the previous depositions, which requires deposition of additional layers to compensate for this. The combination of two gantries or one robot and one gantry can reduce its application time and the process could be designed to overcome the widening of layers, by depositing thinner beads. However, other options have to still be studied to complement the capability of inter-layer rolling, such as side rolling or pinch rolling that can be applied on the final part after completion of the deposition. This can offer a significant reduction in manufacturing time and hence make the process more economic. However, the capability of these processes for reduction of porosity has not been proven yet [11]. Nevertheless, these processes can only be applied on simple geometries, which limits their usefulness in real applications.

Machine hammer peening is a relatively new process, which offers greater flexibility than rolling, since potentially it can be applied on any geometry, and also it does not require heavy load gantry system. Although the process has never been tested on AM parts, it has been used to induce surface modification in various materials in a controlled manner. Other peening variants have proven to be effective in the reduction of surface corrosion, fatigue crack initiation and porosity, but no details on application of this technology for AM parts have been reported [12-14].

Most aerospace grade alloys are used for engineering applications only in the heat-treated stage. To prove usefulness of machine hammer peening on aluminium alloys, first its effect on the material after various heat treatments needs to be understood. Depending on the temperature gradient and the time of exposure, the cold worked material is expected to develop three microstructural phases: recovery, recrystallization and grain growth. At certain point, the enhancement of mechanical properties induced by the combination of cold work and high temperature exposure may decrease and reopening of porosity may occur. For this reason, to obtain a sound part with good mechanical properties a combination of the deposition and cold work processes with appropriate heat treatment should be applied [9,10,14,15].

1.2. Thesis Objectives

The main objective of this study was to build a demonstrator of an aircraft component, which is the largest component ever deposited by WAAM, as presented in Figure 1 and Figure 2. The technical drawing is shown in Appendix A.

To guarantee the deposition of a sound aluminium part with good mechanical properties, cold work has to be applied to the final part. As it is not economically viable to apply interlayer rolling to such a large component, other cold work variants had to be tested. Therefore, one of the objectives was to investigate the benefits of side rolling and machine hammer peening on WAAM deposited walls.

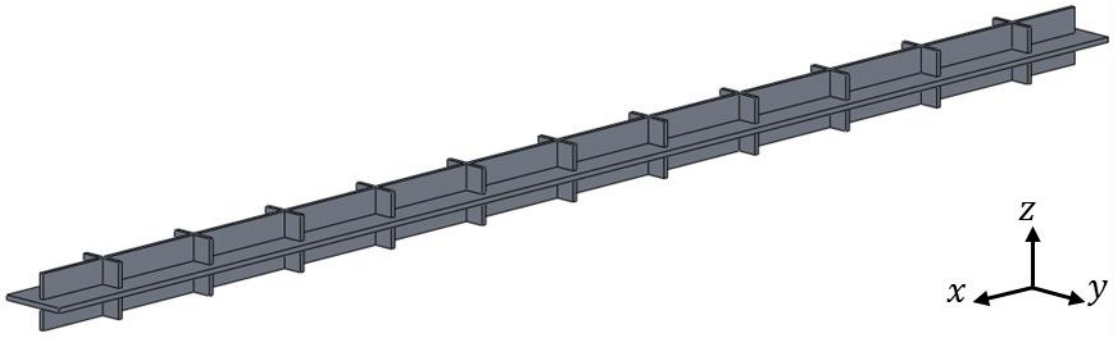

Figure 1 - Intermediate aerospace structure

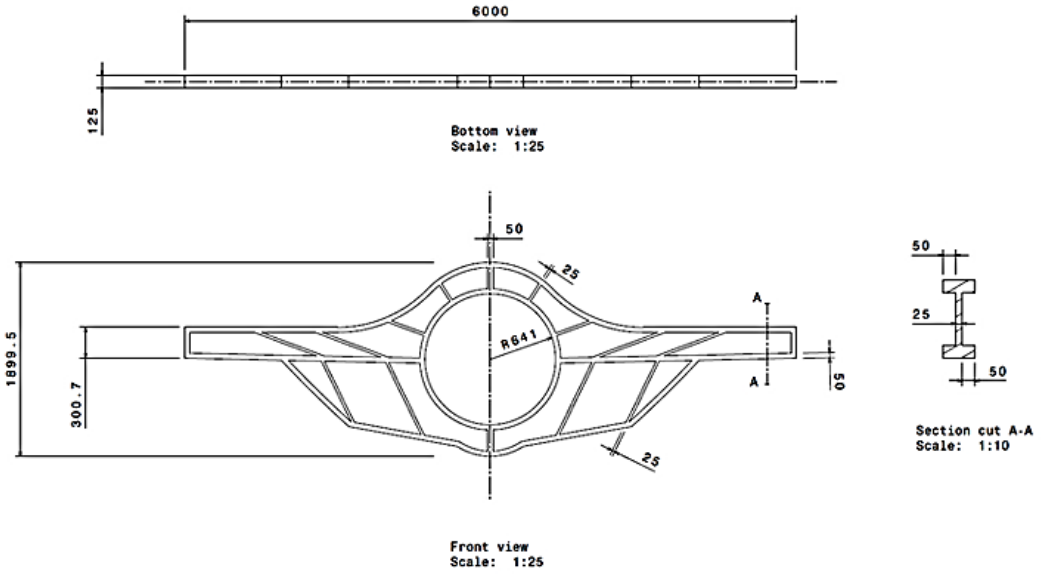

Figure 2 – Final aerospace component

1.3. Thesis structure

The thesis divided into 5 chapters, as follows:

Chapter 2 starts by reviewing the current state of the art on capability of WAAM for manufacturing of large parts. The limitations of aluminium deposition and the need to apply cold work in order to improve the mechanical properties are also reviewed in this chapter. Then the combination of large scale manufacturing and application of cold work, are shown and discussed.

Chapter 3 presents the experimental methods of the thesis. The equipment and material used for each stage of the project are described. The design strategies used for single bead and thick wall deposition are presented. The methodology implemented to determine the effects of cold work on the material is also described.

Chapter 4 presents a discussion of the results obtained throughout this study. This includes procedure to achieve single bead and thick bead crossings, the influence of parameters selection during deposition and the most suitable strategy applied to achieve the final part. Then, the effects of side rolling and machine hammer peening on porosity, microstructure and hardness of thick and thin aluminium walls are presented. At the end, a discussion of the suitability of each cold work process for aluminium is presented.

Chapter 5 shows the conclusions drawn from this study and recommendation for further work.

2. Literature Review

2.1. Additive Manufacturing

Although the first patent on Additive Manufacturing (AM) dates to 1925, only quite recently it has become a developing and booming technology [1]. AM is defined as the “process of joining materials to make objects three-dimensional (3D) model data, usually layer upon layer, as opposed to subtractive manufacturing methodologies”, by the ASTM F42 Technical Committee [16]. Initially AM development was focused on producing prototypes directly from CAD models for polymer inspection and communication tools, which reduced the product development steps. Recently, the aim of additive manufacturing shifted to respond to the demand of the aerospace and automotive industry, to manufacture metal components with complex shapes, which are not economically viable using conventional processes (subtractive and formative processes) [3].

When compared to conventional processes, AM becomes a suitable alternative for the manufacturing of parts with medium to high geometrical complexity at rather low quantities [17]. AM offers several advantages, such as:

- **Complete automation of the process:** fabrication of AM parts can be made directly from a CAD/CAM model. With the use of CNC or robotic manipulators, depending on the desirable application, human intervention and production time can be significantly reduced [18]. Although for CNC machining a direct use of CAD models is also possible, complex parts still require human intervention for re-fixing and calibration, which increases the production time [3].
- **Competitive manufacturing approach for high cost metals:** The capability to produce near--net shape parts reduces the material wastage and consequently the costs associated with it. Materials, such as titanium and nickel alloys, are widely used in the aerospace industry and presently high buy-to-fly ratios (BTF - ratio between the mass of the initial workpiece and the mass of the final component) are achieved with traditional manufacturing. With AM, this ratio can be reduced, e.g. from 10 - 20 for conventional processes to less than 2 [5].
- **Design freedom for complex assemblies:** AM can manufacture complex parts that would be impractical or impossible to achieve with conventional processes. For subtractive and formative processes, several components would be produced independently and assembled afterwards. AM promises the possibility to create a part with the same functionality but as a single-component. This enables the final part to be printed directly from the digital model and save production time and material wastage [5].

For these reasons, AM processes have started to become widely applied. The currently most used AM processes are summarized in Figure 3. Each process can be grouped based on the motion system, heat source and feedstock material used. Because of differences in resolution, productivity and the material availability, different applications are inherent with each option [19].

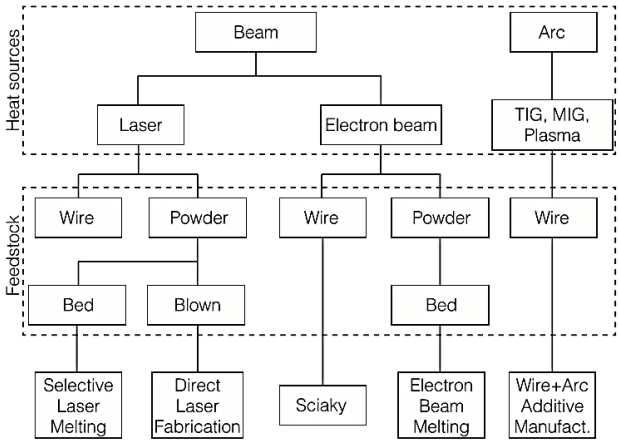

Figure 3 – Main AM processes currently used or under intensive development [2]

Heat sources can vary from power beams (laser or electron beam) to electric arcs. Power beam AM processes are usually associated with relatively low deposition rates and limited part size. For electron beam, there is the need to use an enclosed vacuum chamber, which constrains the part size and, in general, laser achieves low deposition rates. The application of these processes is usually associated with customised and complex products that are difficult or expensive to manufacture in another way. The wastage of material is a determinant factor for these applications, due to the required precision and complexity of machining the final components. In contrast, arc-based AM processes are associated with relatively high deposition rates and large working envelopes. The application of these processes is usually inherent with medium or large components where the AM process offers reduction of manufacturing time, costs and material wastage [20,21].

AM processes can also be defined as powder-feed/bed and wire-feed processes. Powder-feed/bed are often associated with multiple heat and mass transfer modes, which imply non-equilibrium in the depositions. Nevertheless, these processes are capable of achieving high geometrical accuracy. Typical values for layer thicknesses range from 20 to 100 µm with a dimensional accuracy of ± 0.05 µm and surface roughness of 9 to 16 µm. However, poor powder utilisation efficiency and high powder costs make these processes less attractive for medium and large depositions. As the deposition rate is also relatively low (approx. 10g/min), the application of these processes is usually limited to small size components. In contrast, wire-feed processes have nearly 100% material utilisation and do not expose operators to the hazardous powder environment. Although deposition rates vary with the material, much higher values can be achieved. Thus, these processes are associated with the manufacturing of medium to large size components [3].

The most commonly used motion systems are Computer Numerical Control (CNC) gantries and robotic manipulators (Figure 4). The CNC gantry system is the preferable option when high positioning accuracy is required or when additional cold work and/or machining must be integrated. However, to achieve the desirable working envelop a system with several axes is required, which increases drastically the cost of such systems. Robotic arm systems have higher flexibility and wider working envelope. In this way,

they are associated with lower equipment costs and manufacturing of very long parts. When rotation of the part or a global inert environment is required, this is also the most suitable option. However, the accuracy of robotic arms and payloads are lower, as compared to gantry systems [18].

Figure 4 – Robotic and CNC gantry systems [2]

The combination of motion system, heat source and feedstock material can work for different applications. However, for medium and large manufacturing, the most suitable option would be to combine the use of an electric arc as the heat source and wire as the feedstock. These processes are referred to a wire plus arc additive manufacturing and are commonly integrated with robotic manipulators, but not only.

2.2. Wire + Arc Additive Manufacturing

Wire plus Arc Additive Manufacturing (WAAM) uses an electric arc and a wire feedstock to make a layer-by-layer deposition until the final part is achieved. As previously implied, this technology has a lower accuracy when compared with power-feed/-bed technologies (±0.2 mm) and a minimum feature resolution of around 2mm [3]. Thus, WAAM cannot be directly applied, without post machining, to high precision parts but is a promising manufacturing option for medium to large parts, which are widely required by the aerospace and aeronautic industry.

WAAM is also associated with low costs of equipment and material and high deposition rates. The hardware for a WAAM system is similar to a regular welding system. It requires a Cartesian or robotic manipulator with which a welding torch, power unit, shielding gas source and wire feeder unit are integrated. For most materials, a local shielding system is enough to provide the necessary protection of the material against atmospheric oxygen. However, for more sensitive materials (e.g. titanium), an inert-gas filled chamber can be added to the system at relatively low costs [2,22]. Other benefit of WAAM is the lower costs of feed stock material. In WAAM all the wire that is fed is utilised for deposition, i.e., nearly 100% of material utilisation. For each material, the costs vary depending upon wire diameter and alloy composition. For most steels, the feedstock prices vary from 2€/kg to 200€/kg, for aluminium between 7€/kg and 120€/kg and for Ti-6Al-4V from 120€/kg to 300€/kg [1,2]. Considering the high deposition rates of 10kg/h for steel and 1kg/h for aluminium and titanium, WAAM becomes a suitable

low cost technology for manufacture of large components. Although the main focus of WAAM was mainly on materials like titanium and nickel alloys, in recent years this technology has proven to be also viable for materials, such as aluminium and steel [23]. The interest in aluminium of the aerospace industry has also increased in the last years and thus it is a recurring subject of recent projects [1,6,9,10].

WAAM is a near-net shape technology and it requires a final finishing operation after the conclusion of the deposition, since the surface waviness inherent to WAAM deposition is not compatible with requirements of most functional surfaces [24]. However, the required machining of the part presents a very low material wastage when compared to subtractive processes, which require machining of a billet or block of material to achieve the final part. Although in these cases some machined material can be recycled and reused, most times it is a costly inefficient operation. For these reasons, WAAM reduces significantly the BTF ratio and offers a more economically viable option. The incorporation of both systems, WAAM and machining operations into a hybrid machine can improve the economic impact further [25].

Summarising, WAAM stands out from other AM processes in aspects, such as mechanical properties, build rate, working envelope and cost savings, as presented in Figure 5. These are the key factors in large scale additive manufacturing and thus WAAM becomes the most suitable process for such applications.

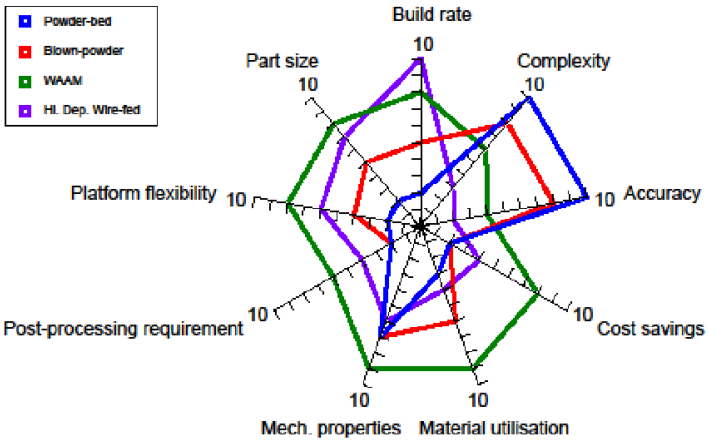

Figure 5 – Comparison of different AM processes [26]

However, the capabilities of this technology are still limited mainly due to lack of commercial systems, high expertise required to run these processes and difficulties in controlling the bead geometry. The most challenging defects are distortion (residual stresses), crack initiation sites and porosity. These defects hamper the achievement of sound and complex components and they can occur depending on the material and process used. Cold work can be applied to mitigate some of these defects and in most cases also enhance the mechanical properties of the material. Build strategies are also crucial in WAAM deposition. Since large manufacturing usually requires large scale features, thicker walls with crossovers and overlaps are needed. Thus, it is crucial to develop tool path strategies to guarantee

defects-free deposition and high efficiency [4]. To develop the capability of WAAM on industrial scale, further studies on manufacturing of large parts and elimination of defects have to be carried out.

2.2.1. Manufacturing of large parts

As mentioned previously, the manufacturing of large engineering components is mainly required by the aerospace industry [1,6]. Besides the dimensions of the part, several other requirements must be satisfied in order to produce parts with the demanded quality, such as:

- **Deposition without defects or flaws**: The integrity of the material must not be compromised by flaws or defects and a high quality of deposition must be guaranteed.
- **Good mechanical properties**: The mechanical properties of the deposited material should be higher or equal to the wrought material achieved with conventional processes, such as forging or machining.
- **Non-restricted working envelop**: An open architecture process allows flexibility and does not limit the dimensions of the parts. Also allows visual inspection during deposition, if required.
- **High build rates**: Production time must be at least similar to the current processes but preferably much lower. Several case studies on applications of WAAM have proven to reduce the production time from months to weeks or even hours.
- **Competitive production cost**: To justify the implementation of WAAM, the production costs have to be lower or similar to the currently used processes.
- **Competitive equipment cost**: The capital cost to invest in WAAM equipment cannot be an impediment to its application [1,3].

Before being able to produce complex components, which could satisfy all the above requirements, firstly, development of basic features has to be studied, such as, vertical and horizontal walls and intersections.

One dimensional walls are relative simple features because of their similarity to welding. Normally after understanding deposition behaviour for a particular material based on the deposition of straight walls, the influence of other parameters on the bead geometry are investigated, i.e. welding position, overlap, heat input, shielding environment [24].

As WAAM is a welding process, it relies on solidification process to control the profile of deposited beads. A lot of effort has been spent on studying parameters that control bead profile in WAAM [27,28] to achieve the geometry as close as possible to the CAD/CAM mode. The main challenge is to control the bead geometry of each deposit and the shape of the overall deposition by processing parameters. Many studies to optimise the process parameters according to the geometry of deposits have been carried out [3,27,28,29]. The most basic relationship between the processing parameters and bead shape can be achieved by the ratio of WFS/TS, which defines the volume of deposited material per unit length. It was shown the correlation between this ratio and the total wall width (TWW) and effective wall

width (EWW), as well as the height. As shown in Figure 6 (c), TWW is the largest width that could be achieved in the deposition and EWW the actual wall width that can be obtained after machining the WAAM part. These parameters allow the study of the deposition geometry but also permit an estimation of the material wastage after machining. A considerable difference between TWW and EWW implies a lot of machining and lower buy-to-fly ratio. As, for most applications, the surface finish requirements are higher than the deposition made by WAAM, finishing procedures, such as machining, have to be carried out. The amount of material to be removed can be determined by the difference between TWW and EWW and is defined as the surface waviness (SW) that is calculated by:

$$\mathrm{SW} = \frac{\mathrm{TWW} - \mathrm{EWW}}{2} \qquad (1)$$

Ayarkwa et al. [30] also studied the influence of different WFS/TS ratios on the height of AA2319 walls. Non-linear surface profiles, such as humps and waviness, are identified, according to the difference between the peak heights and an average surface height (Figure 6 (a) and (b)). For variations higher than 0.3mm, the walls were considered inadequate for deposition and these ratios were excluded. The maximum allowed deviation was determined by the arc stability on the subsequent layers. Such instability, not only affects the height of the bead but also the wall width because there is fixed relationship between width and height of bead for a given volume of deposited material. This will then increase the material wastage due to the fluctuation of wall width and height of the depositions. Similar studies were carried out for a wide range of conditions and materials [24,31,32]. However, a precise empirical model has not been yet developed with the required accuracy. Thus, further development is required to guarantee the desired dimensions for a specific application [3].

Effect of positional deposition was also studied. Kazanas et al. [24] shown that it is possible to deposit in different positions using CMT process, for aluminium and steel (Figure 7 (a)). Initially defects such as hump formation and acute angles developed very close to the substrate. As a solution, a pyramid like deposition was proposed for the first three layers. In this way, it was proven that walls at different angles, ranging from 0º to 180º, could be deposited without any supporting structures or rotation of the part. These features can be deposited on already produced parts, as added features, which increases the flexibility of part design. This then led to manufacture of fully enclosed parts. Figure 7 (b) presents these features, which proves the capability of the process to manufacture hollow features. However, with the alteration of the angle of the torch and the shielding gas, EWW varies and also the WFS/TS ratio directly affects the EWW. To achieve the most optimum deposition, all these parameters have to also be considered [24,33].

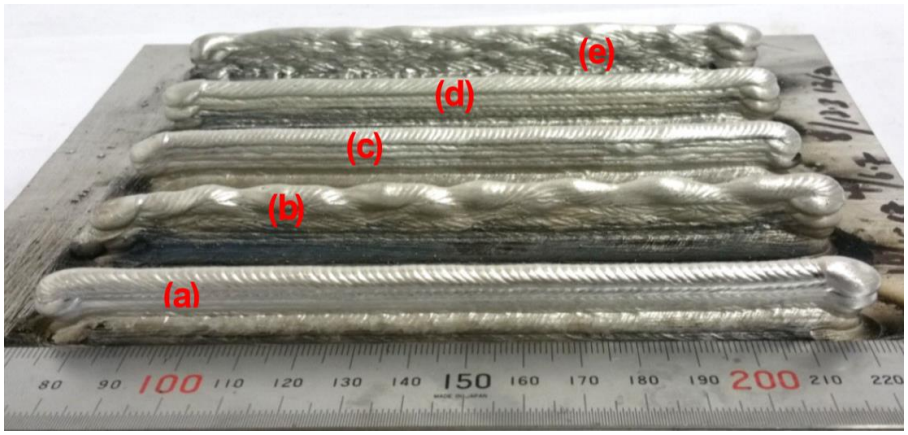

(a) Deposition of walls at constant wire feed speed to travel speed ratio of 10 with different input parameters

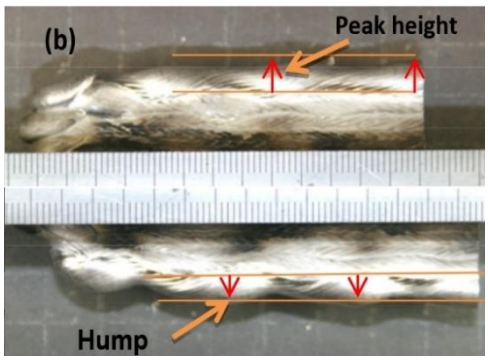

(b) Hump and peak height defects

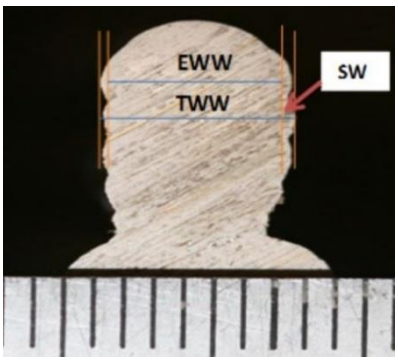

(c) Representation of EWW and TWW

Figure 6 –Influence of welding parameters on the bead geometry in aluminium [30]

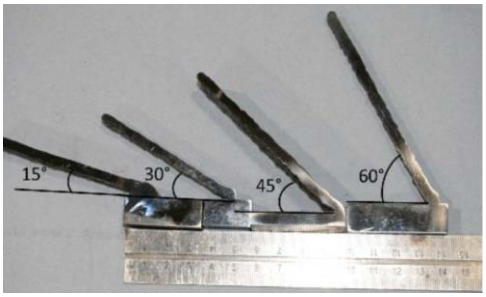

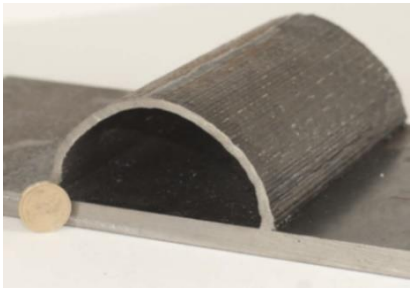

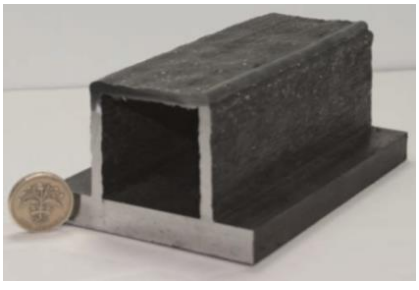

(a) Inclined and horizontal walls

(b) Enclosed shapes

Figure 7 – Geometrical features deposited with WAAM [24]

Another challenge in manufacturing of complex components is control of bead shape in crossovers and T-crossing intersections. Mehnen et al. [24] studied several deposition crossing strategies for mild steel,

as presented in Figure 8 (a). Defects and instabilities of bead profile with characteristic peaks and valleys in the intersections were observed (e.g. Figure 8 (b)). With deposition of the successive layers, this effect can add up to a bigger defect and eventually lead to arc instability. To eliminate this defect different deposition strategies were proposed, as shown in Figure 8 (c). The most consistent layer height was achieved with the Opposite Angles 2 strategy, which consists of overlapping multiple corner sections of walls deposited in such a way that, every time the deposition direction is altered, as shown in Figure 8 (c). In this way, the most suitable strategy for the deposition of mild steel was achieved.

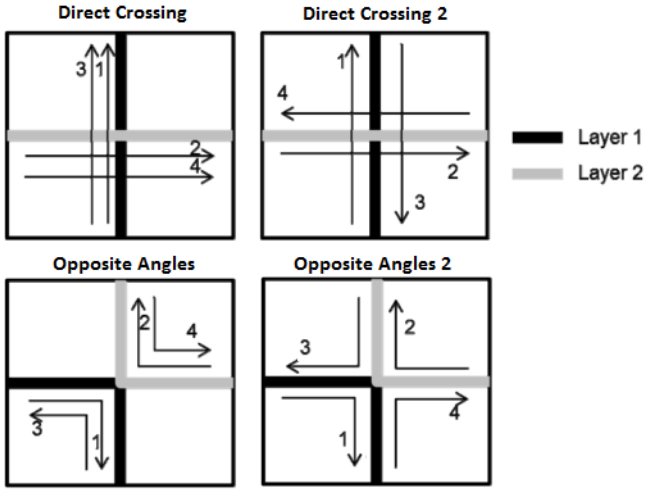

(a) Layer deposition strategies for crossing

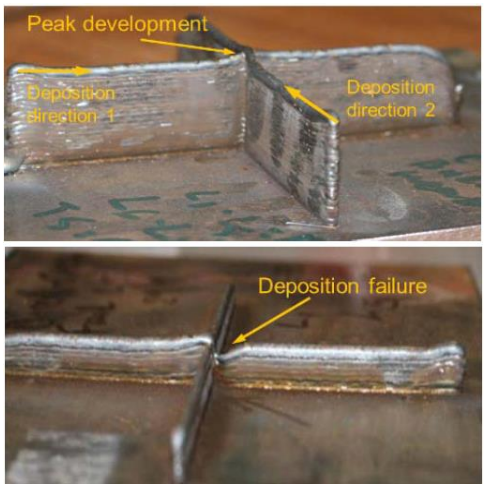

(b) Examples of defects for Direct Crossing strategy

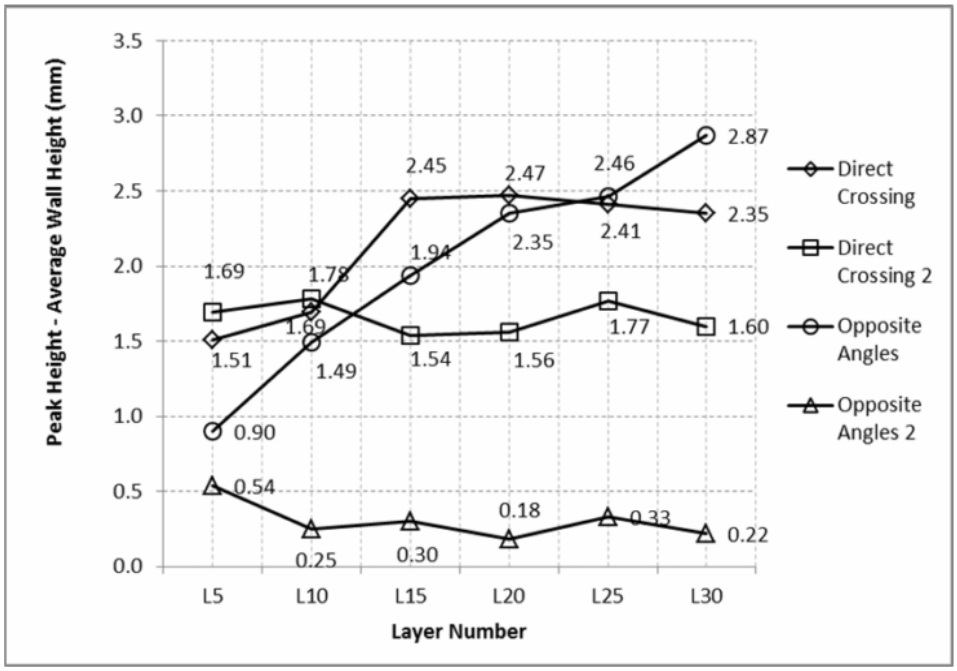

(c) Peak height measurements for different crossing build patterns

Figure 8 – Crossing deposition strategies for mild steel [24]

For T-crossing features, Venturini et al. [4] studied deposition strategies for carbon steel, as presented in Figure 9 (b). The only strategy with an unacceptable deposition was S3, shown in Figure 9 (a) by a

red arrow. By further optimizing the direction and order of deposition, the most suitable strategy was found, (S3_I2), presented in Figure 9 (b) and (c). Many other deposition strategies were dismissed due to slow and non-continuous toolpath, possible instability of the arc and sharp internal corners. Note that the tool path and direction in S3-I2 is similar to the Opposite Angles 2 strategy. Thus, if complex parts require crossovers and T-crossing features, some solutions are likely to work.

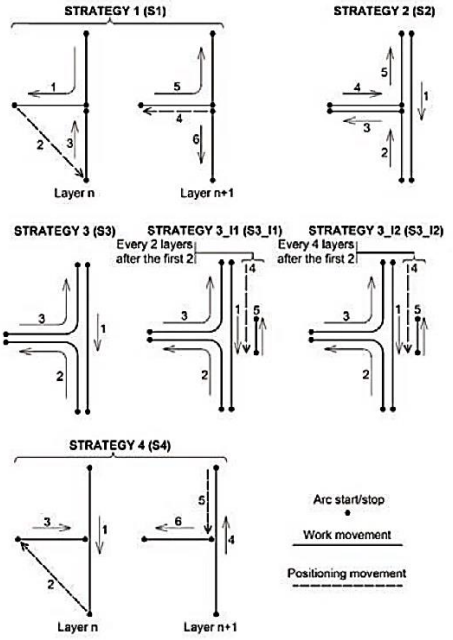

(b) Deposition strategies for T-crossing

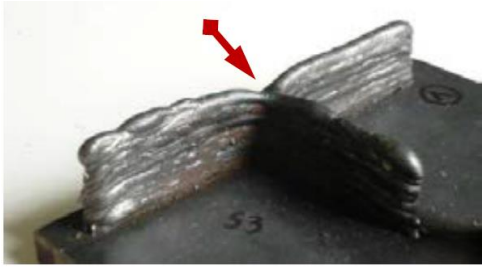

(a) Deposition failure in central zone of S3 strategy

(c) Sound T-crossing using S3_I2 strategy

Figure 9 – T-crossing deposition strategies for carbon steel [4]

Similar was studied for aluminium and titanium. Crossing features were successfully manufactured in both materials, as presented in Figure 10. However, deposition strategies and exact parameters to build these features were not found in the literature. The crossing features of the landing gear rib in Ti-64 were manufactured using an oscillated deposition strategy but no more information could be found [5]. In that work authors selected the oscillated strategy because the required wall width was higher than in the case of single bead walls.

(a) Aluminium stiffened panel [33]

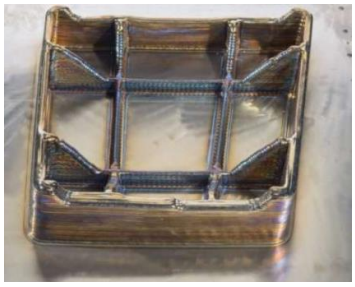

(b) Ti64 landing gear rib [5]

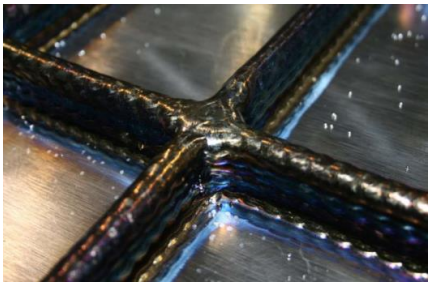

(c) Image of crossing of (b) [5]

Figure 10 – WAAM manufacturing with crossing features in aluminium and titanium

When the required wall width of the bead is greater than the capability of single wall deposits there are different strategies to achieve the desired dimensions. The two most common strategies are the parallel build and oscillated build strategy, presented in Figure 11.

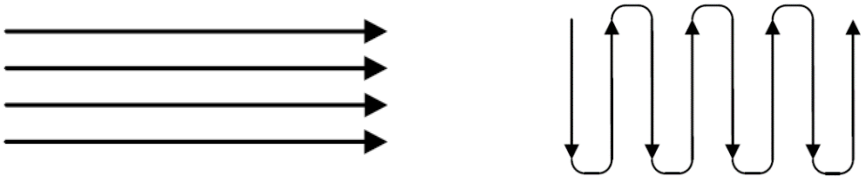

(a) Parallel wall deposition strategy (b) Oscillated wall deposition strategy

Figure 11 – Building strategies for thick walls [34]

Parallel build strategy consists of deposited beads side by side with a defined overlap, as presented in Figure 11 (a) and Figure 12 (b). The number of side depositions is determined by the individual wall width for the set of parameters and the thickness of the final part to be achieved. The ultimate goal is to achieve as flat and square wall as possible. Several works studied the solution for obtaining this effect [35,36]. The overlap was listed amongst the most important parameter in that case. The overlap has to take into consideration the width of the single bead, since it is determined by the amount of overlying beads. Normally, there is the trade-off between productivity (number of beads to complete the wall), flatness of the merged bead and likelihood of lack of fusion defects [32].

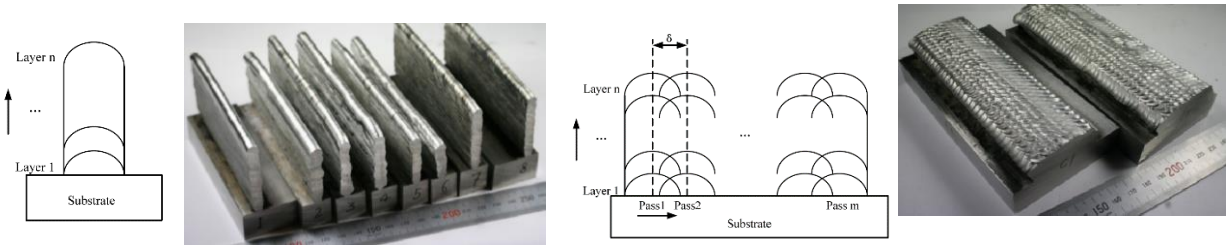

(a) Deposition strategy for single bead walls (b) Deposition strategy for parallel walls

Figure 12 – Comparison of single bead and parallel walls [32]

Online et al. [35] shown the effect of overlap in multi-bead deposition of 5 layers for the geometry of the final wall. The best result was achieved for an overlap of 73.8%. However, in Figure 13 (b), waviness of the top surface is still shown, which suggests that further improvement is required.

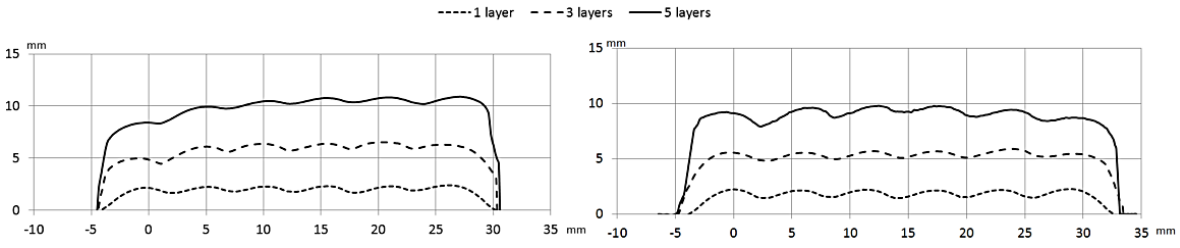

(a) Deposition with 66.7% overlap (b) Deposition with 73.8% overlap

Figure 13 – Influence of overlap in parallel wall multi-layer deposition on transverse cross section of the wall [35]

The oscillated build strategy is shown in Figure 11 (b). In contrast, the oscillated wall build strategy is achieved by oscillating the torch in the transverse direction to the deposition direction. This results in widening the deposited bead by the movement of the welding torch. In this approach, the amplitude of oscillation and the overlap are the main parameters to be determined. Although the use of this strategy was presented in several works [5,34], no detailed information is available. The main advantage of this strategy is the capability of varying the dimension of the total thickness during continuous deposition. Also, higher deposition rates are possible for titanium (1.2 kg/h), in contrast to 0.7 kg/h for parallel strategy. However, oscillated wall strategy usually leads to a higher surface waviness (0.7 to 1.0mm) when compared to parallel wall strategy (0.3 to 0.5 mm) for titanium deposition [5].

Ding et al. [5] compared both strategies when building a titanium rib presented in Figure 10. Parallel wall strategy resulted in necking and depression and simultaneous increase of the bead height in the intersections caused by the greater heat sinking from the additional material. By combining parallel and oscillated walls, the part was made successfully. In the same work, a 2.5-metre long aluminium rib structure was manufactured (Figure 14). For this component, oscillated wall was used to build the base followed by single bead deposition. In addition, the capability of using two robots depositing simultaneously was proven.

Figure 14 – Deposition of 2.5-metre long aluminium rib [5]

Up to date, most research and development on WAAM was focused on titanium and steel [37]. As shown in Figure 14, the ability of WAAM technology to build large functional components with symmetric shapes, such as ribs in aluminium alloys has been demonstrated. However, the implementation of traditional welding-based WAAM process for aluminium is currently limited by high likelihood of defects, such as porosity and solidification cracks [6], which will compromise the mechanical properties of built parts. For these reasons, further studies have to be implemented for aluminium alloys.

2.2.2. Aluminium and WAAM

The importance of aluminium alloys in the aerospace, aeronautic and automotive industry has grown increasingly. After the discovery of the precipitation hardening effect, the aluminium alloys became a high interest material for applications, which require a high strength to weight ratio and excellent

mechanical properties [38]. Because of the challenges with welding of most aluminium alloys, many critical components are manufactured by machining from a solid billet, which is very inefficient and complex. The high material waste and complexity of machining is one of the reasons for high interest in additive technologies, such as WAAM [39]. However, in several applications of aluminium deposition and specifically WAAM [10,40,41], control of defects and material properties is the key challenge to ensure integrity of the built components.

The most occurring defect is porosity due to hydrogen contamination [8]. The formation of porosity can greatly affect the fatigue characteristics of aluminium alloys and with mean diameters greater than 50 to 100 µm, gas pores become a preferential crack initiation site. Also, the material strength is compromised and premature fracture can occur due to the reduction of tensile load bearing capacity of the material with porosity. [10].

Aluminium alloys are much more susceptible to porosity due to the big difference in solubility of hydrogen between the liquid and solid phase (Figure 15). The ratio of the maximum hydrogen solubility in superheated liquid aluminium and hydrogen solubility of the liquid at solidification temperature is much superior to any other structural metal [8]. Therefore, the smallest trace of hydrogen in the contamination source (substrate, atmosphere, wire, etc.) can exceed the concentration limit needed to nucleate pores in the melt pool. Depending on the local hydrogen concentration levels and diffusion rate, the newly formed pores can grow or shrink [42]. The behaviour of generated gas pores depends mainly on the solidification mode, cooling rate, degree of convection fluid flow, welding parameters and bead shape. The chemical composition of the alloy and hence its microstructure is also important [8].

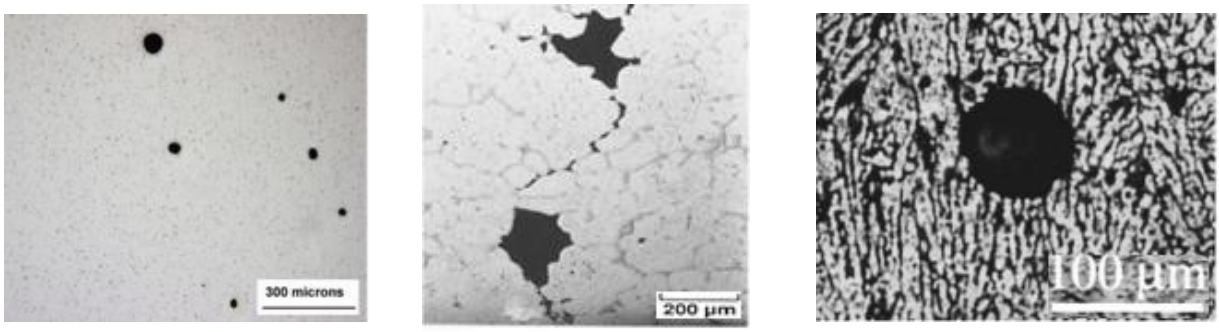

(a) AA 5087 [10] (b) Al-4.5 %wtCu-1.4 %wt Mg [40] (c) AA4043 [41]

Figure 15 – Examples of porosity in Aluminium depositions

The melt pool of liquid aluminium alloys solidifies rapidly due to the high thermal conductivity of the material and the resulting microstructure is very sensitive to the temperature and cooling rate that the material experienced. Therefore, a wide range of different grain structures are normally presented in welded or cast structures [10]. Figure 16 shows the influence of the temperature on the development of microstructure. In the base metal, the grain growth is due to the reheating of solidified material to a high but below melting point temperature. In the next region, the grains develop from planar to cellular to columnar dendritic, since, with the increase of temperature, the cellular grains have the need to divide. Near the centreline, which has the highest temperature, the developed grains are equiaxed dendritic. In

this zone, the growth of columnar dendritic arms is constrained from both sides of the deposition. Thus, there is a need for further branching and consequently finer grains are formed. The grain development influences greatly the quality of the deposited material, due to the grain boundaries formed. Finer grains have a higher number of grain boundaries, which limit the movement of dislocations and consequently strengthen the material. On the other hand, columnar dendritic or cellular grains do not offer such resistance due to their already oriented structure and limited number of grain boundaries [43].

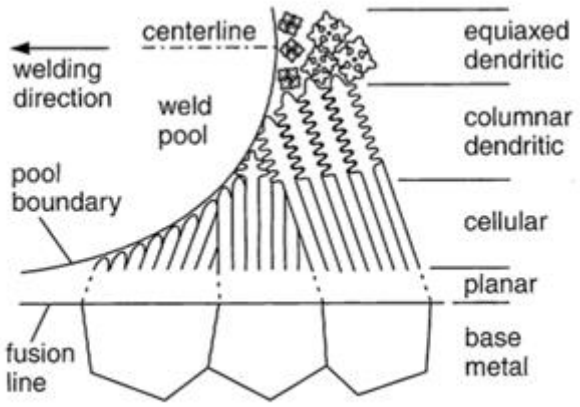

Figure 16 - Influence of temperature gradient on solidification mode for welding with P-GMAW [44]

The grain growth also highly influences the generation of porosity. As the solubility of hydrogen in interdendritic regions (area between grains) is much higher than in the grains, nucleation of hydrogen pores occurs in this region and, as the dendrite arms grow, a porosity entrapped zone is formed [10]. These are interdendritic pores, which often appear and are growth-substructure controlled, i.e., they are defined by the shape, size and growth rate of the structure [8]. Consequently, finer grains have narrower interdendritic regions and thus have less porosity in this microstructure configuration.

The cooling rate of the molten pool is another crucial aspect to consider for the entrapment of porosity. After nucleation of a pore, its growth requires time for hydrogen diffusion and coalescence. Rapid cooling rates decrease the time available for the diffusion and coalescence and thus constrain the pores growth and development [8]. On the other hand, if an extremely low cooling rate is applied, the pores will reach a critical size, which is enough to reject porosity. Gas pores with a diameter greater than 700 μm can overcome the surface tension of the solid-liquid interface and escape the deposited material [45]. However, as previously discussed, the high thermal conductivity of aluminium hinders the application of very low cooling rates, unless preheating or high heat input heat sources are used. Furthermore, for intermediate cooling rates, the conditions become favourable for the generation of high concentration of porosity. Therefore, for aluminium, the most favourable situation is the application of rapid thermal cycles [8].

Dynamic stimulation of the molten pool also produces a substantial reduction in porosity and grain size. In order to increase the turbulence flow in the melt pool, variable polarity and pulsed current can be applied. Variable polarity causes a systematic change in the magnetic field of the molten material.

Subsequently, there is an increase in turbulent convection, which stimulates the branching of cellular dendritic arms and thus produces finer grains. The effect of pulsed current on mitigation of porosity is attributed to the increase of oscillation of the melt pool as a result of periodically occurring electromagnetic force at high peak current. This arc pressure force opposes the surface tension and makes the melt pool more dynamic, which increases likelihood of pores to escape [8,46].

Welding characteristics, such as weld bead shape and size, have a great impact on the control of the amount of porosity. The bead shape defines the distance from which porosity can escape. Beads which are narrow and/or high crown have a higher escape path distance. Nevertheless, the bead width influences the amount of contamination, since it defines the extent of contact between the bead and substrate and thus the amount of hydrogen contents. For this reason, a high crown bead can have low porosity provided that the bead width is extremely reduced and so is the need for porosity escape. Also, the bead shape is mostly affected by the welding current since this parameter strongly influences the volume of molten metal. When increasing current, the depth of melted base material also increases and so does the porosity escape path [8]. The heat input affects not only porosity but also has a significant effect on the microstructure and mechanical properties, as previously presented.

Another important factor is the chemical composition of the aluminium alloy. Figure 17 represents the impact of different alloying elements on hydrogen solubility. The decrease of hydrogen solubility with the addition of Cu, Si, Zn and Fe elements reflects the positive impact of these elements on formation of porosity. This implies that the atomic bonding of these elements with Al atoms is stronger than with hydrogen and subsequently leaves less Al atoms to bond with hydrogen. In conclusion, through the addition of these elements the propensity of hydrogen-induced defects in deposited aluminium can be reduced [47].

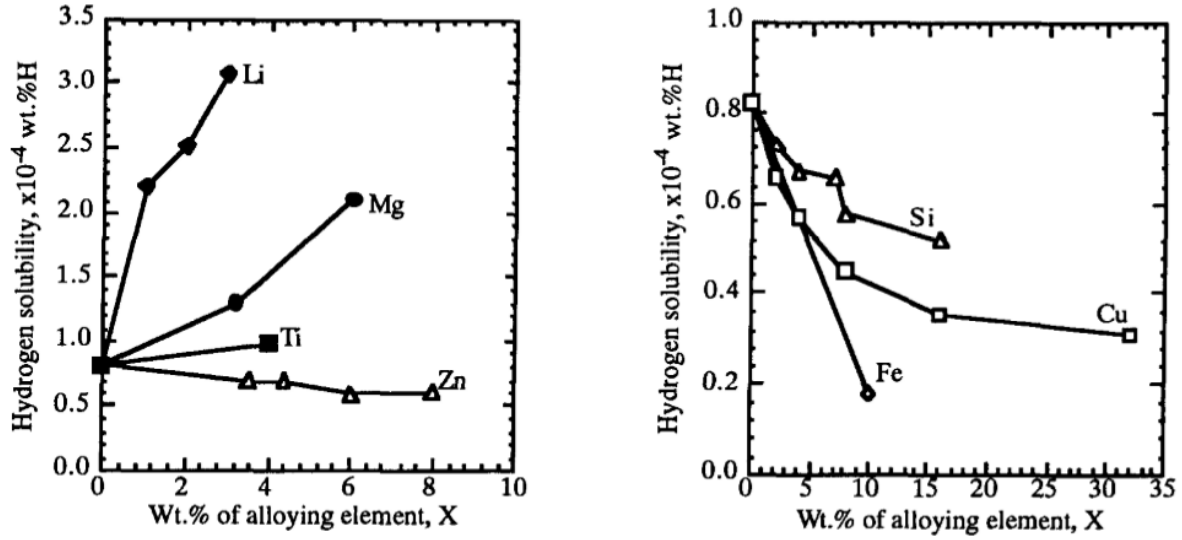

Figure 17 – Effects of alloying elements on hydrogen solubility in liquid aluminium at 973 K [47]

The influence of alloying elements of aluminium on porosity formation was studied by Gu et al. [10]. The authors compared porosity of additively manufactured AA2319 with Cu and AA5087 with Mg as the main

alloying elements. Although in this study number of pores was higher for AA2319 than for AA5087, the diameter of the pores was almost two times larger for AA5087. The electron microscopy images confirmed higher content of microporosity (2µm) for the Mg alloy. The difference was attributed to the influence of alloying elements and their bonding energy with aluminium on solidification and porosity formation.

The concentration of the alloying elements, among others, also defines the physical and mechanical properties of the material. For high strength alloys, a structure with a ductile matrix with dispersed particles is desired. These particles or precipitates interact with dislocations and affect their mobility [48]. To achieve such structure, it is necessary to select an alloy which is single phased at high temperatures and during cooling precipitates another phase in the matrix. A thermal treatment (precipitation hardening or strengthening) can be implemented to obtain the desired precipitation dispersion and refinement of the grain structure [15].

The precipitation hardening procedure can be described in three phases, as follows:

- **Solution treatment** is firstly applied. In this stage, the material is heated until reaching a sufficient temperature to dissolve the alloying atoms into the solution.
- **Quenching** is subsequently applied, which consists of rapid cooling of the homogeneous solid solution and generation of metastable phase. Through this process, the atoms of the alloying elements cannot diffuse out of the solution due to the extremely fast cooling and the solute becomes supersaturated.
- **Aging**, the alloying atoms diffuse out of the solution to contradict the imposed stress in the lattice in the as-quenched condition. The solute particles strengthen the material by diffusing into clusters and promoting a further movement constraint [9,15].

Aerospace industry demands very high quality built aluminium WAAM components, which usually requires the use of high strength aluminium alloy, such as aluminium alloys of 2XXX series. These materials have solutionized copper and/or magnesium, the strength of which can be further improved through precipitation hardening [39]. Figure 18 presents this process for copper-aluminium alloy 2319. The phase diagram is presented to show the variation of phases and composition of the alloy in different stages [15].

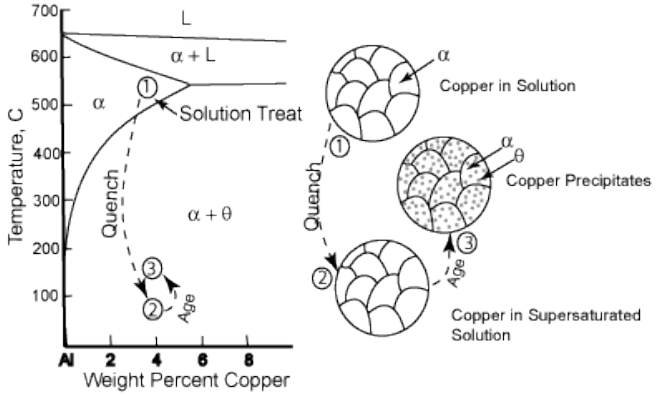

Figure 18 – Schematics of heat treatment procedure for AA2319 [15]

Although heat treatment causes the improvement of the material mechanical properties, it can have a negative impact on porosity. At high temperature, small pores coalesce into larger ones if the material is exposed to high temperature for a sufficient period of time. Consequently, the formation of porosity with critical diameters increases [10].

In multi-layer deposition, the continuous heating of deposited layers alters the morphology and structure of the material. Until an equilibrium between the heat input and dissipation ability of previous depositions is reached, heat is constantly accumulated. After the steady-state is achieved, the deposited material is maintained at the same temperature until the end of the deposition, which acts as a heat treatment [41]. As the development of the microstructure is highly dependable on the time and temperature, often thermal softening of the material occurs. For precipitation hardened alloys softening occurs due to over aging, which is caused by over growing of precipitations. In this case, the precipitations grow to a similar size of the structure grains offering no further constraint for movement of dislocations. For non-heat treatable alloys, the excessive exposure of heat increases the dendritic grain growth and the segregation may constraint the improvement in material strength. As the solute atoms remain in the solid solution, i.e., only solution treatment can be applied to these alloys, no loss of strength on the account of solute atoms diffusion is presented [43]. Thus, for these alloys, softening causes grain growth and the material microstructure is altered, subsequently compromising their strength.

In order to minimise the negative effects of heating and cooling of material during the deposition process and to maintain the mechanical properties of built parts, aluminium alloys should be deposited in very specific conditions. The conditions selected for the deposition should consider microstructure, mechanical properties, size and shape of deposits and defects, such as porosity and lack of fusion.

2.2.3. Cold Metal Transfer

The Cold Metal Transfer (CMT) process is a rather recent process [49], which was developed for welding of materials that require lower heat input, such as aluminium and thin sheet steel [50]. For thin sheets of aluminium, the most used process was conventional MIG welding. However, due to its high heat input, this process became unsuitable for this application, creating burning through and distortion. Short circuiting metal transfer was also a possibility due to its low heat input but it produces excessive spatter. Therefore, the company Fronius invented the new process called CMT [51]. This process is a modified Gas Metal Arc Welding (GMAW) process which creates nearly spatter free beads, has a low heat input and excellent welding quality [6].

The main innovation of this process is the direct integration of the wire motion into the welding process and the overall process control. As the digital process control detects the occurrence of short circuit, it interrupts the power supply and retracts the wire helping the detachment of the droplet created. In this way, the metal can be transferred into the welding-pool without electromagnetic force, just by surface tension [49,51].

Another consequence of this wire motion is decrease of heat input. As the wire is moved forward and after each short circuit cycle it is retracted immediately, during the arcing period, the time of open arc is relatively short. Consequently, the heat input is substantially lower than in other MIG processes.

The mechanical motion of wire provides additional control of the droplet detachment even in the absence of the electromagnetic pinch force, which results in an almost spatter-free metal transfer. Good control and feedback unit and mechanical movement of wire provides additional control of the arc length and good stability of the process [50].

This innovation is the reason why this process is nowadays often used in applications which were previously considered impossible or requested an enormous amount of time and effort [49].

2.2.3.1. CMT Variants

The CMT process is a variant of digitally controlled pulsed MIG welding. The material transfer is initiated in the short circuit period of the cycle which allows for operation in the relatively low power range. The main difference between the standard pulsed MIG and CMT is the control of current during the short circuit period and mechanical control of wire. It is by incorporating this mechanical process in the electrical control that allows the detection of short circuit and therefore a cut in the current (Figure 8), reducing in this way greatly the heat input to the workpiece [52]. This is schematically explained, in Figure 19.

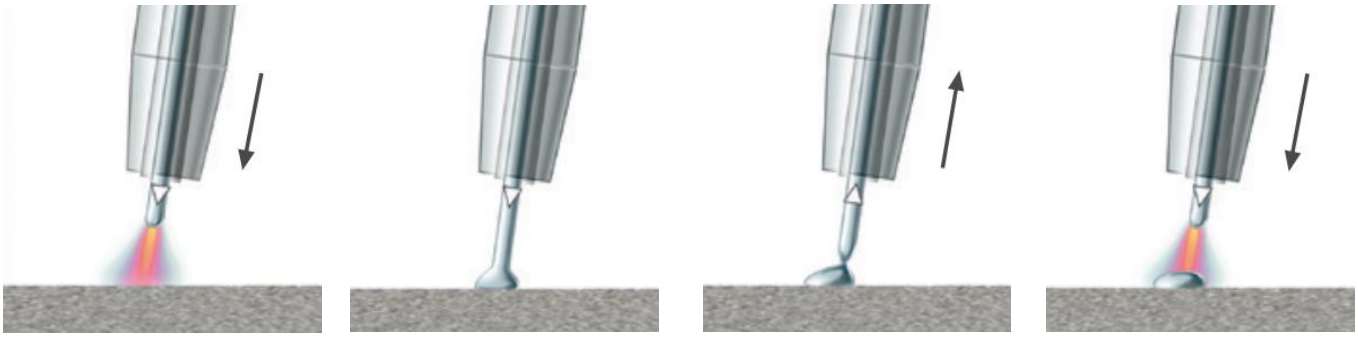

1. During the arcing period, the filler metal is moved towards the weld-pool.

2. When the filler metal dips into the weld-pool, the arc is extinguished. The welding current is lowered.

3. The rearward movement of the wire assists droplet detachment during the short circuit. The short-circuit current is kept small.

4. The wire motion is reversed and the process begins all over again.

Figure 19 – CMT standard process steps [49]

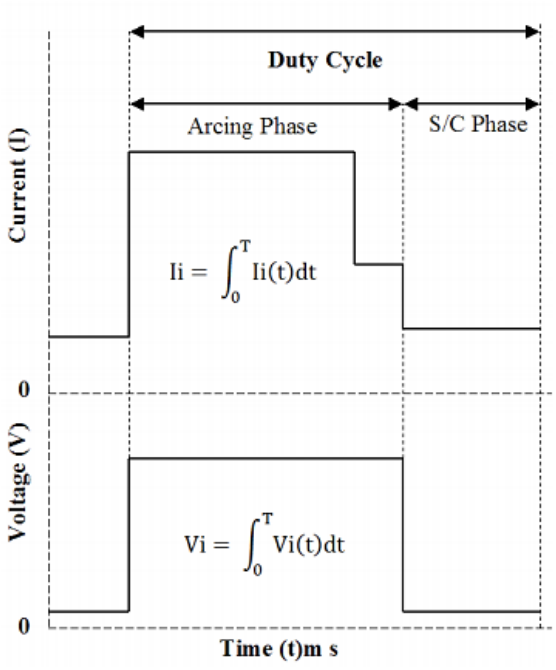

Figure 20 – Control of current during the short-circuiting period in CMT [53]

The control of the arcing phase of the cycle and wire feed rate can produce enough energy to melt both the substrate and the filler wire. Thus, in the short circuit cycle, the necessary arc energy for material transfer is low and consequently there is a reduction of heat input in the deposition [53].

However, the main disadvantage of CMT is low heat input and limited ability to increase the heat input without increasing wire feed rate. In that case, they combined good stability and low spatter of CMT and additional heat of pulsed MIG into one waveform [50].

CMT-Pulse (CMT-P) combines CMT cycles with pulsing cycles, which makes the metal transfer alternate between short circuit and transfer of molten droplets. Therefore, creates a stable arc and an elevated power performance of pulsed welding, which produces an increase in process heat input [49-51].

To further improve the control of distribution of heat between the wire and workpiece another process, CMT Advanced (CMT-ADV), was designed. This process combined CMT or CMT-P with AC MIG process. (Figure 21). The polarity change occurs in the short-circuit phase in order to guarantee the stability of the process. The goal is to reduce and control the thermal input, while increasing the melting rate at lower temperatures than CMT process. Also, due to the cleaning effect that the polarity change implies, the quality of the deposition increases [54].

All the three processes are shown in Figure 21.

CMT Pulse (CMT-P)

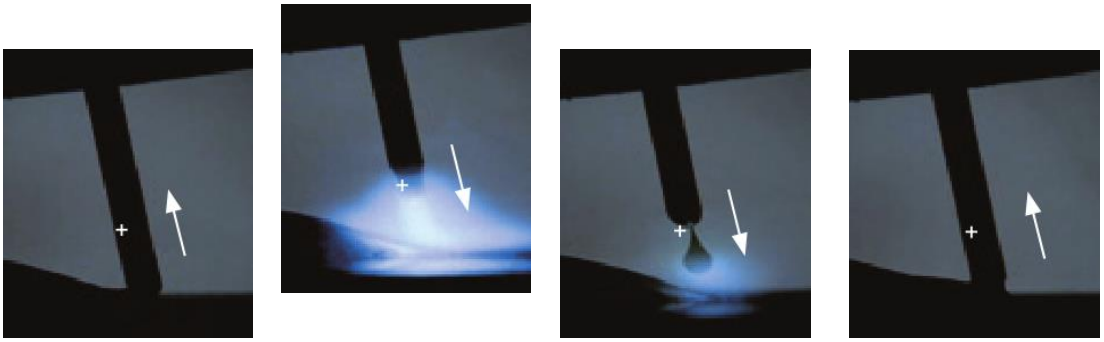

1. CMT **2.** Pulsed-arc positive **3.** Pulsed-arc positive **4.** CMT

CMT Advanced (CMT-ADV)

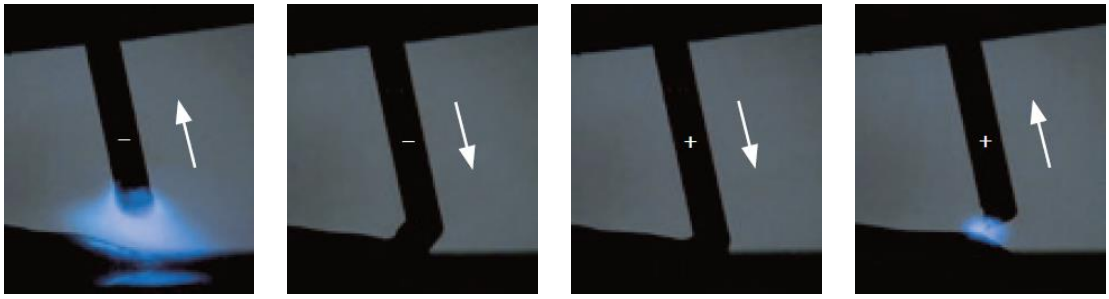

1. CMT negative **2.** CMT negative **3.** Initialisation **4.** CMT positive

CMT Advanced Pulse (CMT-PADV)

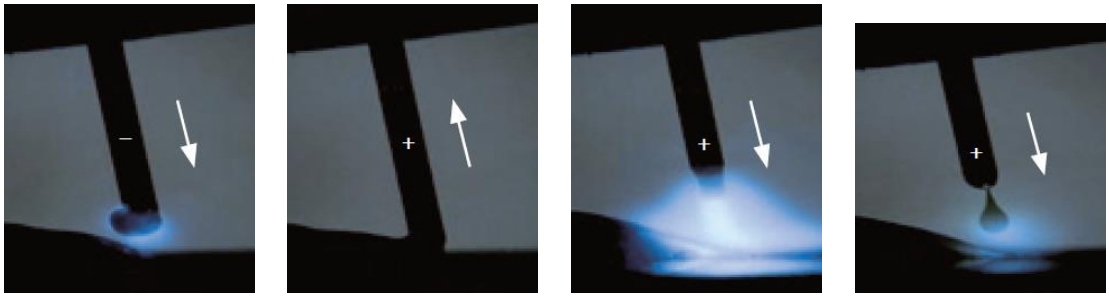

1. CMT negative **2.** Initialisation **3.** Pulsed-arc positive **3.** Pulsed-arc positive

Figure 21 – CMT Variants process steps [49]

2.2.3.2. CMT for deposition of aluminium alloys

CMT has proven to be a suitable process for aluminium deposition, due to its automatic adjustment of contact tip to work distance, lower spatter and mostly for its low heat input [6]. Cong et al. [7] investigated the influence of each variant of CMT process for single layer and multilayer deposition of AA2319 in wrought AA2219 (T851).

For single layer depositions and regarding porosity, CMT standard process was the one with a higher number of pores and larger diameters. Although CMT-P reduced significantly the number and size of the gas pores, CMT-ADV had even better results. In CMT-PADV, gas pores were nearly eliminated, as presented in Figure 22 (d) [7].

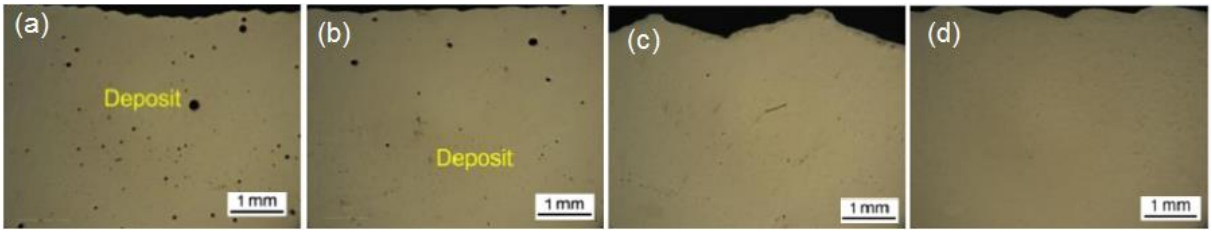

Figure 22 – Micrographs of cross sections of single layer deposit porosity for TS=5m/min using: (a) CMT, (b) CMT-P, (c) CMT-ADV, (d) CMT-PADV [7]

Figure 23 presents the transverse section of single layer deposition for a constant Travel Speed (TS) of 5m/min. CMT process presents a narrow finger shaped molten pool and, although it has nearly the same height of deposition as CMT-P, the dilution is higher. CMT-ADV also has a finger shaped molten pool but with a significant reduction in dilution when compared to CMT. In the case of CMT-PADV was observed a spherical-shaped deposition with an extremely low dilution [7].

Hydrogen in the substrate and filler wire surfaces is a known cause of porosity in aluminium deposits. Among other affecting factors, the reduction of contact area between the bead and substrate surfaces can greatly decrease porosity [44]. As referred previously, CMT-PADV has low dilution and, for this reason, the contact area with the surface is very narrow. Consequently, there is practically no contamination and nearly no porosity. However, the narrow finger shaped pool of CMT-ADV is not beneficial for pores escape. As its penetration is much shallower than CMT, the influence on the ability of gas pore to escape is significantly reduced. On the other hand, CMT and CMT-P present a larger contact area. As CMT-P has a higher heat input, the bead width is greater while the pool height is lower when compared to CMT. Although its contact area is higher, the gas pores escape more easily since its escape distance was reduced (bead height) [7,44].

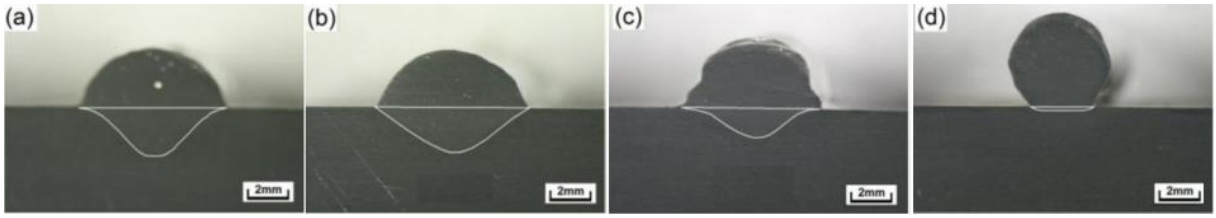

Figure 23 – Transverse sections of single layer deposit samples for TS=5m/min using: (a) CMT, (b) CMT-P, (c) CMT-ADV, (d) CMT-PADV [7]

Regarding the microstructure, CMT and CMT-P processes resulted in a columnar grain structure, while CMT-ADV deposits exhibited a mixture of equiaxed and finer columnar grain structure. However, when using CMT-PADV, a finer equiaxed grain structure was obtained [7,55]. As the grain size and morphology are highly dependable on the HI, the low heat input provided by CMT-PADV results in finer

grain structure of the material. Also, as the grain boundaries limit the dislocation length and motion, finer grains strength the material [1]. Therefore, this last process is the most suitable for the deposition of aluminium considering only microstructure phenomenon [7].

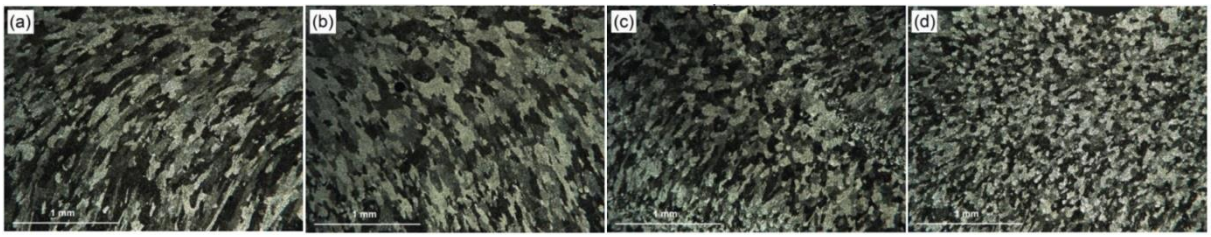

Figure 24 – Microstructure of single layer deposit samples for TS=5m/min using: (a) CMT, (b) CMT-P, (c) CMT-ADV, (d) CMT-PADV [7]

In CMT-P, the variation of arc pressure leads to the aspiration of air in the weld pool, which highly reduces the porosity in the deposited beads. In CMT-ADV, the alternating polarity adds the benefit of the oxide cleaning effect, which consequently reduces the hydrogen content in the melt pool and porosity [56]. Also, with the polarity change in every cycle, the molten pool is stirred and its movement is beneficial for gas pores escape. CMT-PADV is the combination of both CMT-P and CMT-PADV and allies the advantages present of both processes [44].

In conclusion, the authors did not recommend pure CMT process for deposition of aluminium alloys due to its undesirable effect on porosity and microstructure. In Figure 25, porosity of multi-layer depositions using CMT-P, CMT-ADV and CMT-PADV is presented. The difference in porosity shown for each process was expected considering the results of single bead depositions. In further studies, Ayarkwa et al. [30] used CMT-PADV for multi-layer deposition and the porosity concentration was much higher. This contradiction has been explained by Gu et al. [57] who showed that porosity is highly influenced by the cleanness and quality of the wire.

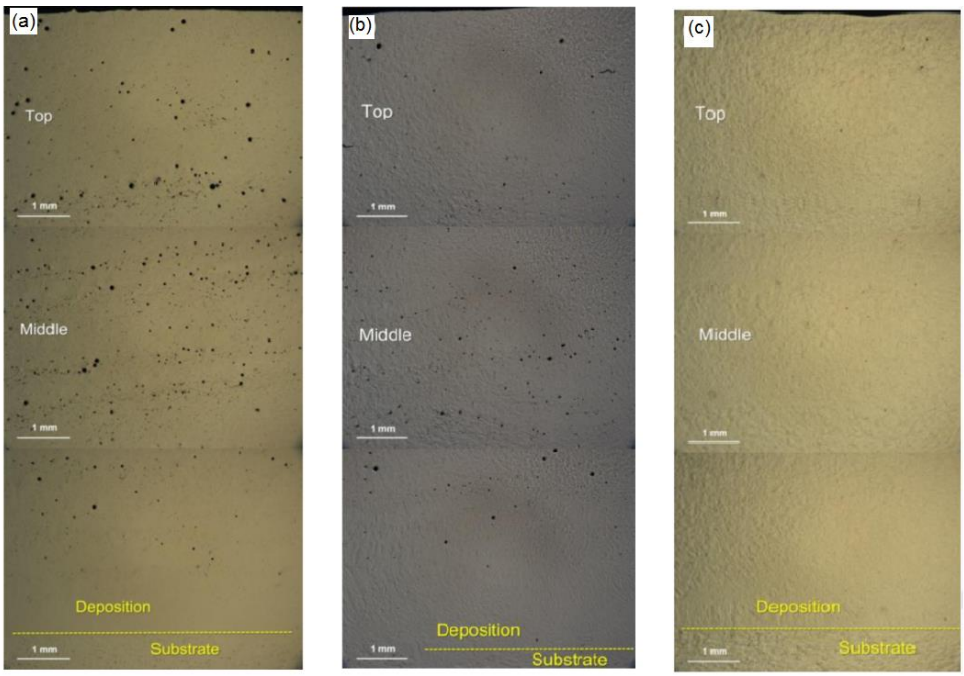

Figure 25 – Micrographs of multi-layer deposit porosity for WFS=6m/min using: (a) CMT-P with TS=0.8m/min, (b) CMT-ADV with TS=0.8m/min, (c) CMT-PADV with TS=0.6m/min [7]

With the subsequent top deposition, a portion of the previous layer is remelted and the entrapped pores become efficient heterogeneous nucleation participles. New pores are then formed and a higher concentration of porosity is formed in the layer boundary, as presented in Figure 26 [30].

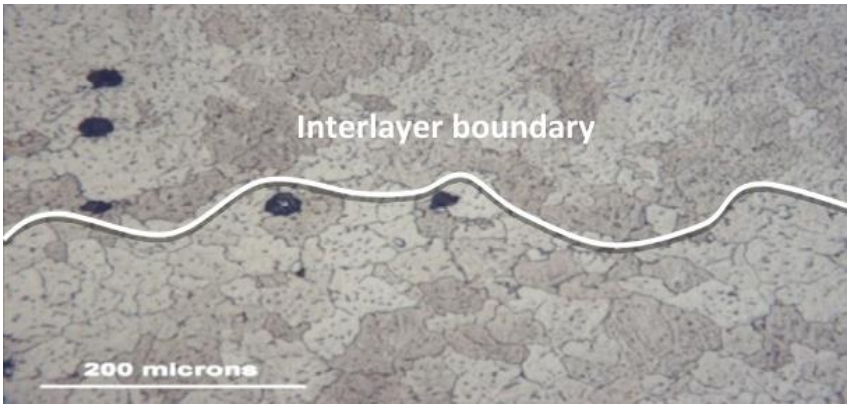

Figure 26 – Porosity in interlayer boundary [30]

From the four variants, CMT-PADV has presented the most promising results. With a careful selection of wire batch and process parameters, aiming for a low heat input, a deposition with fine grains and virtually no porosity can be obtained. To further improve the mechanical properties and eliminate porosity, cold work options and heat treatment can be applied.

2.3. Cold Work Processes

In the previous section, the defects in aluminium during deposition were presented. The incapability to avoid defects and control mechanical properties in aluminium alloys only by controlling deposition parameters, leads to the need of post processing [9]. Cold work, unlike heat treatment, works universally on almost all aluminium alloys. It can help to improve the mechanical properties and mitigate defects. Due to the increase in dislocations in the material induced by cold work, the material becomes constraint. This results in a decrease in mobility of the dislocations and, in this way, increases the strength of the material and decreases its ductility. This strengthening must be applied at low temperatures in order to impede the atoms rearrangement [15].

The most used cold work process for WAAM features is **cold rolling**. This process relies on applying a defined load through a roller, which depends on the application and material used. This method can be applied vertically between every layer or at the end of deposition (Figure 27 (a), (b) and (d)) and on the sides of the wall simultaneously (Figure 27 (c)) or only on one side at the time, as presented in Figure 28. Cold working has been proven to be an effective way of controlling residual stresses and distortion, improving material properties, refining microstructure and reducing porosity [11].

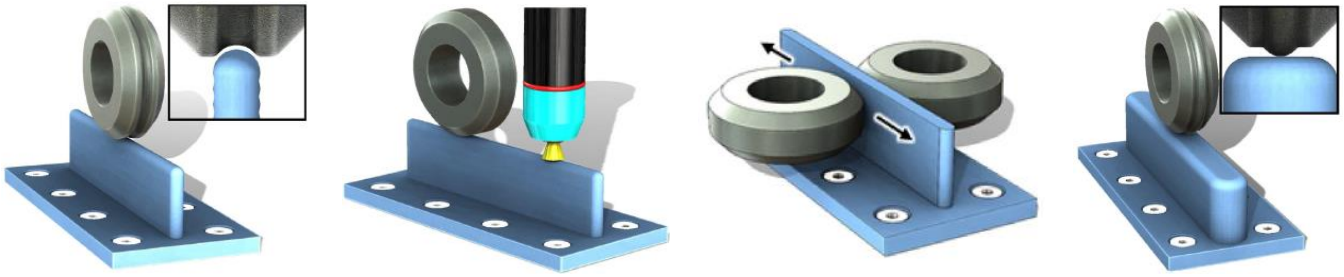

(a) Vertical rolling with profiled roller

(b) In-situ rolling

(c) Pinch rolling

(d) Rolling with an inverted profiled roller

Figure 27 – Schematics of the main rolling methods [11]

Several works have studied the influence of cold work on residual stresses and consequently distortion [19,58,59]. When compared with the improvements reported in cold worked welds [58], similar results were expected for AM applications when applying vertical rolling. However, on rolling of every layer (inter-layer rolling), the compressive stresses induced are outbalanced due to the lack of restraint in the transverse direction and moderate improvement of residual stresses was obtained. For this reason, side rolling, pinch rolling or slotted profile rollers have proven to be more effective option for reduction of residual stresses [59].

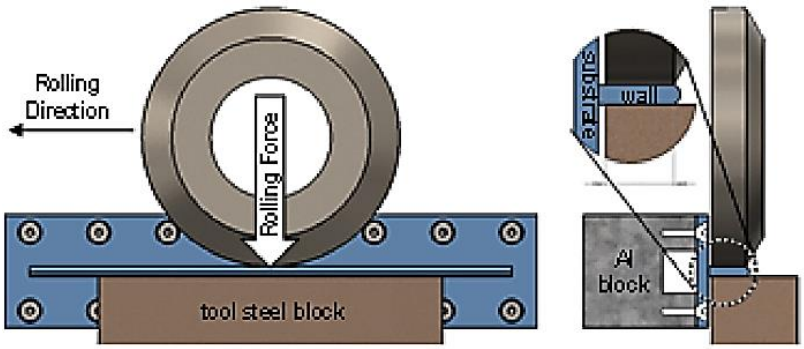

Figure 28 – Schematic of side rolling application [59]

The improvement of mechanical properties in cold rolled AM parts was mainly reported for titanium. As this material has tendency to develop columnar grains in as-deposited condition, by the application of rolling, the grains are deformed and become much finer and equiaxial, as presented in Figure 29 (a) and (b). This effect increases the strength of the material [19] and allows the use of titanium for high strength applications. For aluminium alloys, cold rolling does not present a much greater improvement in terms of grain refinement, since the microstructure of these materials is usually already composed of fine grains. However, in Figure 29 (c) and (d), the dispersion of precipitates is highly changed. It is shown that the microstructure of the alloy is deformed and that the precipitates are flattened. In this way, the concentration of precipitates increases and the mechanical properties of the material are improved. High improvement of microstructure and mechanical properties was also obtained for the deposition of steel [59].

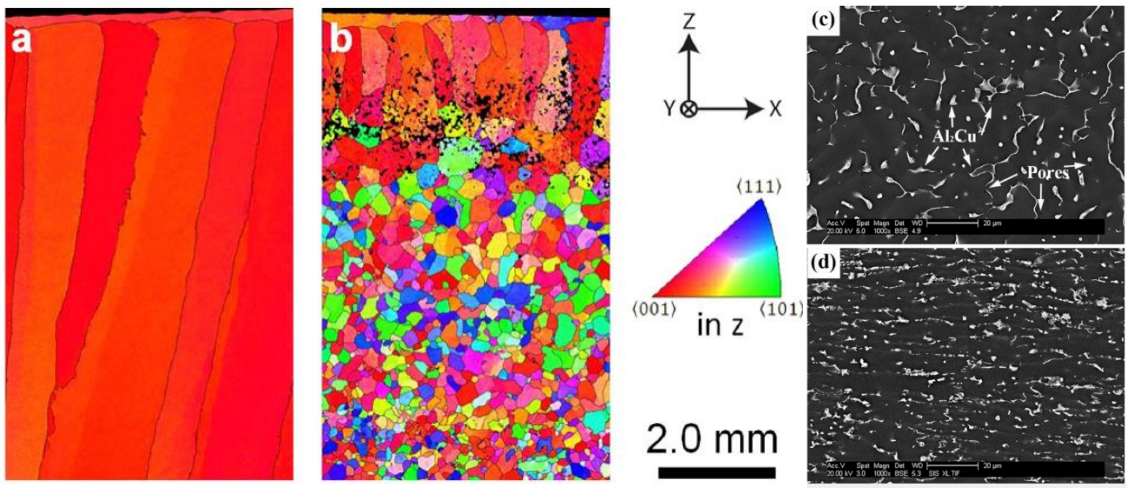

Figure 29 – Effect of rolling on microstructure of titanium and aluminium; (a) Ti-6Al-4V as deposited [11] and (b) Ti-6Al-4V rolled between every deposited layer [11] (c) 2319 aluminium as deposited condition [9] (d) 2319 aluminium inter-layer rolled with a load of 45 kN [9]

Particularly for aluminium, porosity generally appears in the deposited material, as presented in Figure 29 (c). Gu et al. [9] proved that by applying inter-layer rolling, reduction of porosity was achieved and for a load of 45 kN was completely mitigated. Also, due to the elimination of this defect the ductility was improved. However, this study only covered the results for inter-layer rolling, which is a time-consuming process. After deposition of each bead, the rolling is applied. Yet, it has one undesirable effect of flattening the beads shape, which requires deposition of additional layer to compensate for it. According to data shown by Toda et al. [14] the elimination of porosity should occur when a sufficient amount of compressive strain in the material is induced. For this reason, pinch rolling could be also a suitable solution for the reduction of porosity. In this way, only after the deposition of the full part, the load would be applied. Although the capability of pinch rolling for porosity closure in AM parts was never studied, it is a potentially promising option. Because of the working principle of pinch rolling is similar to side rolling, the latter could be used initially to test the concept, since the preparation of two rollers acting simultaneously requires more complex set-up and programming [11].

Both, side rolling and pinch rolling, can be applied on parts with relatively simple geometry, such as straight walls or revolved sections. For this reason, the application of alternative ways of inducing cold work, more suitable for WAAM applications, should be explored [11].

Machine hammer peening (MHP) is a relatively new technology and no literature was found regarding its application for AM parts. The peening process consists of the oscillation of an axially guided plunger, which is activated by either a pneumatic or electromagnetic actuator. This system can be integrated in a machine tool or robotic arm allowing greater versatility than rolling. The flexibility of MHP allows it to be applied in a wide variety of geometries and at different stages of deposition. If the capability of this process is proven, the application of inter-layer cold work would not be necessary and can be replaced [61].

MHP impacts the surface with very well directed impacts, which allows a controlled surface modification. In other peening processes, such as, shot peening, the intensity of impact is not uniform, which makes MHP a suitable process for precision machining. Also, the correlation between the compressive strain applied and the peening intensity was reported in the literature [61-63].

Several works have proven the capability of MHP and other peening variants to enhance the material properties. Peening processes are often used for surface finish, since by selecting the correct line pitch and ball diameter, surfaces can have a very low roughness and mirror-like finishing. Surface corrosion resistance was also studied and its improvement shown, particularly when shot peening and ultrasonic peening were used. However, this effect was observed to only a very narrow region near the peened surface. Also, the processes capability of enhancing fatigue life and increasing fatigue strength in different materials has been proven. However, when exposing the cold worked material to high temperatures, the benefits of cold work were generally reduced [12,13,64].

The influence of peening on porosity in cast aluminium was studied by Toda et al. [14]. A reduction of porosity in the near peened surface, after 420 seconds of application of peening, is presented in Figure 30 (b) and compared to as deposited condition Figure 30 (a). After exposing the material to a temperature of 813K, the reappearance of porosity in region D is visible. This was explained by the rearrangement of grains and relaxation of stresses applied during the deposition and peening.

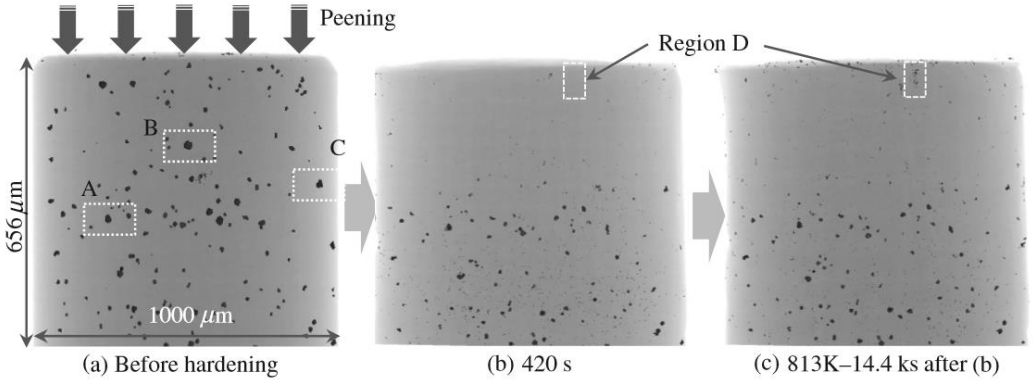

Figure 30 – Representation of the micro pore distribution during the surface hardening and subsequent heat treatment [14]

When a cold worked material is exposed to high temperature, the strengthening effect can be reversed, i.e., softening occurs. During heat treatment, three phases can occur, that are represented in Figure 31.

The recovery stage is characterized by the increase in atomic diffusion due to high temperature that starts reliving the strain energy applied by cold work. This allows the atoms to recover their normal position in the lattice of the material, i.e., move to unstrained positions. In this way, residual stresses decrease, since dislocations moved to lower-energy positions. The strength and hardness of the material do not change in this stage [43].

Recrystallization occurs when the material is exposed to even higher temperatures. At this stage, the nucleation of new strain-free grains occurs in the grain boundaries or inside old distorted grains. Since this occurs to revert the strain hardening grains, the mechanical properties of the material start returning to the initial non-hardened state with higher ductility. The development of this stage is highly dependable on the amount of cold work, i.e., the more cold work applied the faster recrystallization occurs. In this stage strength and hardness start decreasing, while ductility increases [15].

When the material is already recrystallized but is still exposed to high temperatures, the grain size starts to grow. This is the grain growth phase and is characterized by the diffusion of grains across the intergranular boundary. This is explained by the smaller surface area of grain boundary per unit of volume of large grains, which allows further growth at the expense of smaller grains. Thus, the strength of large grains is reduced but the ductility is increased [15].

As presented in section 2.2.2., the exposure to high temperature leads to the nucleation of precipitates, which increase the strength of the material. For this reason, a compromise between the amount of cold work and temperature exposure has to be achieved to enhance the mechanical properties in the most suitable manner.

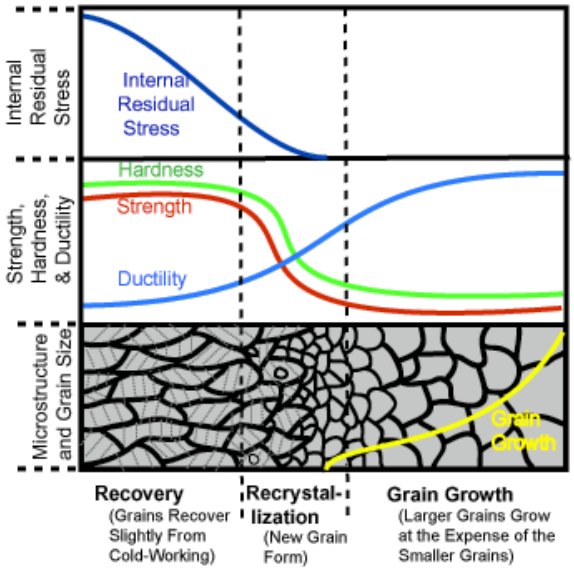

Figure 31 – Three stages of cold worked material exposed to high temperature [15]

2.4. Summary

From the literature, it can be concluded that the lack of commercial systems, high expertise required to run the processes and difficulties in controlling the bead geometry are the main limitations to the application of WAAM technology. Furthermore, build strategies for large manufacturing often require tool path strategies for large scale features, such as crossovers of thicker walls and overlap of single beads. These are crucial to guarantee defects-free depositions and high efficiency and are a key progress in the present work.

Great attention needs to be paid to control defects in aluminium. The most challenging defects are distortion, crack initiation sites and porosity, which are caused mainly by residual stresses, material shrinkage and hydrogen entrapment. These depend on the material, process used and parameters. The microstructure, mechanical properties, size and shape of deposition are also crucial during building of large components. CMT-PADV was considered the most suitable process for the deposition of aluminium, due to the low heat input and cathodic cleaning effect of the process. Porosity free and fine grained depositions can be achieved with this process, but a very careful selection of wire batch and process parameters should be considered.

To further improve the mechanical properties and mitigate porosity, cold work options and heat treatment can be applied. An inter-layer rolling has been proven to be an effective method to achieve so, but it must be applied on each layer and this can be very time-consuming particularly for large components. Other options, such as side rolling and machine hammer peening, can be also used. Both strategies have not yet been tested in WAAM aluminium components and will be further investigated in this work. Another effective strengthening method for aluminium is heat treatment by nucleation of precipitates. Investigations regarding the effects of heat treatment on aluminium WAAM components have been previously studied. However, the right combination of cold work and a suitable heat treatment has to be achieved to enhance mechanical properties and reduce defects. Thus, to develop the capability of WAAM on industrial scale, further study on manufacturing of large parts, elimination of defects and enhancement of properties have to be carried out.

3. Material and Methodology

Throughout this experimental work, several phases had to be considered before to attain the 6-meter long aerospace structure and enhance its mechanical properties through cold work. The methodology depended on the outcome of the initial experimental work, only the generic set-up and methods used for deposition, heat treatment and cold work are presented in this section, while more detailed explanations are given in subsequent chapters. Moreover, the procedure for metallurgical analysis and mechanical test is described in detail.

3.1. Material

Four different materials were used for the deposition of single bead crossings, hybrid crossings, single bead wall and parallel wall, as presented in Table 1.

Table 1 – Base plate and filler wire for each application

	Base Plate		**Filler Wire**	
	Dimensions [mm^3]	Aluminium Grade	Dimensions [mm]	Aluminium Grade
Single Bead Crossing	250x65x12	AA 6082-T6	Ø1.2	AA 4043
Hybrid Crossing	500x300x22	AA 6082-T6	Ø1.2	AA 4043
Single Bead Wall	250x65x12	AA 2024	Ø1.2	AA 2319
Parallel Wall	250x65x12	AA 2024	Ø1.2	AA 2319

For the manufacturing of the large spar, the deposition was carried out on both sides of a 6082-T6 aluminium plate with 6000x300x22 mm^3. The chemical composition of all used materials is presented in Table 2.

Table 2 – Chemical Composition of all used Aluminium Alloys [65]

	Elements [%wt.]										
	Si	**Fe**	**Cu**	**Mn**	**Mg**	**Cr**	**Zn**	**Ti**	**V**	**Others**	**Al**
Alloy 6082-T6	0.7-1.3	0.50	0.10	0.4-1.0	0.6-1.2	0.25	0.20	0.10	–	0.15	Balance
Filler 4043	4.5-6.0	0.60	0.30	0.15	0.20	-	0.10	0.15	–	0.15	Balance
Alloy 2024	0.50	0.50	3.8-4.9	0.3-0.9	1.2-1.8	0.10	0.25	0.15	–	0.15	Balance
Filler 2319	0.20	0.30	5.6-6.8	0.2-0.4	0.02	-	0.10	0.1-0.2	0.05-0.15	0.15	Balance

3.2. Deposition

3.2.1. Deposition equipment

All the depositions were performed within a cell equipped with 10-metre robot tracks, two 6-axis KUKA robots and a fully interfaced programmable logic controller, presented in Figure 32. One of the robots was incorporated with a CMT welding power source while the other with interchangeable tool mounting which could be incorporated with another functionality, such as, welding, machining, inspection, monitoring and metrology.

Figure 32 – Deposition Cell [21]

For the deposition of single bead crossings, single bead walls and parallel walls, the set-up from Figure 33 was used. Only one of the robots was used and all depositions were performed on a working table. The shielding gas used for all the trials was pure argon (99.99%) with a flow rate of 25 l/min and the contact tip to work distance (CTWD) was kept at 13 mm. A standard welding MIG torch was used with incorporated shielding and no additional shielding devices were used.

For the final part the set-up was modified with a part rotator installed. As the 6-metre long part deposition was performed on both sides of the substrate, a rotation table was required. This additional manipulator is presented in Figure 34 and would rotate 180º every time a layer was completed, until the completion of the part. A custom-made support frame was manufactured to support the part during deposition and minimise distortion. The experimental trials of hybrid crossings were also performed in this set-up.

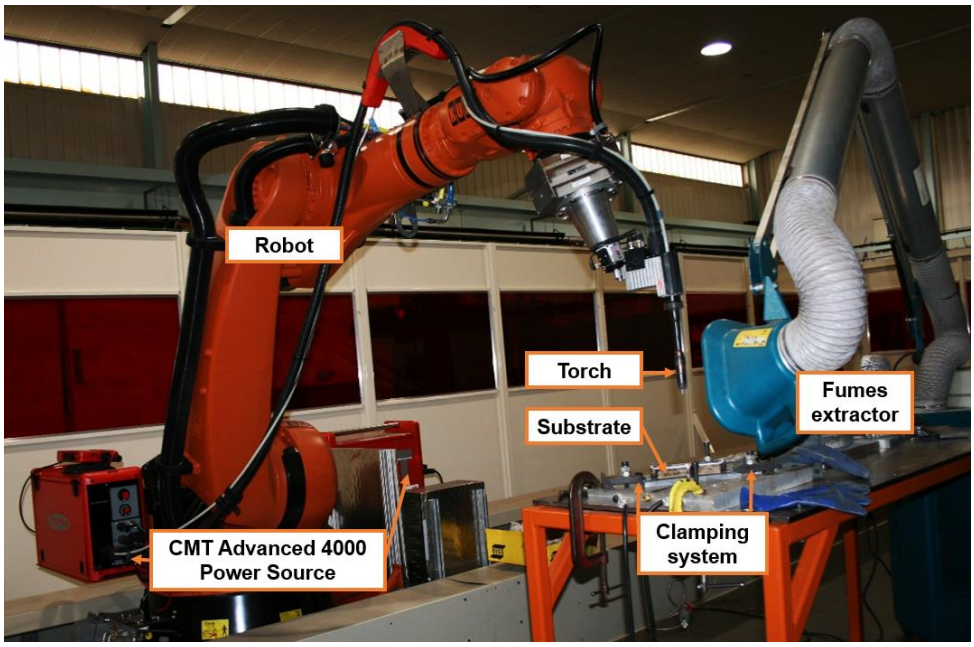

Figure 33 – Experimental set-up for development work

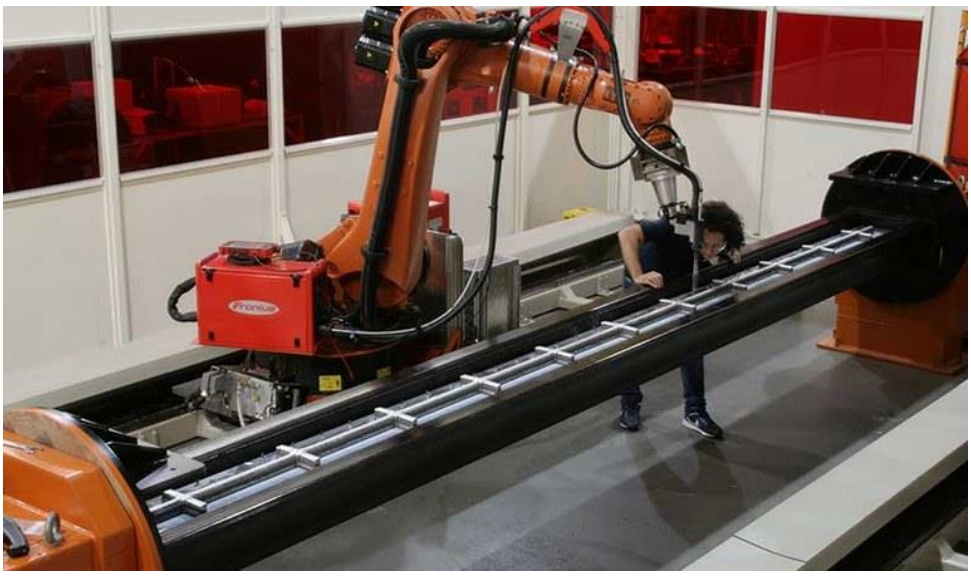

Figure 34 – Rotation table for 6-metre long structure [21]

3.2.2. Deposition procedure

Throughout the experimental approach, different types of walls needed to be manufactured. To meet the initial goal, which was the manufacturing an 8-metre straight wall, a set of initial experiments for the development of optimum process for intersections and crossings was required. To manufacture the 6-metre aerospace spar, two different hybrid crossing strategies were studied. In the first one, the combination of parallel walls and single bead crossings was applied. In the second case, the parallel and oscillated technologies were used together. With the aim to improve the mechanical properties of the large spar, a study of the impact of cold work was carried out for thin and thick walls, i.e., in single

bead and parallel walls respectively. This required manufacture of additional walls. An example of each deposited procedure is presented in Figure 35.

(a) Single bead wall

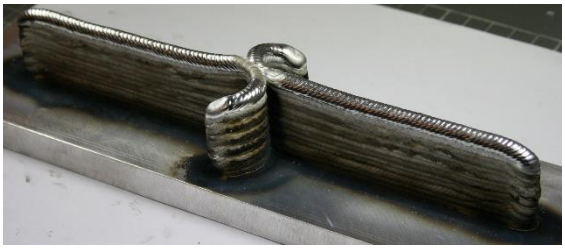

(c) Single bead crossing

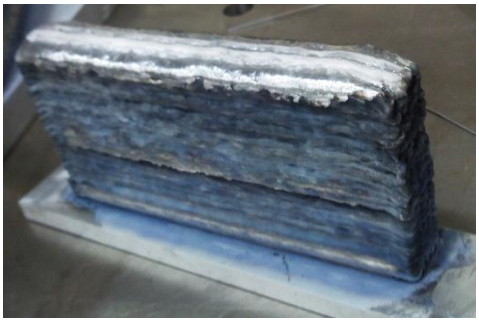

(b) Parallel wall

(d) Hybrid crossings

Figure 35 – Type of deposited walls

- **Single bead wall**

For the deposition of single bead walls, the used process parameters are presented in Table 3. A waiting time of 90 seconds was applied between each layer to ensure the same inter-pass temperature. The deposition parameters were changed in the initial three layers to compensate for thermal loss from the base plate and then parameters were constant after reaching steady-state conditions. This alteration is due to the high cooling of the base plate prior to the actual welding and as CMT-P has a higher heat input than CMT-PADV, it becomes more suitable for the first layer. Consequently, the layer height increment was not constant for these layers and only after the third layer the deposition parameters were constant.

Table 3 – Process parameters used for single walls

Layer number	Process	WFS [m/min]	TS [m/min]
1	CMT-P	7	0.6
2	CMT-PA	9	0.6
3	CMT-PA	7	0.6
4 to n	CMT-PA	6	0.6

n – number of layers for the desired height

- **Parallel walls**

To achieve thicker walls with a substantial thickenss to apply cold work, a parallel wall was built. The spacing between deposits was constant, which resulted in 66% overlap to exclude lack-of-fusion defects. This value was determined based in previous experiments of the welding group at Cranfied University. After the completion of each deposited layer, consisting of five overlapping beads, bulding of the next layer was carried out untill the required wall height was achieved. In each case the direction of deposition for each layer was always maintained the same as indicated by arrows in Figure 36 (a). Then it was reveresed for the subsequent layer.

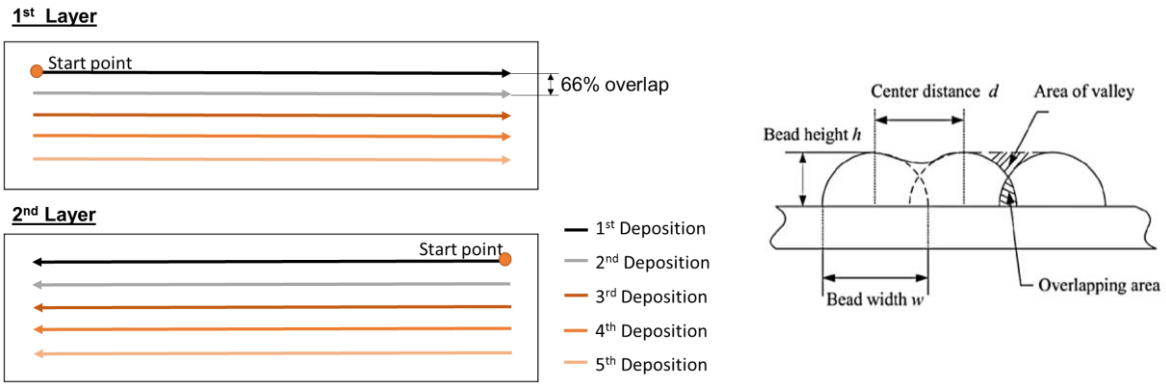

(a) Path strategy for parallel walls (b) Sketch of overlapping beads [36]

Figure 36 – Path strategy for parallel walls deposition of 5 depositions

To achieve a flat top surface in parallel deposition, it is necessary to control overlap. As presented in Figure 36 (b), there is relationship between the overlap area and the valley area. Thus, overlap is given by Equation 2:

$$Overlap\ [\%] = \frac{d\ [mm]}{w\ [mm]} \qquad (2)$$

For the study of cold work, specific dimensions of both single bead and parallel walls were required. In Figure 37, the length and the height of the walls is specified.

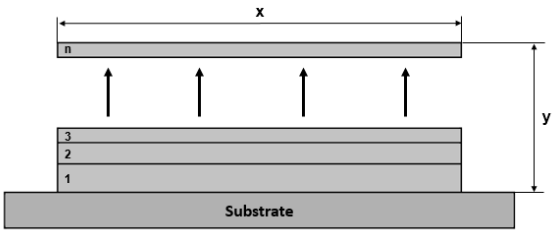

(a) Schematics of layer deposition

	Single Bead Wall [mm]	Parallel Wall [mm]
x	140	160
y	80	100

(b) Wall dimensions

Figure 37 – Schematics of layer deposition for single bead and parallel walls and corresponding dimensions

- **Single bead crossing**

In the study of single bead crossings, each wall consisted of 15 layers and was deposited also with the parameters presented in Table 3. In only one trial, CMT-P was used for all layers, but the remaining parameters were maintained.

The main variables and the deposition path strategy used are presented in Figure 38 and Table 4. More details of the single bead crossings experiments are explained in chapter 4.

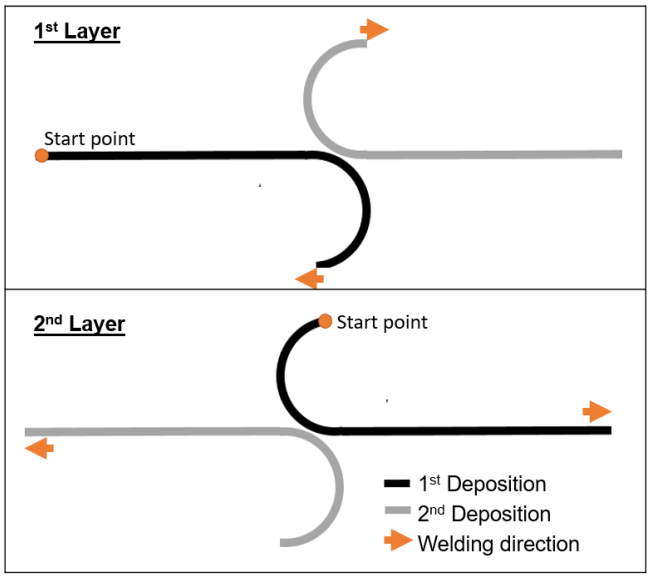

Figure 38 –Deposition path strategy for single bead crossings

Table 4 – Parameters range of single bead crossing trials

Process	Radius [mm]	Overlap [%]
CMT-P or CMT-PA	9.6 or 20	33 – 80

- **Hybrid crossings**

To obtain the 6-metre long frame, two approaches were studied and tested: crossing and parallel deposition and combined parallel wall and oscillated deposition.

The first approach is the combination of single bead crossing and parallel wall technologies, as presented in Figure 39. For this reason, radius, WFS and centre beads distance were the main variables studied. The deposition strategy and variation of these parameters will be further described in chapter 4.

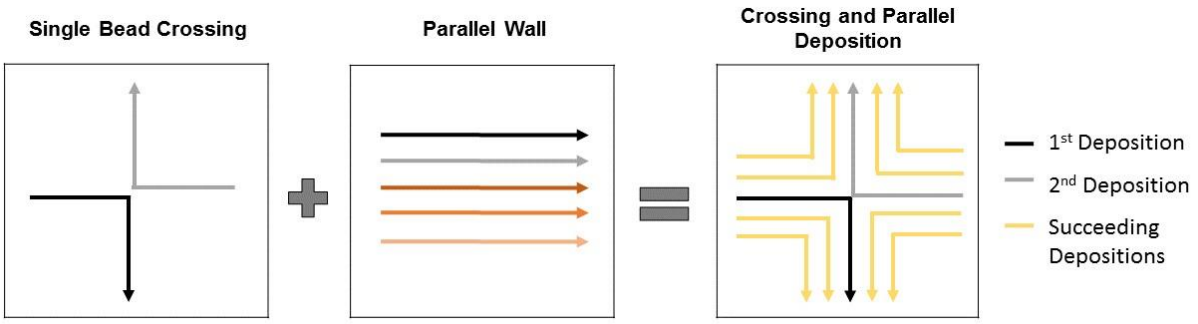

Figure 39 – Schematics of the combination of single bead crossings and parallel walls

The second approach was the combination of parallel wall and oscillated strategy, as presented in Figure 39. The oscillated wall path was produced by an oscillated movement of the torch along a path similar to the one shown in Figure 39. The main variables were the centre distance between the longer parallel beads and the perpendicular distance between them. This approach relied on the sufficient overlap to avoid lack of fusion and defects. The main variables were WFS, perpendicular beads distance and centre beads distance for parallel and oscillated walls. The detailed deposition strategy and variation of these parameters will be further described in chapter 4.

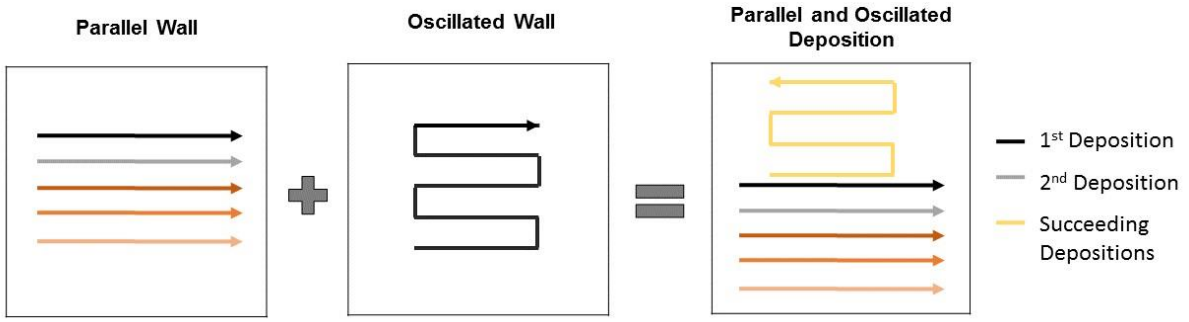

Figure 40 – Schematics of the combination parallel and oscillated wall

3.3. Cold Work

Two different methods of inducing cold work in deposited walls were studied, machine hammer peening (MHP) and side rolling. In both cases the following procedure was applied:

1. Deposition of the wall;
2. Machining the walls on both sides to achieve flat surfaces, on which cold work was performed (represented in Figure 41);

Clamping the machined walls in the flat position and carry out peening or rolling as shown in

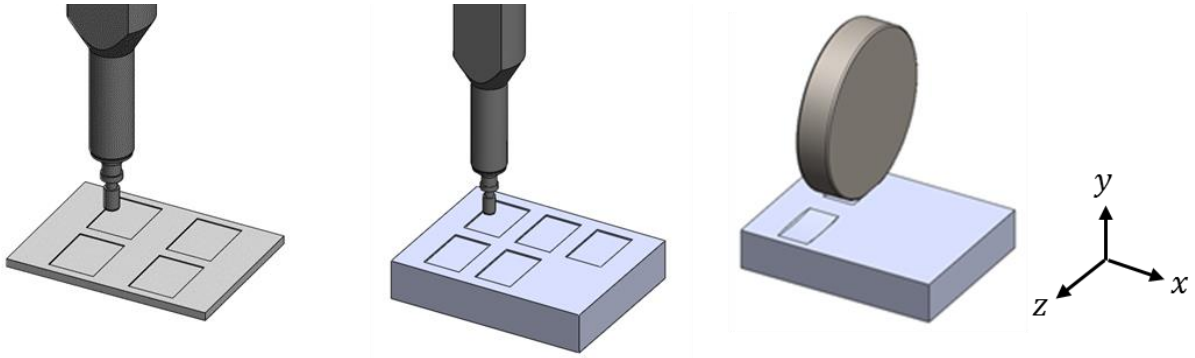

3. Figure 42.

Note that only parallel walls were used for cold rolling, whereas MHP was tested in both types of deposited walls. Different procedures and equipment were used for machine hammer peening and side rolling.

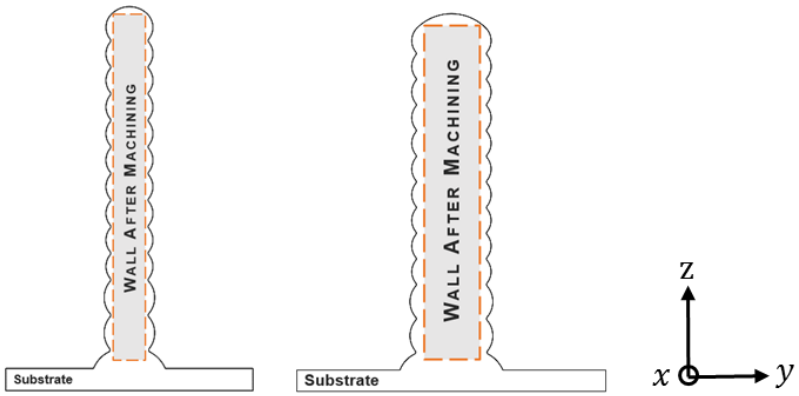

Figure 41 – Cross section of a single bead wall and a parallel wall with indicated part after machining

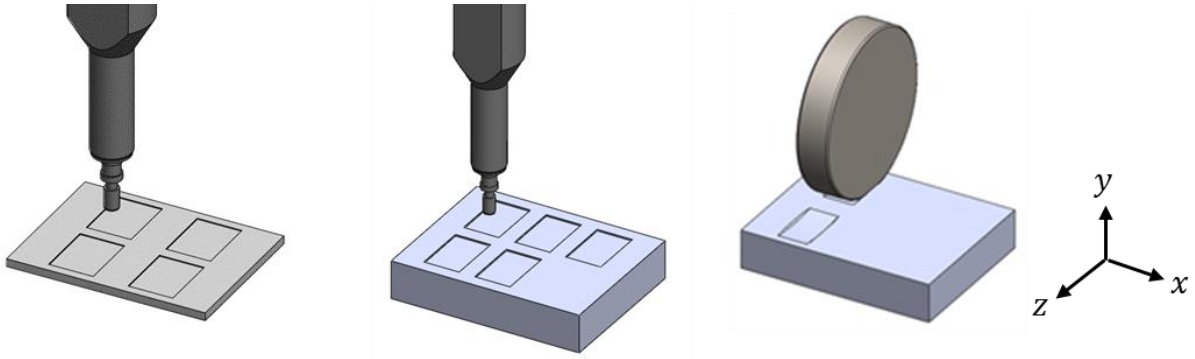

Figure 42 – Illustration of walls being peened and rolled

- **Machine Hammer Peening**

Machine hammer peening was performed in the cell presented in Figure 32 (Section 3.2.1), in which the tool FORGEfix (Air) [66] was installed on the second KUKA robot. FORGEfix is a pneumatic cold forging tool with air cooling which was used for local hardening of the workpieces.

The main parameters of this process are presented in Figure 43 and Table 5. In most experiments only single pass of the peening was applied, but in some cases multipass with different displacements was used, as indicated in Figure 43 (c). For the purposes of this experimental work, the displacement refers to the line pitch divided by the number of required tool path repetitions.

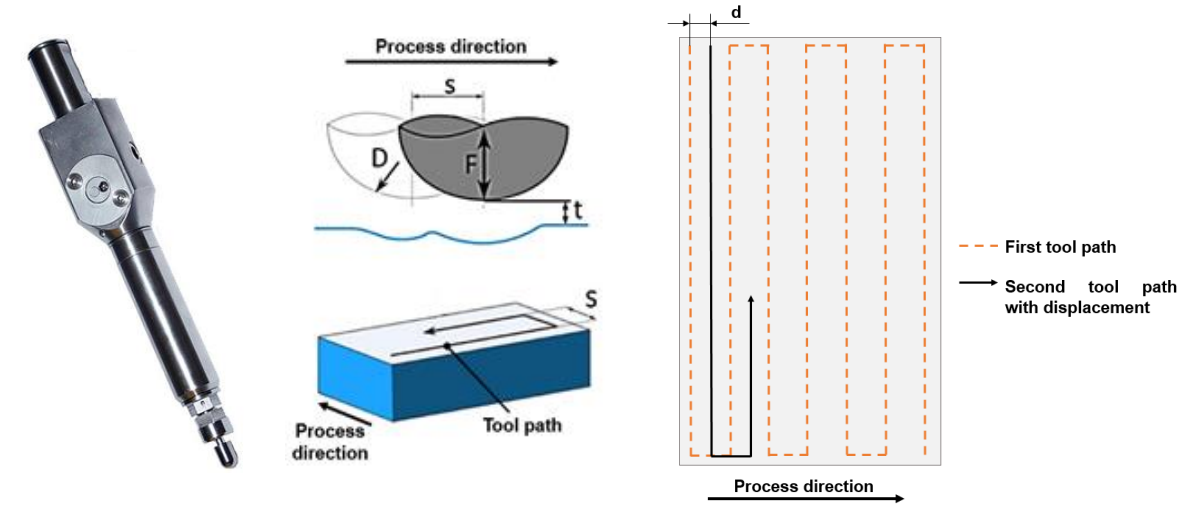

(a) FORGEfix Tool [66] (b) Important Machine Hammer Peening Parameters [62] (c) Displacement when path repeats

Figure 43 – Principle of Machine Hammer Peening and parameters

Table 5 – Main Parameters of Machine Hammer Peening Process [adapted from 62]

Parameter	Unit	Description	Value
Diameter D	[mm]	Diameter of the spherical plunger tip	8
Distance t	[mm]	Distance between surface and plunger tip	0.10
Line pitch s	[mm]	Distance between two MHP lines in the same tool path	0.1 – 0.3
Displacement d	[mm]	Distance between two MHP tool paths	0.1 – 0.15
Travel speed TS	[mm/s]	Speed set for the robot arm movement	25 – 75
Pressure p	[bar]	Pressure of compressed air supply	5
Frequency F	[Hz]	Frequency of the oscillating movement	~ 250

All the trials performed are presented in Table 6. The peening density was calculated using Equation 3:

$$\text{Peening density } [\text{hits/mm}^2] = \frac{\text{F [Hz]}}{\text{TS [mm/s]}\times\text{s[mm]}} \times \text{N} \qquad (3)$$

Table 6 – Variable values for MHP of AA2319 and AA4043

	Trial	TS [mm/s]	s [mm]	d [mm]	Repetitions N	Peening density [hits/mm^2]
AA2319	1	75	0.3	–	–	11
	2	50	0.2	–	–	25
	3	75	0.3	0.15	2	22
	4	75	0.3	0.10	3	33
AA4043	1	75	0.3	–	–	11
	2	50	0.2	–	–	25
	3	25	0.1	–	–	100
	4	75	0.3	0.15	2	22
	5	75	0.3	0.10	3	33

- **Cold Rolling**

Cold Rolling was performed using a hydraulic rolling rig as presented in Figure 44. The rolling equipment consisted of a roller and hydraulic piston which applies force required for cold work. A flat roller of H13 steel with a diameter of 100mm and 20mm width was used. The machined walls were positioned in a flat orientation and clamped prior to rolling. The roller was positioned at a distance of 5 mm from the wall edge and lowered until in contact with the wall. Then compressive force was applied to its surface by the hydraulic cylinder and the roller. The rolling process started with a speed of 600 mm/min and a load of 75kN. After rolling a length of 30 mm, the process was terminated. This procedure was repeated in another part of the same sample with an increased load of 150 kN (Table 7).

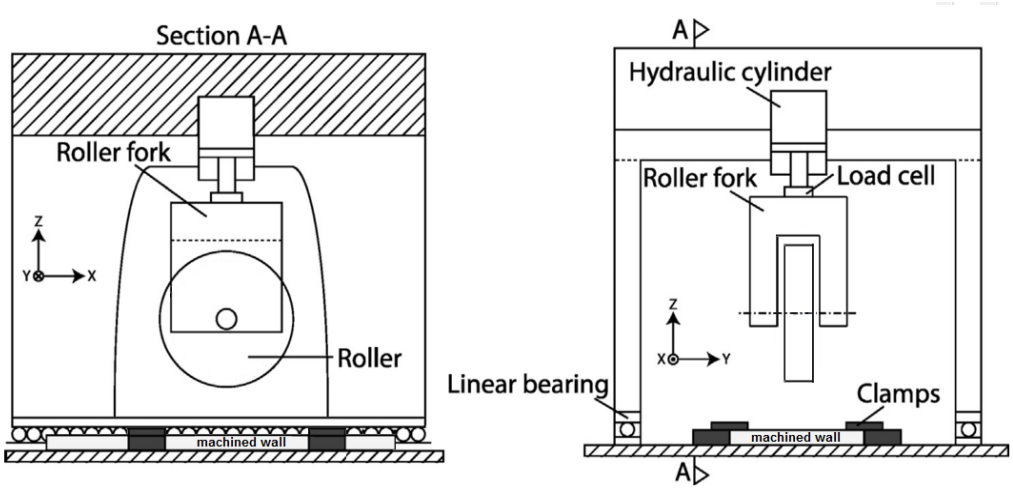

Figure 44 – Schematics of the rolling equipment [adapted from 67]

Table 7 – Parameters used for Cold Rolling

	Trial	Load [kN]	Roller width [mm]	Roller diameter [mm]	Rolling speed [mm/min]
AA4043	1	75	20	100	600
	2	150			

3.4. Heat Treatment of peened samples

Heat treatment was only performed in the Aluminium Alloy 2319, since AA4043 is a non-heat treatable alloy. Two separate procedures were applied, for tensile test specimens and for the samples used for metallographic studies.

- **Tensile test samples**

For the tensile test samples, a T6 heat treatment, which is solution treatment and artificial aging was carried out, as shown in Figure 14. The samples were heated in a furnace to a temperature of 500 ºC with a heating rate of 5 ºC/min and then further heated to 535 ºC with a lower rate of 1 ºC/min. After holding them for 120 minutes, they were quenched in water. Artificial aging was achieved by heating the specimens to 155 ºC with a rate of 5 ºC/min and then to 175 ºC with a rate of 1 ºC/min. After holding at this temperature for 360 minutes, the specimens were air cooled to room temperature.

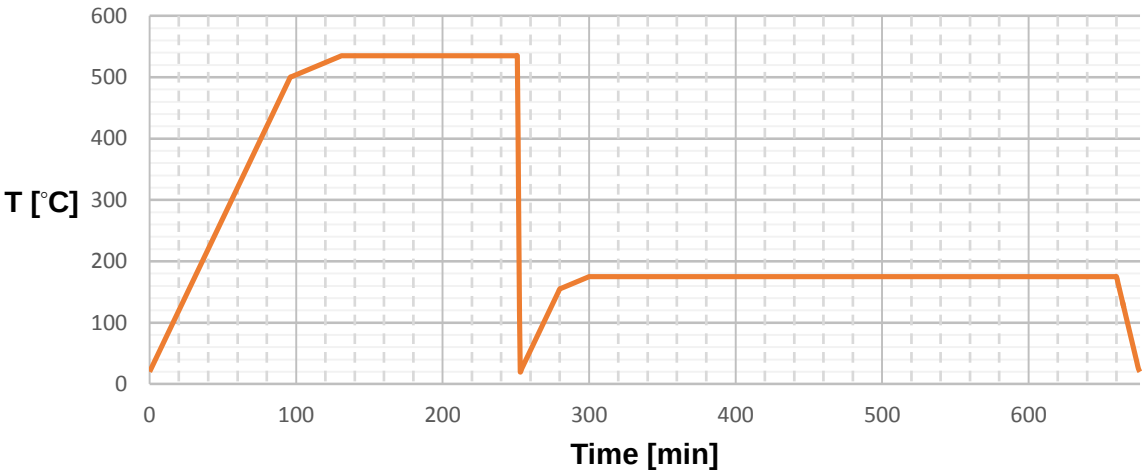

Figure 45 – Temperature profiles of two cycle heat treatment implemented in AA2319

- **Samples for metallography studies**

For the samples for metallography studies, the same procedure was used but with additional waiting time between the solution treatment and aging. After the solution treatment, a natural aging for 3 weeks was done and only after this period the artificial aging was performed.

3.5. Characterisation

3.5.1. Metallographic preparation

For the metallographic preparation, the samples were cut 10 mm from the starting point of peening or rolling perpendicularly to the process direction. Each workpiece was again cut in two halves. One part was used for metallographic examination and the remaining half was examined after being subjected to

heat treatment. This way the peening conditions were exactly the same for the as deposited and heat treated samples. To prepare macrographs, the specimens were cold mounted in 40mm cylinder moulds, grounded, polished and etched with Keller's solution. Then the microstructure was investigated under an optical microscope.

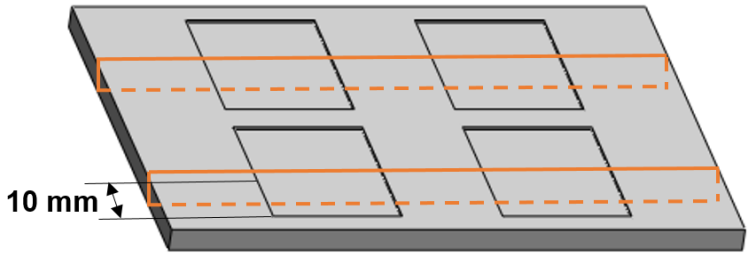

Figure 46 – Representation of the orientation of test specimens in cold worked walls

3.5.2. Porosity free zone and deformation

To evaluate the effect of MHP on the porosity, each set of parameters was analysed by metallographic examination of cross sections, as presented in Figure 47. The deformation was measured by the height difference between the non-cold worked and the MHP surfaces (Y1). The depth of porosity free zone was determined by taking 15 measurements along the band near the MHP surface, until encountered a gas pore with a diameter higher than 20 µm. From these values an average was calculated, which is represented by Y2. The standard deviation was approximately 25% for each cross section.

For side rolling, the deformation values were measured in the same way as the MHP samples. However, the depth of porosity free zone was determined by taking 5 measurements of the distance between the rolled surface and a point at which a gas pore with a diameter higher than 20 µm was encountered. From these values, an average was also calculated.

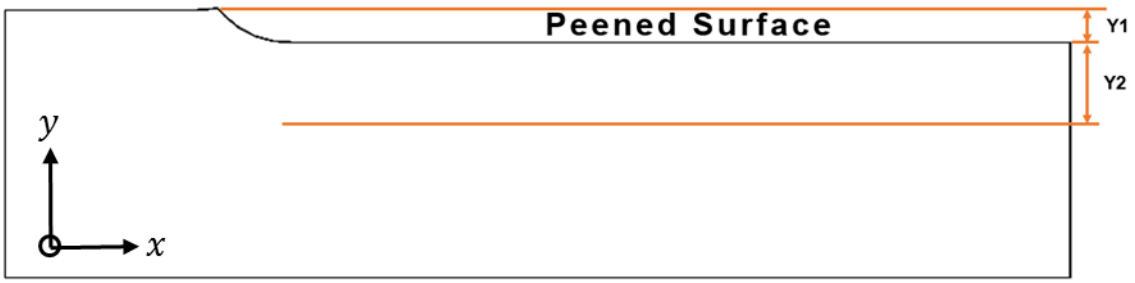

Figure 47 – Representation of measuring procedure for deformation (Y1) and depth of free porosity zone (Y2)

3.5.3. Hardness Test

To assess the effect of rolling and peening, micro hardness was carried out. A Zwick/Roell ZHV hardness machine with a load of 100g and a dwell time of 15 seconds was used. The hardness was measured across the thickness in the transverse direction to the peening direction at different positions

from the edge of the processed zone, as presented in Figure 48 and Figure 49. For rolled samples, an equivalent procedure was followed to the one shown in Figure 49.

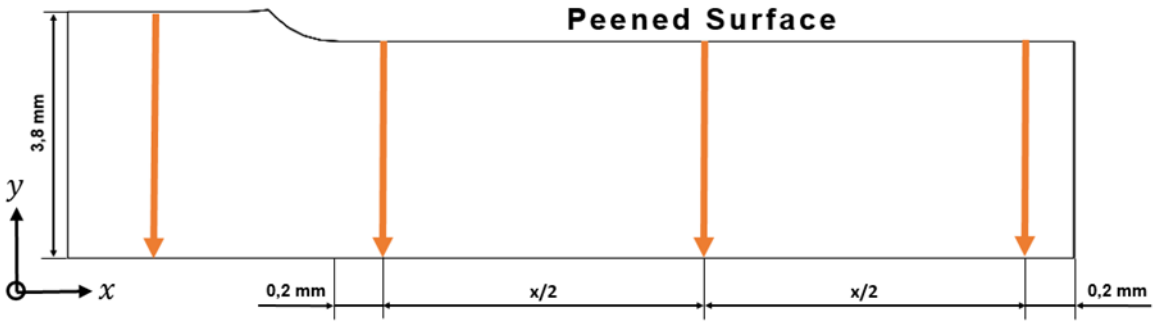

Figure 48 – Representation of direction and location of hardness tests for AA2319

For AA2319 samples, the first indentation was placed 0.05mm from the surface and then a spacing of 0.12 mm between subsequent indentations was used.

Because the samples of AA4043 had a much higher thickness (24 mm), the hardness was measured from the surface to a depth of 6 mm for both the peened and non-peened region. This depth was sufficient to get beyond the peening affected zone into the unaffected material. The starting point for the measurements was 0.05mm from the top surface, and the spacing between subsequent indentations was 0.13mm with a dwell time of 15 seconds. With this spacing, 50 measurements were performed in each line, as shown in Figure 49.

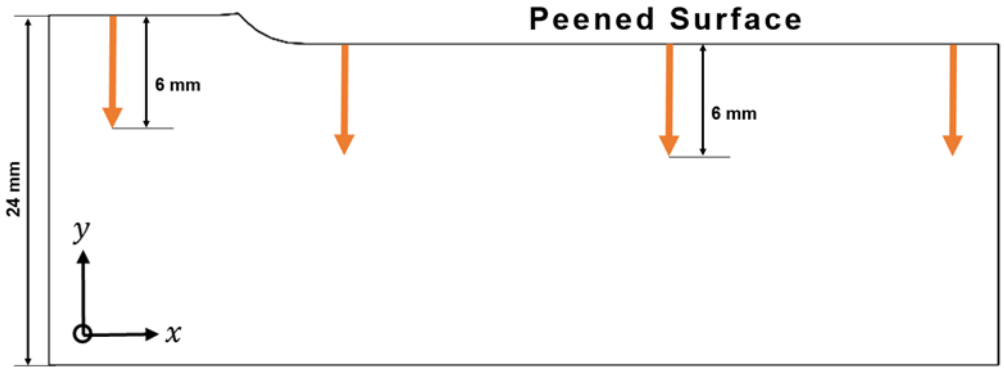

Figure 49 – Representation of direction and location of hardness tests for AA4043

3.5.4. Tensile Test

Tensile testing was performed for only one peening density, which was a representative case of all peened samples. As deposited, as deposited and heat treated, peened, peened and heat treated conditions were tested. The orientation of test specimens in a wall is presented in Figure 50 (a). Three vertical and horizontal tensile test samples were extracted. Each wall was machined to a desired thickness of 2.5mm, as presented in Figure 50 (b). However, for each condition a different procedure was followed.

For the as deposited samples, the wall was immediately machined to the dimensions shown in Figure 50 (b). For as deposited heat treated samples, first the wall was machined to the desired thickness, then heat treatment was applied and only after the shape of the tensile specimens was machined.

For the peened samples, the wall was first machined to 2.5 mm thickness and then the peening was performed on both sides of the wall. The peened and heat treated samples had a similar procedure but after the peening they were subject to the heat treatment.

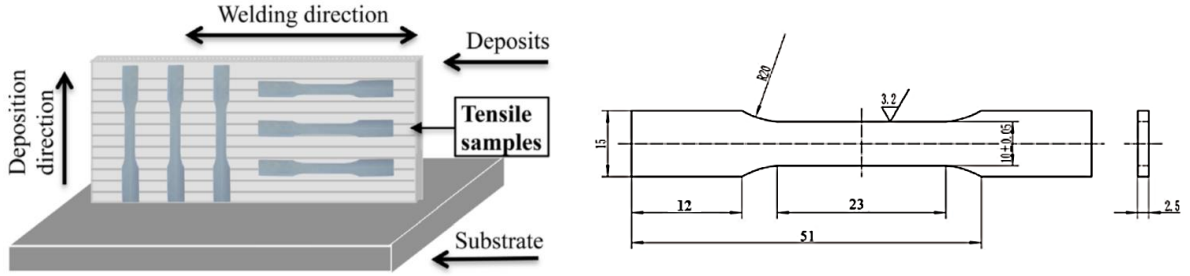

(a) Positions of test specimens in built wall (b) Dimensions of tensile samples

Figure 50 – Orientation of tensile specimens in a wall [67]

4. Results Presentation and Discussion

4.1. Crossing Optimization

The main goal of this project was to manufacture an eight metres long straight wall, and to achieve so various strategies of robot and substrate movement were investigated. This was necessary in order to extend the working envelope of the robots to build this long part. Note that maximum reach of each robot was only 2.5 metres. Three different options of tool path strategy were considered:

- Linear movement of robotic arms and bases
- Linear movement of substrate with stationary robotic arms
- Simultaneous movement of the robotic arms of the two robots

The first method focussed on the tool path control by the movement of robotic arms, i.e., the substrate was in a fixed position in which deposition would be carried out by the robot, which moves with its base on 10 metres tracks along the workpiece. In this case, the robotic arm would follow a straight-line tool path. The main challenge anticipated in this approach would be simultaneous control of the velocity of the base movement and the arm movement. The non-constant speed and other deviations to the linear movement of the robots also have to be considered. Any discontinuity during movement over such a long distance will influence the quality of deposited beads. Although these could be predicted and considered in the programming stage, it would take a considerable amount of time and development, which would increase the cost significantly. Without such a control in place the likelihood of irregular beads and unpredictable deviations from the programmed straight wall is high. For these reasons, this approach was considered unsuitable.

The second method used the same principle, as the previous one, but in this case the workpiece moves and the robotic arms are depositing in a fixed position. The main challenge of this approach would be deviations from the linear movement and various instabilities, such as lumps and humps associated with movement of big size parts. Also, this approach would require twice as long tracks. This approach would be more suitable with processes in which the control of the position of the torch and maintaining of the stick-out distance is critical, such as in plasma or TIG welding. With CMT there is no major advantage and thus this approach is unfeasible.

The third method considered using two robots simultaneously for the deposition, with two different variants of operation. The first option involves the first method (linear movement of robotic arms and basses) but with one robot starting the deposition before the other with a time gap to be studied and optimized. By the conclusions presented formerly, related to deviations from linear movement over this long distance, this method of parallel deposition was excluded. The second option involved movement of the robotic arms with the bases in a fixed position to deposit a particular length at a time. Its main challenge is the limited workspace of each KUKA robot of 2.5 metres, which requires stitching many sections together. Using this strategy to build the final part, it was necessary to understand how a

continuous straight bead can be created. The results and experience of previous work on development of overcrossings in steel WAAM parts was used as the starting point in the current project.

As described in Section 2.2.1, Mehnen et al. [33] studied several strategies of crossing deposition in mild steel. According to the authors, the most adequate option for deposition was the opposite angles 2, presented in Figure 51 (a). In this strategy, the robot path for one bead is given by two angled lines. In this 90º angle the interpolation robotic movement is not considered, i.e., the robot deviates from perfect corner deposit to shorten the path between the two straight lines, which becomes a curved link, as shown in Figure 51 (b) by the red line. Considering this unpredictable deviation and the goal of producing the wall with the least material wastage, a new approach was taken, which included development of a single curve crossings, as shown in Figure 51 (c).

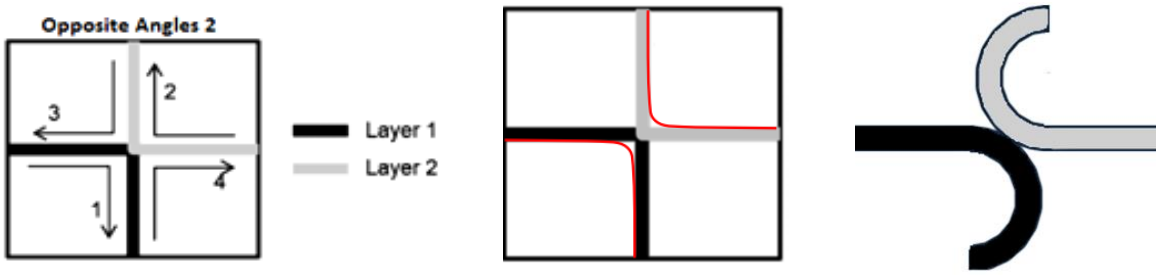

(a) Opposite Angles 2 strategy [adapted from 33]

(b) Robot interpolation for 90º angles

(c) Curved intersection link

Figure 51 – Layer deposition strategies for crossings

For this new crossing strategy new parameters had to be evaluated, according to Figure 31:

- End length: The ends of the weld beads, where the multiple initiation and termination of the process takes place, have high likelihood of porosity in case of aluminium [7,10,30]. Thus, a minimum length was considered to be 30mm.
- Angle: Angle of the curve was optimised to ensure sufficient end length, but to avoid unnecessary material wastage and collisions. The maximum angle of the curve to avoid collision of the torch with already deposited material was assumed to be 180º.
- Radius: Combines both the angle and end length. Considering the angle chosen, the radius would vary in order to achieve the 30mm end length.
- Overlap: To control the overlap, the bead width and the centre distance would be changed.

An optimization model was developed in MATLAB taking in consideration geometrical variables of bead, as presented in Figure 52.

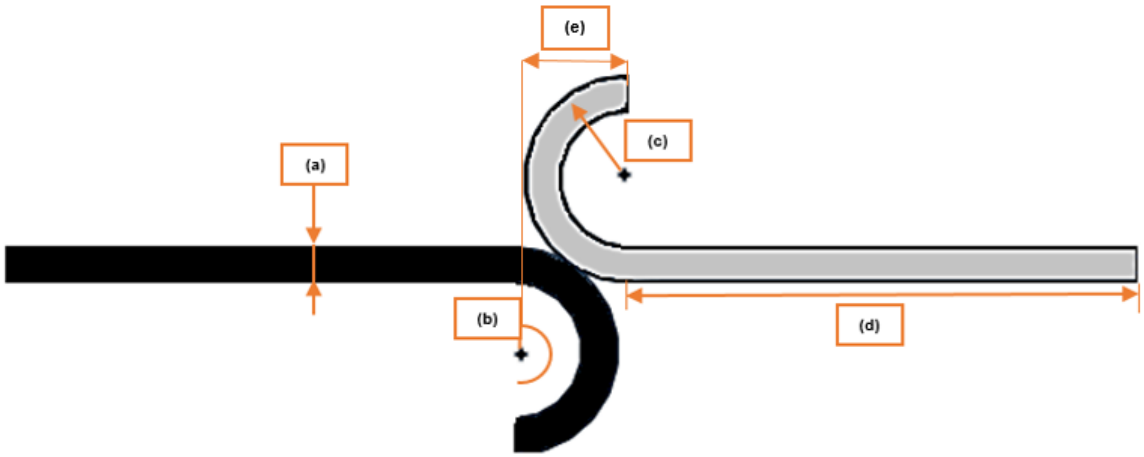

(a) – Total bead width
(b) – Arc angle
(c) – Arc radius
(d) – Straight bead length
(e) – Centre distance

Figure 52 – Crossing model optimization variables (top view)

The output of the program was the remaining area in the crossing zone, i.e. considering a straight bead after machining, the area between two intersecting arcs, as represented by the red region in Figure 53.

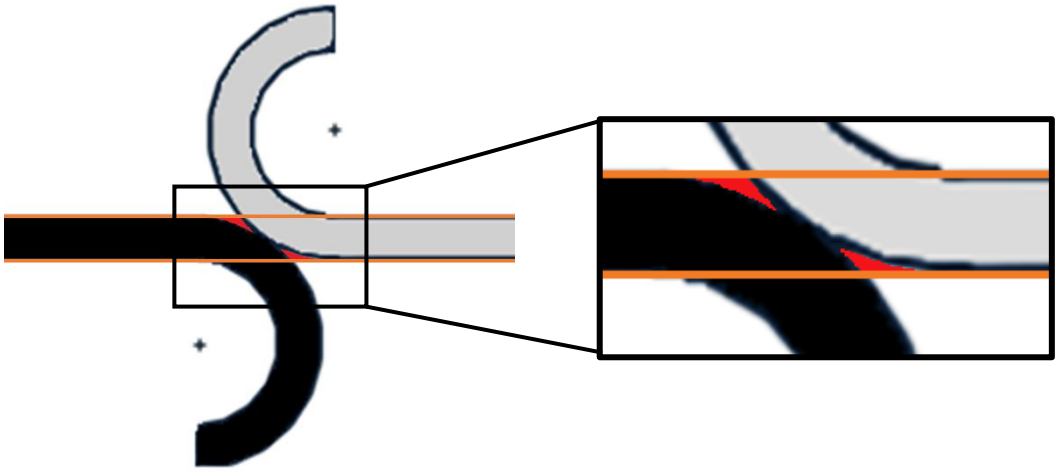

Figure 53 – Representation of the remaining area in the crossing zone

For a certain set of deposition parameters, the bead width is constant. Thus, the only variables in the model will be the arc angle, radius and the distance between arc centrelines (overlap).

Taking into consideration the maximum angle considered (180º), for an end length of 30mm, the minimum radius value is approximately 9.6 mm. These values where the starting conditions in the model and, in the subsequent iterations, the angle was decreased while the radius and consequently overlap were increased. In Figure 54, the outputs of the program are presented. It can be seen, that the empty area increases with increasing the arc radius. Different combinations were investigated theoretically.

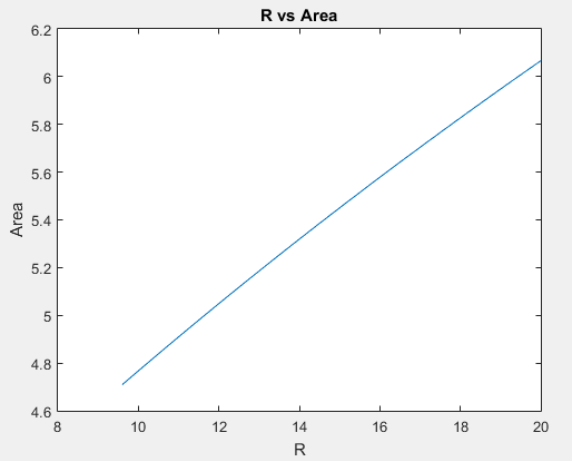

R	Area	Angle	xposition
9.6000	4.7095	179.0493	14.4000
9.7000	4.7240	177.2034	14.4665
9.8000	4.7384	175.3952	14.5327
9.9000	4.7528	173.6236	14.5986
10	4.7672	171.8873	14.6642
10.1000	4.7816	170.1855	14.7296
10.2000	4.7959	168.5170	14.7946
10.3000	4.8102	166.8809	14.8593
10.4000	4.8245	165.2763	14.9238
10.5000	4.8388	163.7022	14.9880
10.6000	4.8530	162.1579	15.0519
10.7000	4.8672	160.6424	15.1156
10.8000	4.8814	159.1549	15.1789
10.9000	4.8955	157.6948	15.2420

Figure 54 – Variation of the area and radius with constant width

Then the model was validated by doing experimental trials. Since only the geometrical aspects of the crossing were considered in the model without physics of melting and solidification, after the first trial, there was no contact between both beads. This was attributed to poor wetting and the lack of contact between the overlapping beads for zero overlap in experimental trials. Therefore, the overlap was increased to 33% for the next trials. The parameters were varied throughout the experiments, but always considering the outcome of the previous trial, as shown in Table 8.

Once the curved crossing was successful, the opposite angles 2 strategy was tested also for different parameters. The results, however, were never satisfactory using CMT-PADV due to too low heat input of the process and poor wetting between the beads. Thus, to guarantee that this strategy could be applied to aluminium, the process was changed to CMT-P. The higher heat input resulted in good bead.

Trials 1, 2, 3, 6, 7 and 8 had lack of fusion defects due to the insufficient overlap and small radius of the curves. Although the low heat input of the CMT-PADV is another factor contribution to this type of defects [32], the viability of the crossing with CMT-PADV was crucial to obtain the best quality deposition for aluminium in terms of low porosity, as discussed in Section 2.2.2. In contrast to the values of the Matlab programme, which did not take in consideration the arc physics and the temperature dependent melt behaviour the increase in radius will increase the contact area between the beads and increases the likelihood of merging them together. On the other hand, if the radius was low or the temperature insufficient poor wetting resulted in a gap between the beads, even if the overlap was positive. For this reason, the programme was proven to consider insufficient data to provide an accurate strategy for the crossings.

In trial 10, the overlap was excessive and crossing of both beads had an unnecessary amount of material. This resulted in a peak at the crossing connection, which promoted an unstable arc in this region. In trial 11, the use of the opposite angles 2 strategy with CMT-PADV resulted in the same problem, as in trial 10. The low heat input of the process could not remelt the metal and flatten the bead and after the deposition of the second layer, a peak of excessive material was created and instability of

the arc occurred. In this situation, the beads overlap could not be changed without compromising the effective width at the end of the deposition. To develop the required straight wall, both beads had to be deposited in a straight-line strategy. However, to achieve sufficient contact required to merge the beads, the tool paths had to off-set slightly. As for CMT-PADV the deposited beads are very narrow (Section 2.2.3.), even a small off-set would cause a considerable reduction in the wall width, therefore it is hard to find correct ratio between the overlap and welding conditions for this process to achieve the required wall width without defects. For this reason, no further studies were carried out using this approach.

This unbalance in the depositions, either by lack of fusion or excessive material, made these parameters unsuitable for single bead crossings.

Table 8 – Crossing experimental parameters and correspondent outcome

	Process	Radius [mm]	Overlap [%]	Outcome
1	CMT-PADV	9.6	33	X
2	CMT-PADV	9.6	50	X
3	CMT-PADV	9.6	60	X
4	CMT-PADV	9.6	66	✓
5	CMT-PADV	9.6	80	✓
6	CMT-PADV	20	33	X
7	CMT-PADV	20	50	X
8	CMT-PADV	20	60	X
9	CMT-PADV	20	66	✓
10	CMT-PADV	20	80	X
11	CMT-PADV	Strategy Opposite Angles 2		X
12	CMT-P	Strategy Opposite Angles 2		✓

In trial 4, 5, 9 and 12, successful crossings were manufactured with both CMT-PADV and CMT-P. Table 9 shows longitudinal and transverse cross sections from which values of effective wall width (EWW) and total wall width (TWW) were obtained and are summarized in Table 10. The variable A was added to describe the effective wall width of the crossings.

Ayarkwa et al [30] performed an evaluation of these variables for different WFS and TS ratios in deposition of single wall in AA2319, using 1.2mm diameter wire and CMT-PADV process. In his study, the EWW varied from 4.9 to 8.0 mm and the TWW from 5.3 to 9.8mm for all the experiments. Specifically for the same range of experimental parameters as the ones used in this thesis (WFS/TS=10), EWW ranged from approximately 5 to 6 mm and TWW from 6 to 7mm [30]. Although the materials were very similar these values were much higher than the ones obtained in this work. The difference can be associated to the difference between crossing and single walls. In single wall deposition, the dimensions of a wall are purely dependent of the volume of deposited metal and the surface tension-thermal balance. In the crossing where two walls merge together, additional effects related to the contact between the walls, wetting, surface tension and cooling effect of the previously deposited wall influence

the wall height and width. Once the walls merge together, rapid cooling increases surface tension force and the resulting lateral depression of the beads can consequently narrow the crossing deposition. Since CMT-PADV has a narrow shape and a high bead height, its surface tension is higher than in the other processes. This effect of surface tension highly influences the connection between both beads. Similar findings were found in the literature [68].

Table 9 – Successful trials of one bead crossing depositions

CMT-PADV	**R=** 9.6 mm	**Ov.=** 66%	**CMT-PADV**	**R=** 9.6 mm	**Ov.=** 80%
					
CMT-PADV	**R=** 20 mm	**Ov**.= 66%	**CMT-P**	Strategy Opposite Angles 2	
			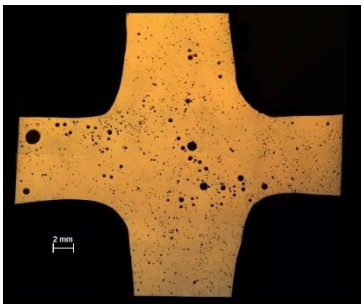		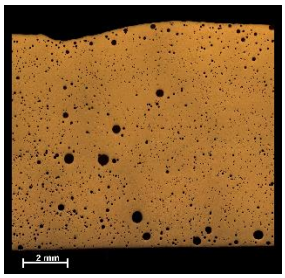

Table 10 – Effective wall width expected after machining

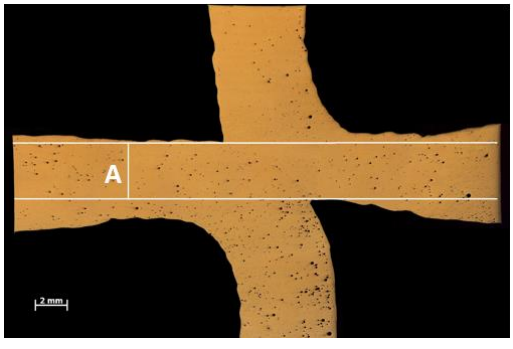

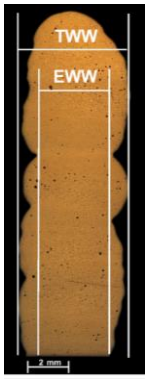

Cross. Nº	A [mm]	EWW [mm]	TWW [mm]
4	3.7	3.1	5.5
5	4.5	3.6	5.2
9	2.9	2.7	4.2
12	6.9	6.4	7.3

Pickin et al [52,53] investigated single bead deposition for AA4043 using CMT and CMT-P and their width ranged from 5.5 and 6.2 mm which are similar the values obtained in 12 trial with CMT-P (Table 10). As this process has a higher heat input the wetting between the beads is smoother and in this way the effective wall width is similar to the values for singles beads. The narrowing due to surface tension is less significant in hotter processes.

The experimental data (Table 9 and Table 10) shows the importance of temperature (heat input), material type and deposition strategy on the dimensions and defects level of the crossings. The possibility of achieving acceptable crossings in aluminium with CMT-PADV and CMT-P has been demonstrated. Different strategies of controlling the dimensions of deposited walls have been presented. These findings were used to develop strategy for building the final part, with much thicker walls than those studied in this section.

4.2. 6-metre Long Preliminary Part

To manufacture the 6-metre long preliminary part, two approaches were studied but only one could be applied to develop crossings with much bigger wall width as compared to the previous experiments. To validate which option would be more suitable, several experiments were carried out on a smaller scale to implement it later in the final part.

4.2.1. Crossing Parallel Wall Optimisation

The first approach used the knowledge already acquired regarding one bead crossing and couples it with the parallel wall deposition strategy. As parallel wall deposition relies on deposition of multiple walls adjacent to one another with a defined overlap, this technique should be easy to apply to the single wall crossings. To obtain a desired overall thickness of 20 mm, the combination of crossing and parallel walls was studied.

Firstly, the path strategy for the deposition had to be determined. This approach was based on the results in Section 4.1 and adapted for the integration of parallel walls. Considering the sensitivity to lack of fusion defects, the higher heat input CMT-P process was used. The path direction of the opposite angles 2 strategy, but with added beads next to the centre line (red lines), was implemented, as represented in Figure 55. The direction of deposition was changed between the layers as indicated by the arrows.

As previously stated, the 90º corner interpolation of robot movement is one of the challenges to consider when programming the deposition path. To guarantee the process repeatability in the corners this feature was replaced by a curve with a defined radius. This radius was one of the variables studied in the experiments. The values of the radius were initially constant for all beads but from the initial results an increase of radius from the inner wall to the outer wall was necessary, represented in Figure 56 (c). The wire feed speed (WFS) and the bead distance (overlap) were also variables in the experiments.

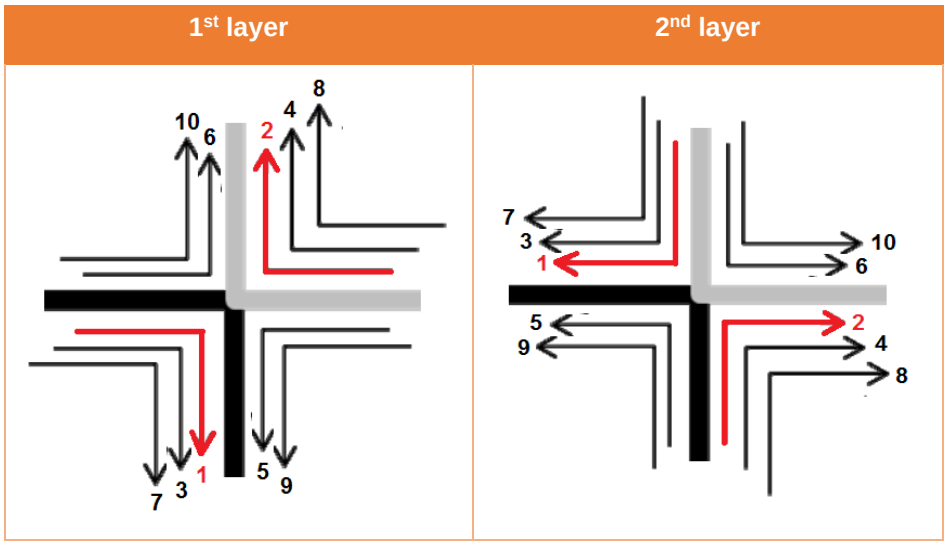

Figure 55 – Crossing Parallel path strategy based in [33]

Table 11 summarizes the experimental parameters used. To manage the heat sink effect and control dimensions of the beads, the wire feed speed was changed between the layers until steady-state conditions, as explained in chapter 4.1. In the first trial, the difference between the exterior beads and the centre of each layer was very significant, as indicated as height difference in Table 11. The best results in terms of smallest difference in height between different beads in each layer was achieved in trial 4, where radius and wire feed speed were varied between interior and exterior beads of each layer and a greater bead distance was used. An average layer height of 2.0mm was obtained for this trial.

Table 11 – Experimental parameters for crossing parallel walls and height difference out come

	Radius [mm]			WFS [m/min]						Bead distance [mm]	Height difference [mm]
	R_1	R_2	R_3	1st Layer		2nd Layer		3rd Layer			
				Centre	Ext.	Centre	Ext.	Centre	Ext.		
1	2.5	2.5	2.5	9	9	7	7	6	6	5	2.1
2	2	2	2	9	8	8	7	8	6	6	1.6
3	2	3	4	9	8	8	7	8	6	6	0.9
4	2	3	4	9	8	8	7	8	6	7	0.7

The variation of radius and WFS in each layer has proven to be effective way of managing the heat and layer dimensions, hence reducing the height difference and producing more even depositions. Still, in the more exterior beads, there is a reduction of layer height, shown in Figure 56 (a) and (b). This is mainly caused by the lack of cooling time between depositions of the same layer to control the interpass temperature. This height decrease was minimised by increasing of bead distance (decreasing overlap). Considering the height difference presented in Table 11, EWW and TWW values ranged from 21 to 22 mm and 31 and 32 mm respectively. These 10mm difference between the EWW and TWW, would cause a considerable material wastage for the large part. For this reason, a compromise between the height

and width to be machined has to be accessed in order to optimize material wastage. Nevertheless, a sound structure was produced and the capability of this strategy was proved.

(a) Top view of 4th trial deposition

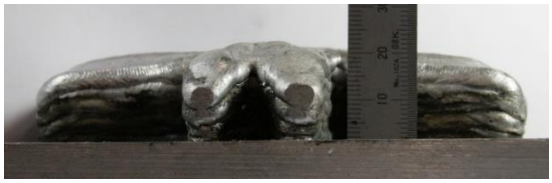

(b) Front view of 4th trial deposition

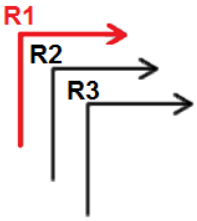

(c) Representation of the 3 radius variation

Figure 56 – Image of parallel Wall crossing and representation of radius variation between inner and outer beads

4.2.2. Parallel Oscillated Wall Optimisation

The second approach combined parallel and oscillated walls, as shown in Figure 57. The parameters used for this strategy were developed in another project carried out at Cranfield University [69].

As this method included deposition of parallel walls with a 6-metre length, the process had to be tested and validated to ensure constant dimensions of each bead. Note that for single bead depositions option, over such as a great length, was excluded in the previous section due the high risk of deviation from the nominal layer height and width caused by inaccuracy of robot movement and other instabilities. Therefore, the option of stitching short sections of walls at crossings was developed. However, during development of intermediate walls with 3 m length, it was proven that no such deviation occurs. No noticeable deviation in the deposited 3-metre long beads was measured. This can be explained by the self-adjusting CTWD of the CMT processes, which was explained in Section 2.2.3, and relatively fast solidification of aluminium. Also, the accuracy of the robot movement was found to be quite high. Thus, the parallel oscillated wall approach was further tested.

Both parallel and oscillated walls used CMT-P process. For the final part, the WFS was 6.2 m/min and the TS was 10mm/s which resulted in an average layer height of 2.2 mm. First, the parallel wall was deposited and after the oscillated walls are added perpendicularly. As presented in Figure 57 (b), for the oscillated wall, the TS increases from 90 to 100% of the set value as it approaches the parallel wall. This variation was defined to prevent the drop of height for different parts of the deposition, as shown in Figure 57 (a) front view. Also, the oscillated wall was defined to build a desired width of 20 mm and the chosen distance between bead centres was 4 mm, giving an overlap of 66%. For the connection area between the parallel and oscillated wall, there is an increase of the contact length to provide a smoother

transition and minimise the heat sink effect. Furthermore, the end point of each bead is outstanding beyond the desired width of each oscillated wall for the final part and will be machined off, hence the likelihood of defects should be minimised. Note that there is a slight depression in the connection of both walls. This could be further optimised by controlling the shape of the final bead in the intersection. This factor could be also compensated at the design stage by careful design of the width of the parallel wall. The results show that this approach can also be considered as a good option for deposition of the large aerospace spar.

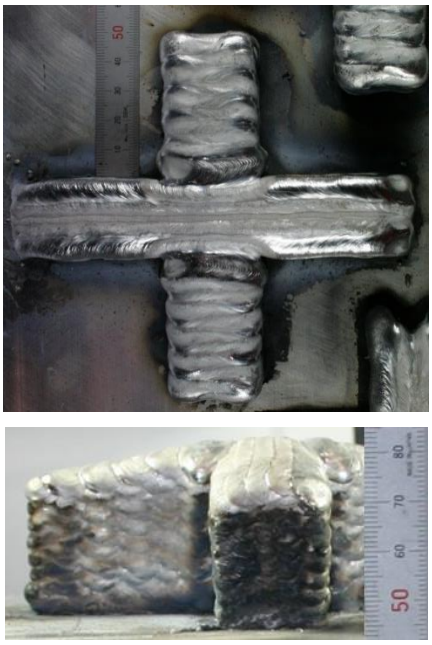

(a) Preliminary trial deposition top and front view

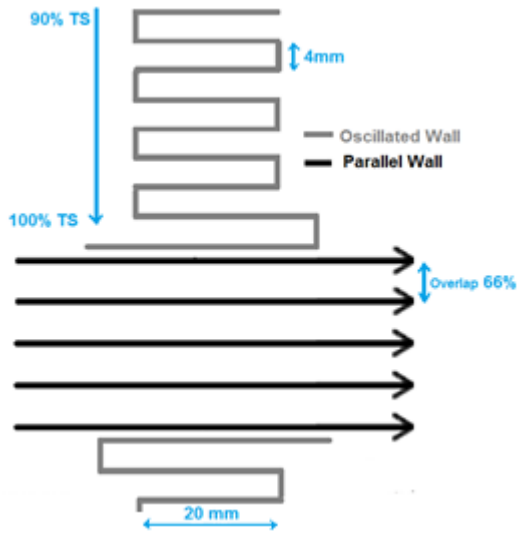

(b) Final deposition parameters

Figure 57 – Parallel and oscillated wall photo and schematics of final deposition parameters

4.2.3. Comparison between Hybrid Deposition Strategies

As both approaches were successfully used to manufacture large parts, to choose the most appropriate option, only theoretical considerations were deliberated.

The main advantage of the crossing parallel wall is the uniform heat sink at the connection. In this way, the necking defects can be eliminated and a good integrity of the part is ensured. However, this approach is more complex at programming stage, since there are many start and stop points required to complete the part. The starts and stops are also problematic for welding process. Normally, in those points, collapse or raise of bead height occur due to unbalance ration of WFS, welding speed and thermal balance. Even with the inversion of welding direction to balance this factor, these points are associated with higher porosity in case of aluminium alloys. For the deposition of the 6-metre part, 120 start and end points per layer are necessary to implement this strategy. For this reason, the end lengths of all those points would have to be removed resulting in big wastage of the material. Both complexity and

start/end points are presented in Figure 58, where the beginning of each line represents a start point and the arrow represents an end point.

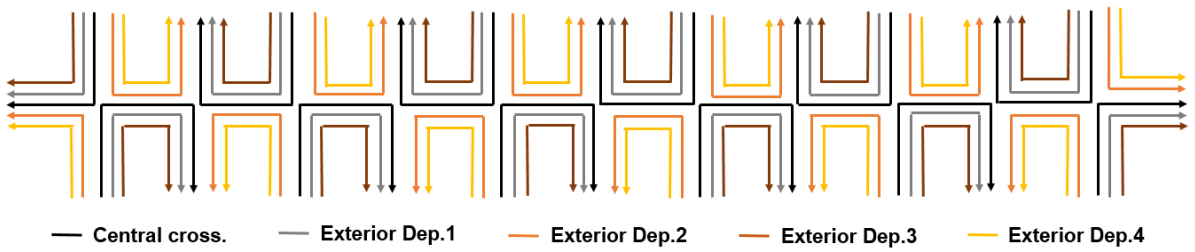

Figure 58 – Representation of the first layer deposited for the large part with crossing parallel deposition

The parallel oscillated walls combine two widely used deposition strategies for WAAM in different materials. Ding et al. [5] presents several large metallic components produced by additive manufacturing, from which a complex titanium frame structures were built with both parallel and oscillated deposition. The highest quality was achieved with a combination of both strategies in one part. Parallel walls were used for a square shaped outer feature with curved edges and the internal structure with intersections was manufactured using oscillated strategy. In this way, the capability of combining both deposition strategies was proven. However, the process used was not CMT-PADV but much hotter plasma and also titanium has different behaviour from aluminium. The biggest concern in strategy is the necking effect in the intersection between parallel and oscillated sections due to greater heat sinking from the parallel wall, which can be hard to control with synergic CMT process. This is undesirable as it can act as stress raisers and can cause crack initiation.

Another crucial aspect to take into consideration is the wall width. In crossing parallel deposition, width in both directions of the crossing is constant. In parallel oscillated wall, each wall can have distinct widths. Also, oscillated walls have the capability to vary their width continuously by varying the oscillation width [5]. Considering that the studied deposition is only for the preliminary part, the combined parallel and oscillated seems to be easier to control and program and therefore should be more adequate option for building the final part. However, to make the final decision, the defects also have to be considered. In the crossing parallel option, more porosity and inconsistency in layer height is expected due to many start and stop points, whereas the parallel and oscillated wall may suffer from lack of fusion defects in the interface if the process is too cold. To make the final decision, cross sections were analysed.

Both strategies are compared in Figure 59 and the cross sections are shown in Figure 60. Section A-A and Section B-B correspond to the parallel oscillated deposition. Section A-A presents only the parallel wall deposition and possibly shows lack of fusion defects, besides the porosity, which is typical for aluminium alloys. Section B-B presents the connection between both walls and lack of fusion defects are also shown. Note that the oscillated wall does not present this defect. Lack of fusion defects are associated with low heat input and reduced overlap [32]. However, since the relatively hot CMT-P process was used, the source of the defects is probably insufficient overlap or still inadequate heat input for these thick intersections. Section C-C and D-D shows the crossing parallel deposition. Section C-C

shows a diagonal cut to access the defects in the central connection, while section D-D presents the parallel wall deposition. In both, some porosity appeared but no other visible defects were detected.

Taking into account all results, parallel oscillated wall strategy seems to be more suitable for the deposition of large parts. The lack of fusion defects in the interface between parallel and oscillated walls can be mitigated by increasing the heat input of the process and the lower number of start and stops makes the process less prone to defects. Unfortunately, due to the lack of material, further optimisation was not possible and this option was chosen to build the final part.

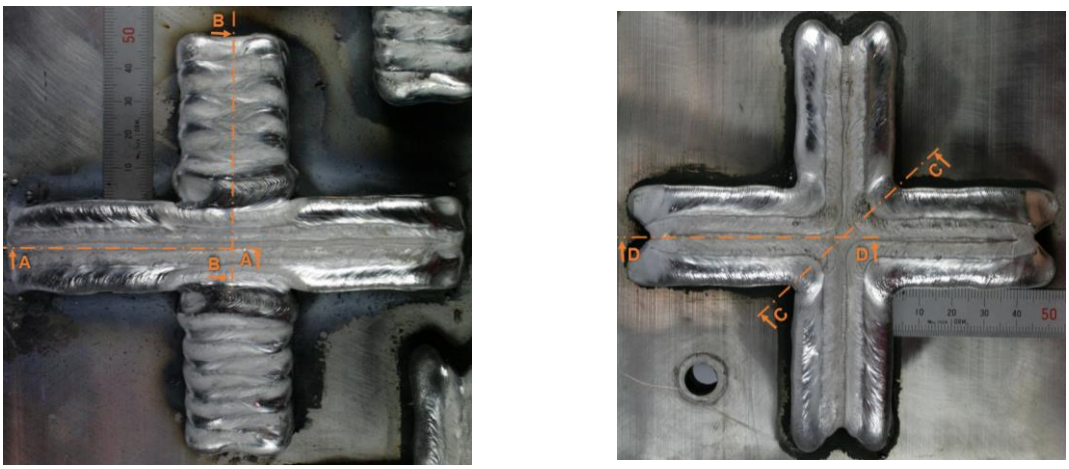

(a) Parallel oscilatted wall cross section

(b) Crossing parallel wall cross section

Figure 59 – Cut location for defect comparison of both path methods

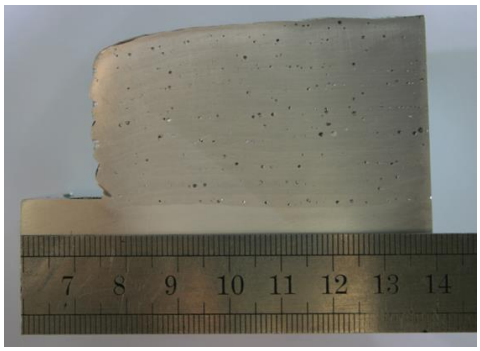

(a) Section A-A

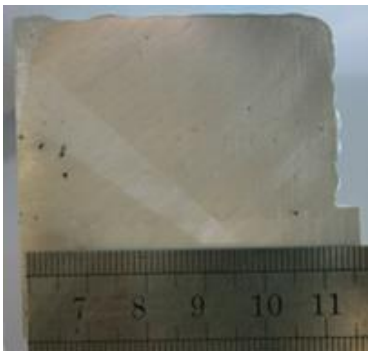

(b) Section B-B

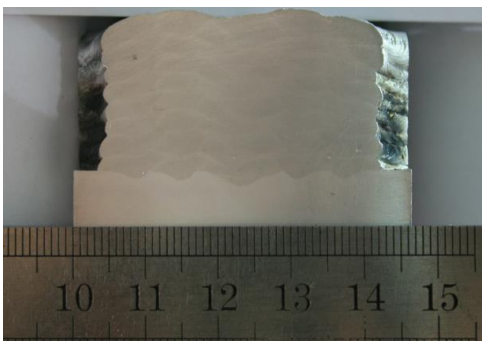

(c) Section C-C

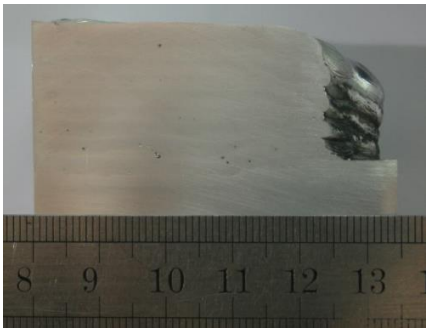

(d) Section D-D

Figure 60 – Cross sections for hybrid deposition

Figure 61 shows the final part deposited with the parallel oscillated strategy. The largest part ever deposited with WAAM was manufactured and the capability to implement this technology was once again proven. The part exhibit good quality intersections and stable wall height and width. Also, distortion of the part was very low, due to double sided deposition on the substrate, and unfortunately the final part could not be sectioned to check for defects.

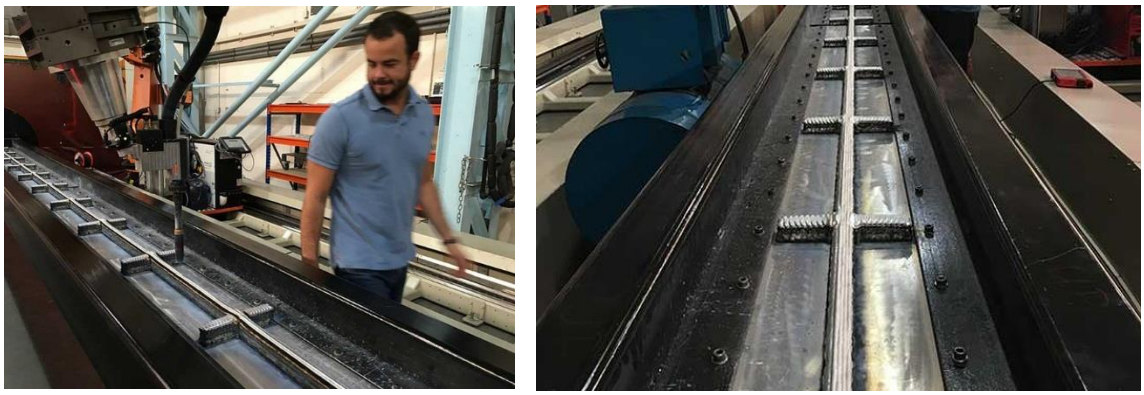

Figure 61 – 6-metre long preliminary part

4.3. Machine Hammer Peening

With the goal to improve the mechanical properties of aluminium, machine hammer peening (MPH) was applied to the sides of deposited walls of AA2319 and AA4043. After performing MHP, the cross sections were examined and porosity and microstructure were analysed as well as hardness measurements. Its effectiveness on microstructure, reduction of porsity and improvement of mechanical properties after different stages of heat treatment was assessed. One representative case for AA2319 with peening density of 25 hits/mm^2 was subject to tensile testing

4.3.1. Effect on Porosity

Cross sections of the peened samples for the two different alloys are shown in Figure 62. A depression zone near the surface can be distinguished, which suggests plastic deformation and its value is approximately 0.20mm. It can be seen that there is a porosity-free region under the peened zone, which suggests that plastic deformation affects the porosity. To determine this influence each peened condition was analysed. Note that the presented samples in Figure 62 are without any heat treatment in as deposited (P) conditions. All data for this and other heat treatment conditions, such as solution treatment and natural aging (P+ST+NA) followed by artificial ageing (P+ST+NA+AA), are summarized in Table 12.

For all AA2319 samples, the deformation was almost constant having a slight increase in samples where a second and third tool pass with offset of the MHP tool was applied. This suggests that the deformation in multi-pass processing is more effective in increasing the depth of cold work in the material than the peening density in a single pass. This may be attributed to the distribution of peened spots. A constant off-set between each pass resulted in more even distribution of compressive strain than overlapping.

With displacement, the peening is not applied always in the same place and in this way the surface is more evenly flattened with an increase of deformation. Also, frequency and temperature may affect this deformation. For high frequency, the material does not have enough time to relax its elastic deformation before the following impact is applied and an increase of temperature at the surface can cause a decrease of the plastic deformation.

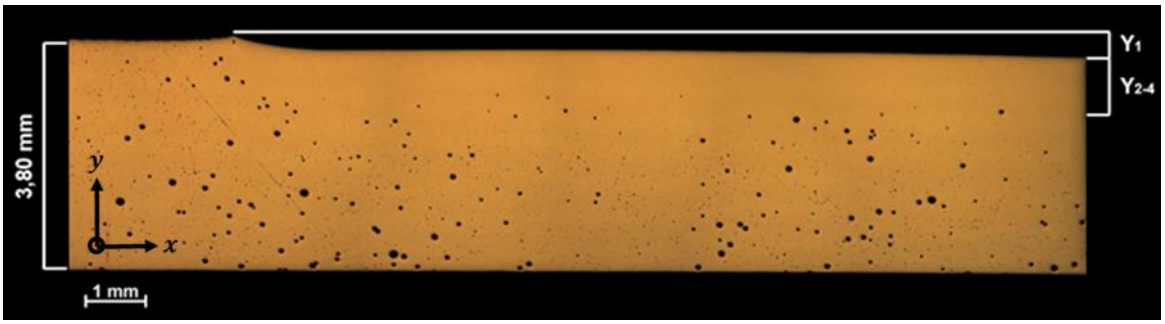

(a) Peened sample of AA 2319 single bead wall

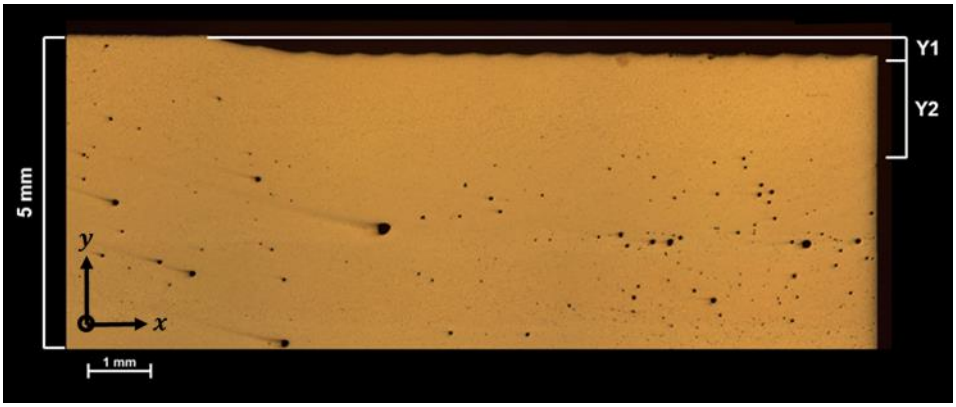

(b) Peened sample of AA 4043 parallel wall deposition

Figure 62 – Depth of porosity free zone for 22hits/mm2 peened samples of AA4043 and AA2319 (unetched)

For AA2319 P condition, the lowest depth of porosity free zone is associated with the lowest peening density. However, the values for the remaining samples are very similar to each other. This implies that after a certain number of hits the peening effect does not increase the depth of porosity free zone. This is in disagreement with Kirk [63] who showed that the layer of compressed depth increased with increasing peening intensity. Moreover, the reduction in porosity can be explained by annihilation of pores by compressive stresses and deformation. It has been shown in the literature [14] that at least 50% of local compressive strain is needed for effective annihilation of pores. This implies that the peening strategy and distribution of strain field should have an important effect on mitigation of porosity. It has also been shown [14] that in some cases the compressive stress field is not homogenous. Some regions were exposed to tension and others to a variable compressive strain. However, in the region right after the peened surface, a high percentage compressive strain seems to be evenly applied. The increase of overlap during peening increases the likelihood of more homogeneous distribution of compressive stress. Most likely the compressed surface layer increases with the increase of peening density but the response is not linear, which means that at a certain depth the strain is not uniform and

thus the annihilation of micro pores is less effective. Since only one surface for each set of parameters was analysed, therefore more definite conclusion cannot be made.

For the P+ST+NA condition, the depth of porosity-free zone increased to an average of 1.10 mm depth. This suggests that after the exposure to the ST temperature and reorganization of the grains during the NA to a steady state, the porosity reduced in the peening affected region. Toda et al. [14] reported that peening seemed to disintegrate the micro pores in even smaller sized micro pores and thus increasing the number of micro pores. These micro pores are stored mainly around dislocation, in interstitial lattices and grain boundaries [70]. In Figure 66 (a) and Figure 66 (b) and in Section 4.3.2, the microstructure for the P+ST+NA and P conditions were compared. A complete rearrangement of the grains in the case P+ST+NA occurred in the material. This change in microstructure is supposed to relocate the micro pores. There is a direct link between the microstructure and porosity. It has been shown in other work that after long exposure of an Al-5.5%Mg alloy to a homogenization temperature of 430ºC for 18 hours, porosity increased [71]. However, for a low hydrogen content alloy (argon shielded), this increase was considerably lower than for the other alloys. Although no increase in porosity for the peened samples was found, it is possible that with the relocation of micro porosity, the smaller sized pores merged together in other location, hence explaining the increase in depth of porosity free zone (Table 12 and Figure 63).

For the P+ST+NA+AA condition, the depth of porosity free zone decreased considerably, achieving lower values than for the AD condition. This suggests that further exposure to high temperature lead to the re-opening of crushed and/or annihilated pores. Toda et al. [14] presented a similar result when applying peening to an aluminium alloy and subsequently heat treating it. For non-annihilated pores the exposure to a higher temperature can cause their growth and porosity merges due to the Ostwald effect. The annihilation of pores occurs when enough compressive deformation is applied and a non-equilibrium stress state is induced. In this way, dissociation of the internal molecular hydrogen to hydrogen atoms into the aluminium alloy can occur. However, this porosity can heterogeneously nucleate in the material again and re-open the previously corrected defects. The same effect was reported for different sources of cold work [6,10,11,14,71].

The deformation for AA4043 increases with the increase in peening density in a coherent way. The AA4043 P case has an increase of depth of porosity free zone with an increase of peening density, as described by Kirk [63]. Similar to the AA2319 P condition, for the samples with multi-pass peening a higher increase in peening depth was observed. This reinforces the notion that the peening pattern highly influences the depth of porosity free zone. Also, as AA4043 is a softer material than AA2319, the microstructural resistance to cold deformation is lower and thus the impact in porosity increases.

Figure 63 shows micrographs for each condition discussed in this Chapter. Points A, B, C and D correspond to different depth levels from top to bottom of each sample. In all cases the micro-porosity disappeared near the peened surface but only for a limited depth. However, for AA4043 samples peened with 11 hits/mm^2 and 33 hits/mm^2, pores with diameters larger than 100µm are trapped near the surface,

as presented in Figure 64. This suggests that MHP is useful for eliminating micro porosity but does not supress or reduce macro porosity.

Table 12 – Deformation and depth of porosity free zone

	Density [hits/mm^2]	Deformation (Y1) [mm]	Depth of porosity free zone		
			P (Y2)	P+ST + NA (Y3)	P+ST+NA+AA (Y4)
AA 2319	11	0.21	0.60	1.09	0.61
	25	0.21	0.91	1.19	0.75
	22 (m.p.p.)*	0.25	0.92	1.15	0.71
	33 (m.p.p.)*	0.27	1.02	0.99	0.66
AA 4043	11	0.22	1.06	–	–
	25	0.32	1.29	–	–
	100	0.56	1.85	–	–
	22 (m.p.p.)*	0.32	1.64	–	–
	33 (m.p.p.)*	0.35	1.69	–	–

*multi-pass peening

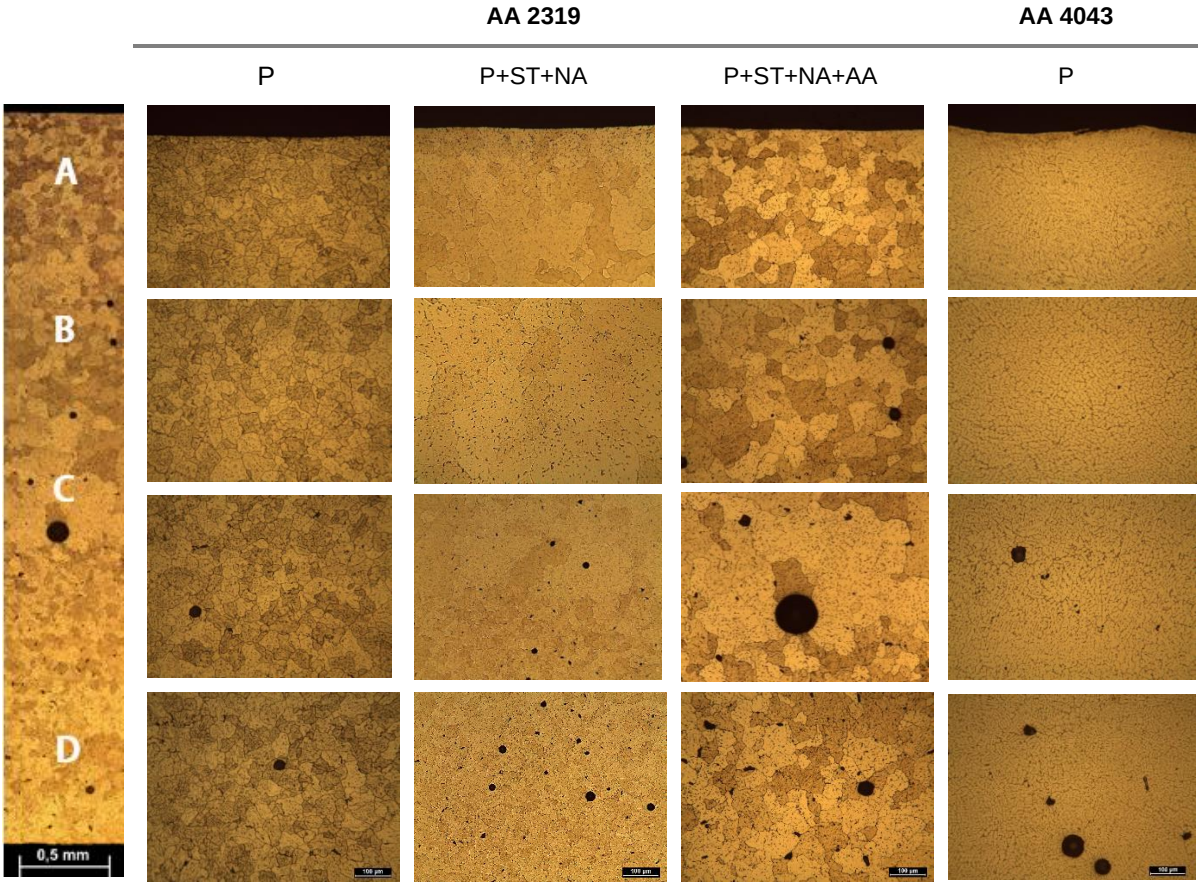

Figure 63 – Micrographs of peened AA2319 and AA4043 after different heat treatments taken from different depth levels (A, B, C and D); peening intensity 22his/mm^2

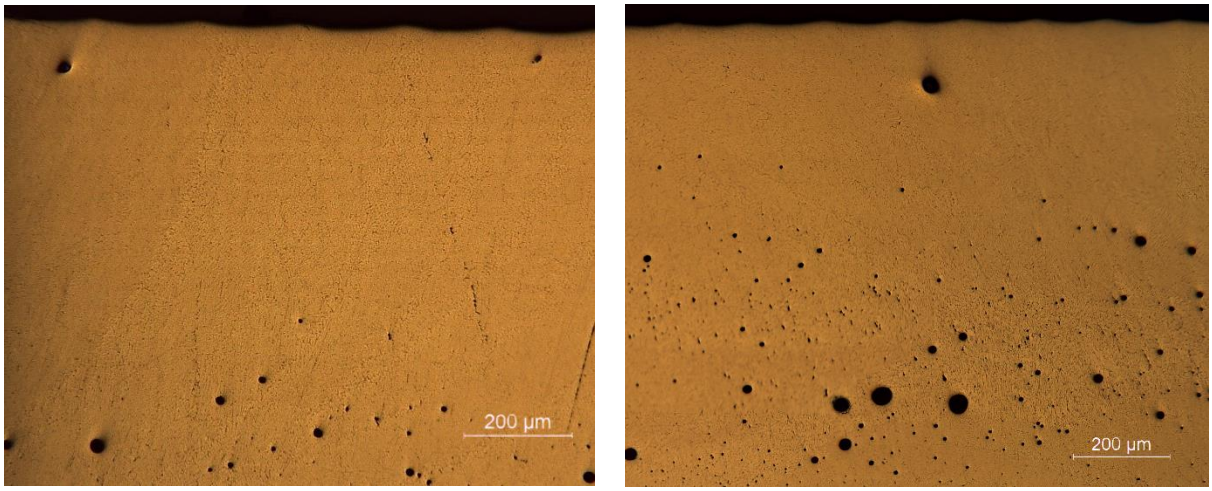

(a) Macro porosity for 11 hits/mm^2 (b) Macro porosity for 33 hits/mm^2

Figure 64 – Representation of macro porosity of peened AA4043 samples

In the next step, double side peening was investigated. These samples were used to extract tensile test specimens. In Figure 65, both P and solution treatment and artificial aging conditions (P+ST+AA) are shown. A band of porosity appears in the middle line between both peened regions for both conditions. As discussed previously, after P+ST+NA+AA the sample is subjected to the Ostwald ripening effect, which reduces the number of pores, but leads to formation of larger pores, which appears to have happened particularly in the non-peened area. In the peening affected area, porosity appears to have reduced after P+ST+NA+AA. The Ostwald effect can also justify this difference, the pores can redistribute themselves during the microstructure rearrangement and coalesce in different locations.

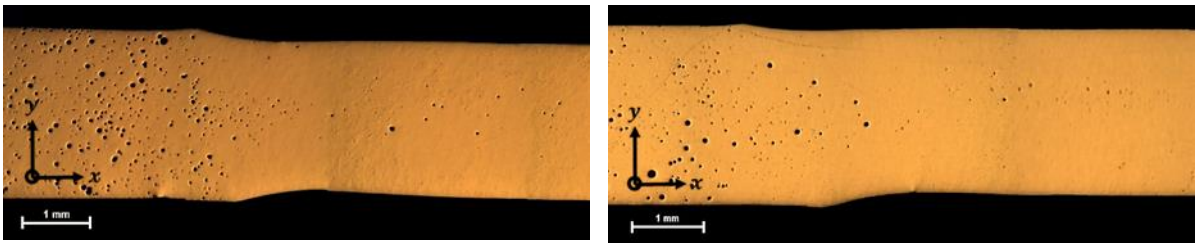

(a) P condition (b) P+ST+AA condition

Figure 65 – Porosity of samples peened with 25hits/mm^2 on both sides

4.3.2. Effect on Microstructure

To analyse the effect of MHP on microstructure etched cross sections were studied. Figure 66 shows the microstructure of the sample peened with 22 hits/mm^2 in the P, P+ST+NA and P+ST+NA+AA conditions for AA2319 deposition. The behaviour presented is constant for all the parameters of the process. Figure 66 (a), presents a fine grain structure across the sample. However, Figure 63 shows the near peened surface (point A) of the P condition with a darker region, which indicates a severely deformed surface, similar to one reported in a study carried out by Chen et al. [64,72]. Figure 66 (b) and (c) present a boundary between two different microstructures. This suggests that a boundary between the microstructure zone which was affected by the peening effect and the non-affected zone was created. The influence of the exposure of the cold worked metal to high temperature (recovery,

recrystallization and grain growth) cannot explain this effect, because the microstructure appears to follow the recrystallization and grain growth stages in the downward direction. The expected behaviour would be recrystallization or grain growth but not both simultaneously. By exposing the material to a higher temperature for an extended period of time, only the grain growth stage should appear uniformly in the peened affected zone.

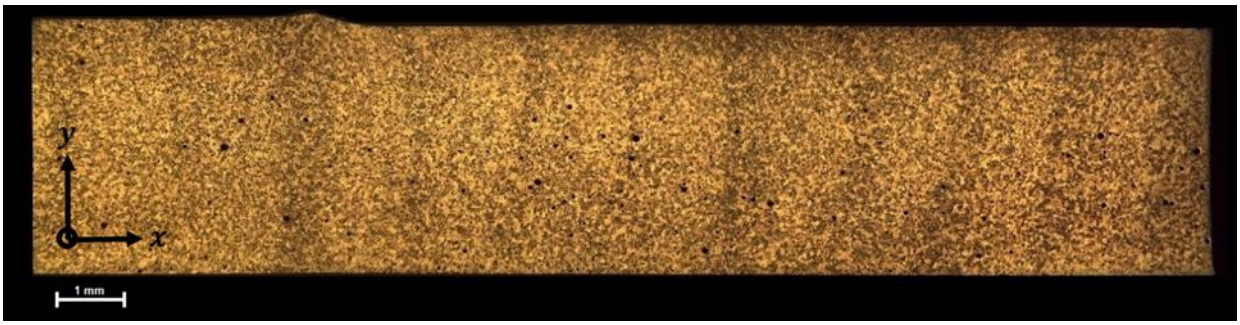

(a) Microstructure of peened sample in as deposited condition

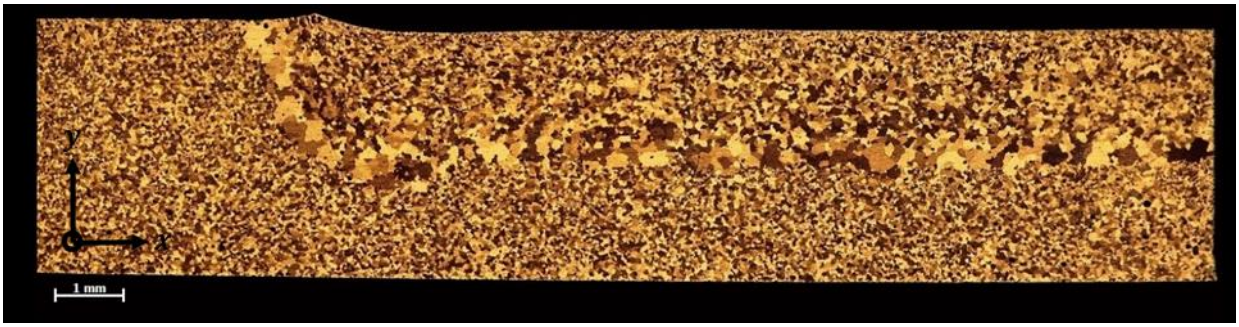

(b) Microstructure of peened sample after solution treatment and natural aging

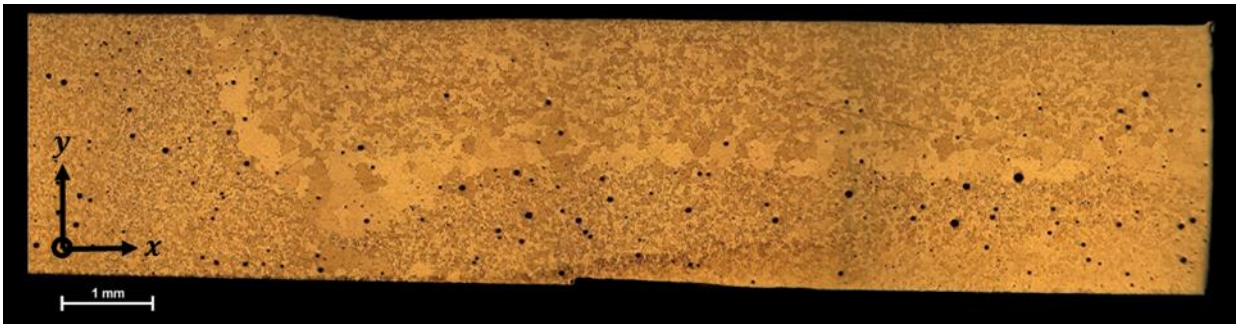

(c) Microstructure of peened samples after solution treatment, natural aging and artificial aging

Figure 66 – Microstructure of sample with 22 hits/mm^2 before and after heat treatment for AA2319

In Figure 67, the same micrographs for the sample 22hits/mm^2 P+ST+NA are shown with higher magnification. The microstructure development from finer grains to coarse grains is shown. Figure 67 (b) shows very fine grains at the peened surface when compared to Figure 67 (c) which is a non-affected zone. This behaviour is characteristic of new grains nucleation, generated to replace the deformed and distorted grains affected by MHP, which happens at the recrystallization stage. However, this behaviour is not consistent across the depth and at certain level an increase in grain size occurs and the boundary which is characteristic of the grain growth stage. The P+ST+NA and P+ST+NA+AA conditions exposed

the material to high temperature for a sufficient period of time so the material reached a steady state condition. For this reason, the microstructure distribution should be homogeneous. According to literature [72], the high deformation applied by peening should develop this distribution faster than without plastic deformation. However, the behaviour presented in Figure 66 and Figure 67 is not consistent with the expectations.

The microstructure distribution the boundary layer was studied previously [73]. The influence of the process parameters and material flow in the formation of abnormal grain growth (AGG) in friction stir processing of aluminium alloys was shown (Figure 68). AGG is a microstructure instability, which depends on two key factors: thermal input and material flow. The deformation pattern for FSP is inhomogeneous and for this reason the AGG appears in an irregular manner across the material microstructure. In contrast, deformation by MHP has a well-defined strain band, which changes accordingly with the applied peening density [63]. Thus, is expected that AGG appears in a more regular way, as occurred in Figure 66 (b) and (c) and Figure 67. In the two HT conditions, the thermal conditions in the material were changed. In the P+ST+NA condition, there is gradient of grain size, from fine grains near the surface to coarse ones in the boundary of grain growth. This implies that the AGG developed gradually until the grain redistribution in the deepest layer of material affected by peening was achieved. The significant growth in this region is then caused by the material flow, since this boundary is the limit from which the material was deformed by the compressive strain caused by MHP. In the P+ST+NA+AA condition, Figure 66 (c) shows a slight increase in the grain growth and the boundary created is then expanded. This can be explained by the further exposure to the high temperature and consequently further AGG.

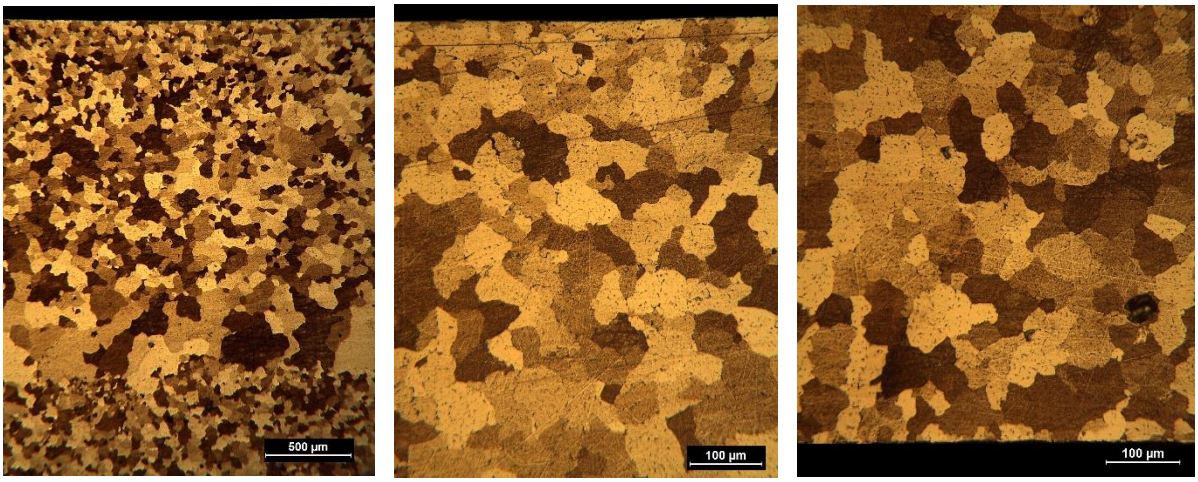

(a) Image of the peened surface with a magnification of 10

(b)Image of the peened surface with a magnification of 20

(c) Image of the bottom non-peened surface with a magnification of 20

Figure 67 – Grain growth after P+ST+NA condition of samples peened with 22hits/mm^2 for AA2319

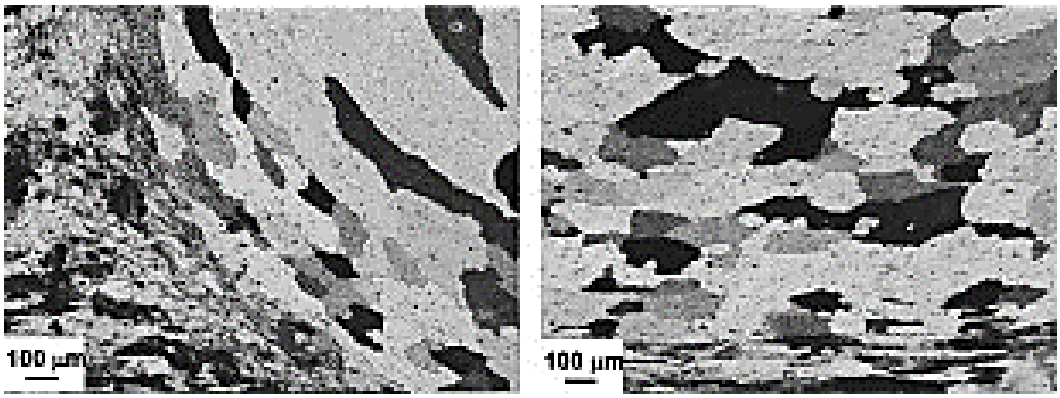

Figure 68 – Abnormal grain growth in aluminium after friction stir welding [73]

Figure 69 presents the microstructure of a sample peened in both sides with a density of 25hits/mm^2 only for ST+AA condition, since P condition showed the same results. However, the grain growth boundary does not appear in this situation. By peening both sides, all microstructure under the peened surfaces is affected by the peening effect. The darker boundary on both peened surfaces implies again that sever deformation has been applied to the material. As the sample thickness is considerably smaller, 2.5mm, there are no regions with coarse grains and the material presents a slight increase of grain size from the surfaces to the centre of the sample, but the grains are still fine and equiaxed. In this way, when the MHP is applied on both sides with enough density, a refined microstructure can be obtained.

Figure 69 – Microstructure of samples peened in both sides with 25hits/mm^2 and heat treated for AA2319

Figure 70 presents SEM images of P and P+ST+NA+AA conditions for the sample peened on both sides with 25 hits/mm^2. The white phase particles appear to be distributed along the grain boundaries and in the intra-grain regions. Although the chemical composition of the particles was not analysed here, Gu et al. [9,10] defined similar particles for WAAM deposition of AA2319 and defined them as Al-Cu eutectics (α-Al and θ phases). As in WAAM depositions, the material is exposed to multiple thermal cycle from the heat of subsequent layers, the presence of these particles in P and P+ST+NA+AA conditions is justified. The dispersion and quantity of precipitates for P+ST+NA+AA condition is higher mainly due to the further exposure to high temperature cycles, which allowed the formation of new precipitates that were still solutionized in the P condition (chapter 2.2.2). This effect was also studied by

Cao and Kou [74] who concluded that, when reaching eutectic temperature, θ phase particles formed distinct composite eutectic particles for the deposition of AA2219 with GMAW.

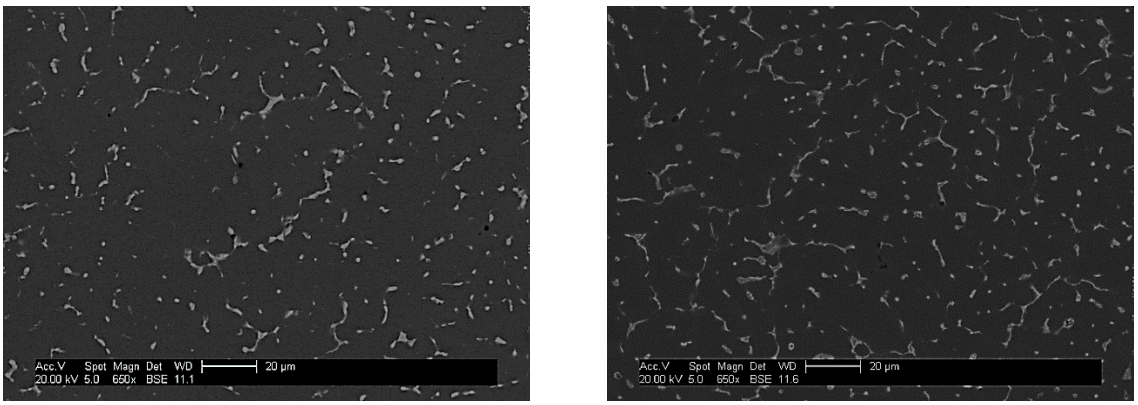

(a) P condition near peened surface

(b) P+ST+NA+AA condition near peened surface

Figure 70 – Scanning Electron microscopy image of AA2319 for P and P+ST+NA+AA conditions

For AA4043 deposition, only the P condition was studied. As shown in Figure 63 and Figure 71, the microstructure of the material changes considerably throughout the WAAM deposited material. Wang et al. [41] observed the same microstructure changes in different deposited layers due to different heating and cooling rates during the process. As the wall was deposited with parallel strategy, with overlapped multiple beads, the already deposited material is highly influenced by the multiple thermal cycles. The fine grains shown in Figure 71 (a) are due to the cold work induced by the MHP. However, in non-affected areas, such as the one presented in Figure 71 (b), the microstructure exhibits columnar slender grains with high number of pores. To eliminate these coarse grains, the cold work would have to be induced to the deeper region, but, as presented in Table 12, the MHP can affect up to 1.85 mm from the surface. In that case, double sided peening could be applied.

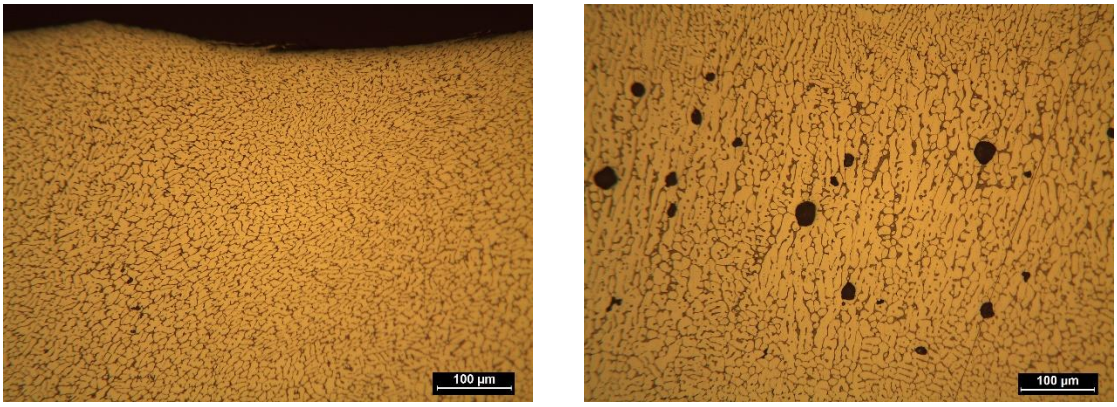

(a) Microstructure of the peened surface

(b) Microstructure at approximately 3 mm depth from peened surface

Figure 71 – Microstructure of AA 4043 in P condition

4.3.3. Effect on Micro-hardness

Micro-hardness measurements were carried out to determine the depth of cold worked zone induced by MHP. As a reference, all values were compared against the bulk average value measured in the non-affected region by peening. The micro-hardness results for AA2319 deposition for each condition are presented in Figure 72, Figure 73 and Figure 74.

Figure 72 presents the micro-hardness results for samples peened with different densities for the P condition. It is shown that there is a considerable increase in the surface micro-hardness, which drops until values near the bulk average. The surface hardness is approximately 50% higher than the bulk average. For the peening density of 33hits/mm^2, the values present an unstable variation throughout the thickness, particularly at the end. The surface hardness increase can be explained by an increase of density of dislocations, which do not allow for their further movement and the material is more resistant to deformation, as presented in section 4.3.2. Similar results were reported in the literature [72,75]. The scattered results for the samples with 33hits/mm^2 implies that the peening density was too high, which resulted in inhomogeneous compressive strain field and thus the hardness was not enhanced as for the other peening densities.

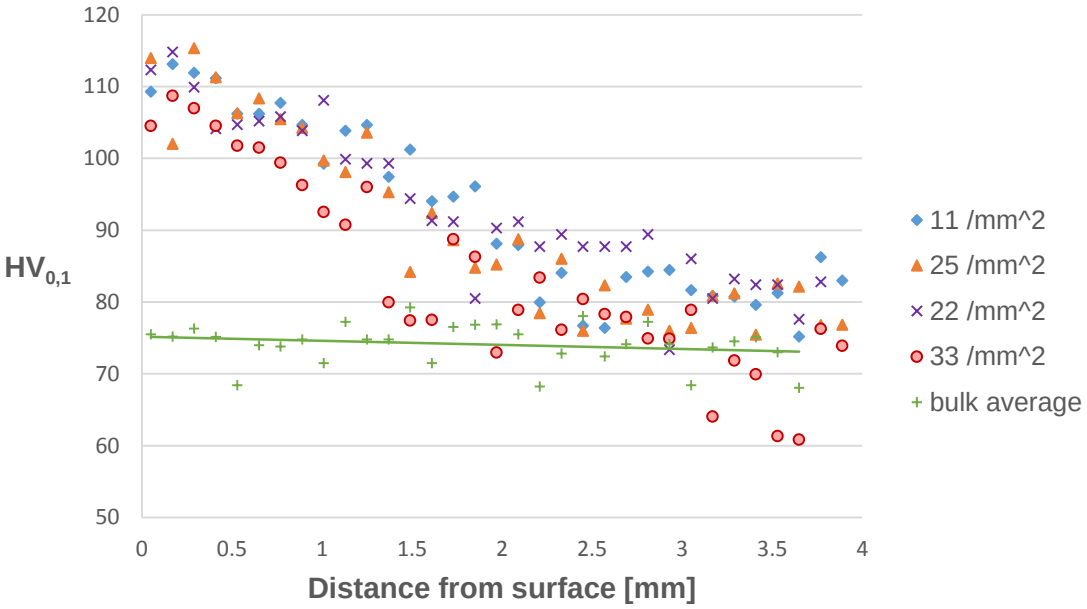

Figure 72 – Micro-hardness results for as deposited MHP AA 2319 with different peening density

Figure 73 presents the micro-hardness of samples peened with different densities for the P+ST+NA condition. The peened samples have similar behaviour for all the peening densities. The first measurement points near the surface have lower or equal to the bulk average. This softening near the surface can be associated to the coarsening of precipitates as the result of high temperature exposure during the heat treatment. The large precipitates with similar size to the grains do not offer resistance to the deformation or refinement of the material and thus the hardness decreases. However, the further regions below the surface present a considerable hardness increase. The microstructure presented in

Section 4.3.2 for this region was composed of fine and equiaxed grains with a slight increase in grain size at deeper regions. The samples with 22 and 25 hits/mm^2, have an increase in hardness of approximately 15 to 20%. In contrast, the values for 11 hits/mm^2 were lower because the plastic deformation for this density was lower. However, the sample with 33 hits/mm^2 peening density shows only a slightly higher hardness than the 11 hits/mm^2 sample, which supports the conclusion that the excessive cold work does not increase hardness further. In further distance, 1.5 to 2.0 mm below the surface, a sudden drop of hardness was recorded, even lower than the bulk average. As this region is associated with the grain growth area, this decrease was expected. In contrast, the microstructure in deeper region under this grain growth region, has again a fine grain structure similar to the one in the non-affected peening region. This was previously explained by the fact that this microstructure was not further affected by the peening effect. However, the hardness results did not follow exactly the same trend. For a depth between 2mm and 3.8mm the values are considerably lower than the bulk average (non-affected material). This can be attributed to complex correlation between compressive and tensile stress and hardness, as described by Pharr et al. [76]. It was shown that an increase of hardness only occurs in the region with compressive stresses and reduction in hardness in tensile region. No measurements of compressive stresses were performed for the present study, but the hardness variation suggests that in that case some regions with tensile strain were induced. When it comes to recrystallization both compressive and tensile strains will be beneficial. This may explain the difference between different response of hardness and microstructure to peening. In several works, different distribution of stresses was reported, which may mean that it depends on the peening conditions. Liu et al. [77] observed a decrease of compressive stress with the increase of the distance from the peened surface. Toda et al. [14] showed that residual stresses for peening were always compressive for a narrow band near the surface. For the rest of the material, an inhomogeneous stress distribution appeared with compressive and tensile stresses. For this reason, the sudden drop of the hardness values is most likely related with the development of tensile stress in this region.

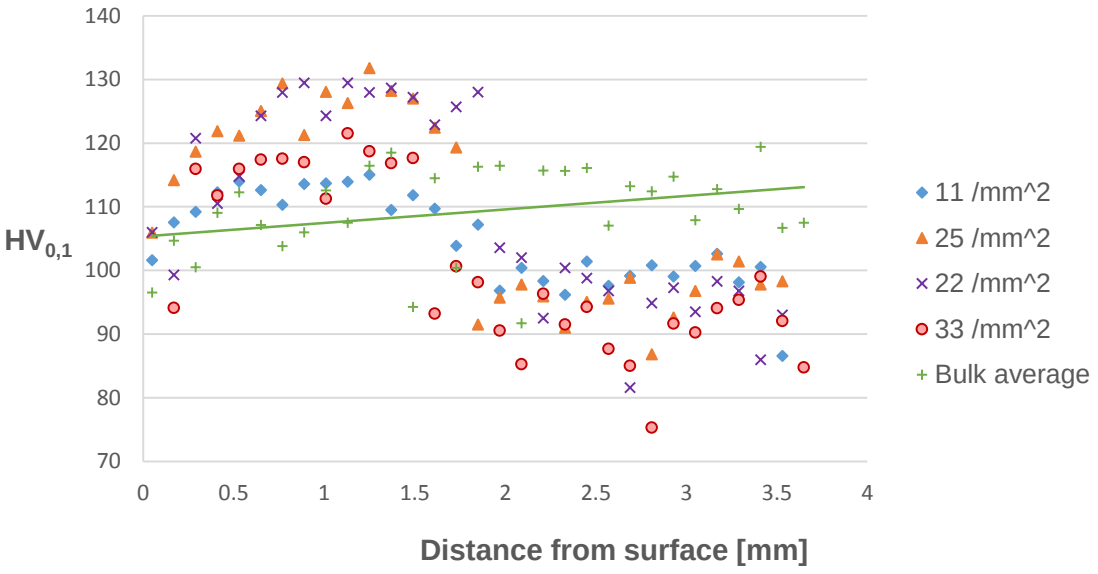

Figure 73 – Micro-hardness results for MHP AA2319 after solution treatment and 3 weeks natural aging

Figure 74 presents the micro-hardness results for samples peened with different densities for the P+ST+NA+AA condition. The micro-hardness values follow a similar trend regardless of the peening density and are the same as the bulk average. This suggests that after artificial aging, the hardness is normalized and that the cold work of the peening process does not have any effect on the hardness. With the exposure of the material to high temperature for a certain period of time, generation of precipitates all over the material occurred. As these precipitates appear not only in the grain boundaries but also in intra-grain regions, the microstructure stops having any significant impact in the hardness results. Similar results were obtained in the literature for cold worked and heat treated specimens [10].

Figure 75 summarizes the micro-hardness results for the sample peened with 25 hits/mm^2 in P, P+ST+NA and P+ST+NA+AA conditions. For this peening density, high values of micro-hardness have been achieved. The bulk average line was additionally presented as a reference for each condition. Comparing the values of the P bulk average and the P+ST+NA+AA condition, an improvement of approximately 110% was achieved for the later. However, when comparing the same condition with the P near the surface, this increases only approximately 35. From all the results presented, the P+ST+NA+AA condition presents the highest improvement in hardness. However, as this improvement is independent of the peening effect, no peening would be required to achieve these results. When P+ST+NA+AA or P+ST+NA cannot be applied to the part for dimensional or practical reasons, peening presents a considerable superficial hardness improvement. By applying peening to both sides of the sample, the extension of the affected region could be achieved. Due to the limited time of the project this approach could not be experimented for all cases.

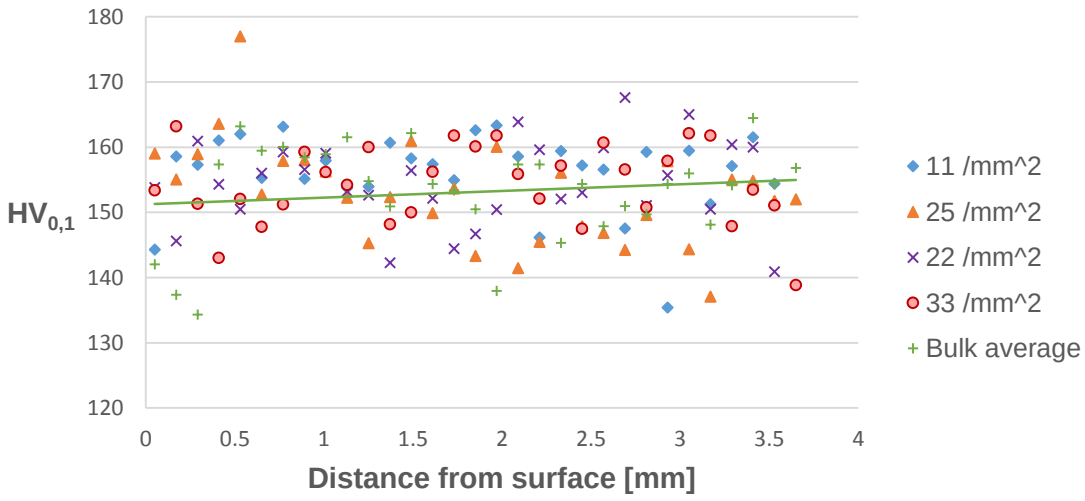

Figure 74 – Micro-hardness results for MHP AA2319 after artificial aging

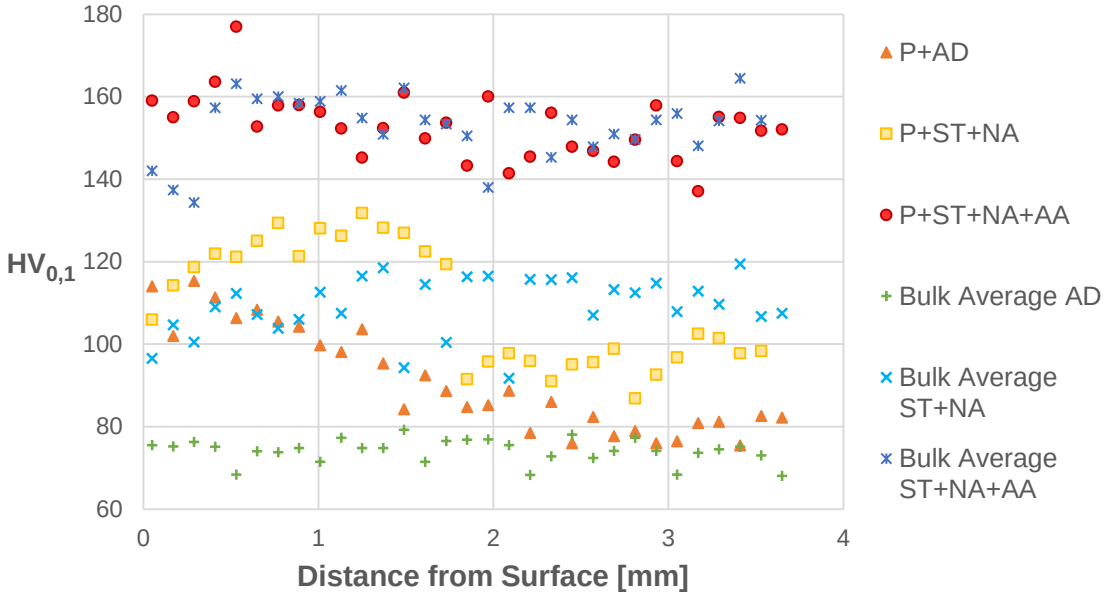

Figure 75 – Micro-hardness results for the sample peened with 25 hits/mm^2 for all the conditions

Figure 76 presents the micro-hardness of AA4043 for different peening densities. A similar result for AA2319 was explained and represented in Figure 72. As A4043 is a less resistant to dislocations and material deformation, the peening affects much greater depth and the thickness of the region with increased hardness is much greater, as compared to AA2319. Also, for this material, the influence of peening density on the hardness is much lower, which suggests that significant improvement of hardness can be obtained for a smaller peening densities.

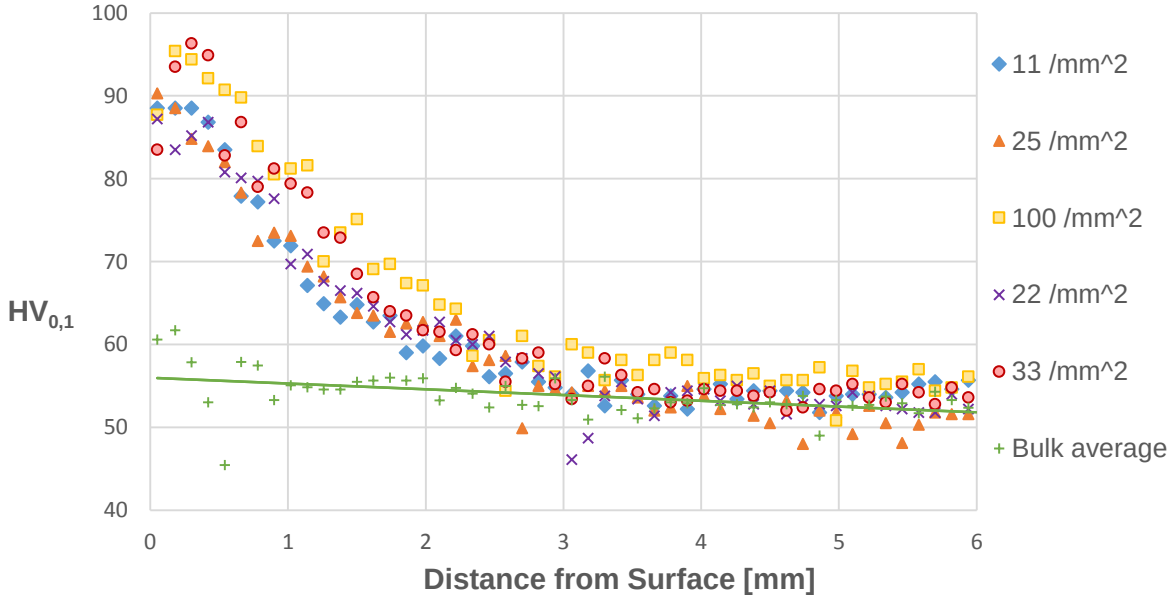

Figure 76 – Hardness results for as deposited MHP AA4043

4.3.4. Tensile Test

From the micro-hardness study for AA2319, the samples with peening intensities of 22hits/mm^2 and 25hits/mm^2 presented a similar increase of hardness increase in all conditions. However, the process time to peen with 25hits/mm^2 is reduced compared with 22hits/mm^2, since the multi-pass with tool offset was applied in the second case. For this reason, the tensile tests specimens were peened with a density of 25 hits/mm^2 on both sides. All results are compared in Figure 77. Note that peening (P) was applied to half of the specimens and no cold work (as deposited - AD) was applied to the other half. Also, solution treatment and artificial aging was applied, to study the influences of HT in peened and non-peened specimens (AD_{HT} and P_{HT}). The vertical direction (Ver) refers to the samples across the built layers, whereas the horizontal direction (Hor) refers to the samples along the layers.

For the non-peened or as-deposited samples, the values of ultimate tensile strength (UTS) and proof strength (PS) are similar for both directions. The results are consistent with work published by Gu et al. [3]. However, the elongation in the vertical direction of their specimens was higher than obtained here. Nevertheless, the horizontal value was higher than for the vertical direction and the trend was similar to the one presented in Figure 77.

When peening is applied, the UTS and PS values increase when compared with AD, but the elongation decreases. As the increase of material strength is due to the increase in density of dislocations and deformation of the material, the mobility of the dislocations is constrained. In this way, the ductility of the material is compromised and thus the elongation decreases.

When HT is applied to the AD material, the UTS and PS values increase. The same increase was reported by Gu et al. [39] study. The values presented were higher than the ones achieved in this experimental tensile test, but only for the UTS value. The increase in strength and decrease of elongation can be explained by the further constraint of dislocations, due to the formation of precipitates during the HT.

For the heat treated peened specimens, the UTS and PS values obtained are lower than the ones for the peened samples without HT and AD with HT. However, the values obtained do not represent the strength drop characteristic for the grain growth behaviour, as presented in the Section 4.3.2 the microstructure for both sided peening is presented with a fine and equiaxed grains. However, the elongation increase, particularly when compared with the AD_{HT} condition, suggests exactly what is expected in the grain growth situation. Most likely, the slight increase in grain size in the middle section of the both sided peened sample, explains this duality in results.

The presented results give a range of possibilities depending on the desirable application. For applications, in which the higher strength is desirable, as-deposited heat treated and peened conditions are the most suitable. For applications where elongation is necessary and high strength values are desirable, the peened heat treated condition should be applied. Anyway, it was proven that the

application of cold work and/or heat treatment will increase the strength and/or elongation and therefore enhance the mechanical properties of the material.

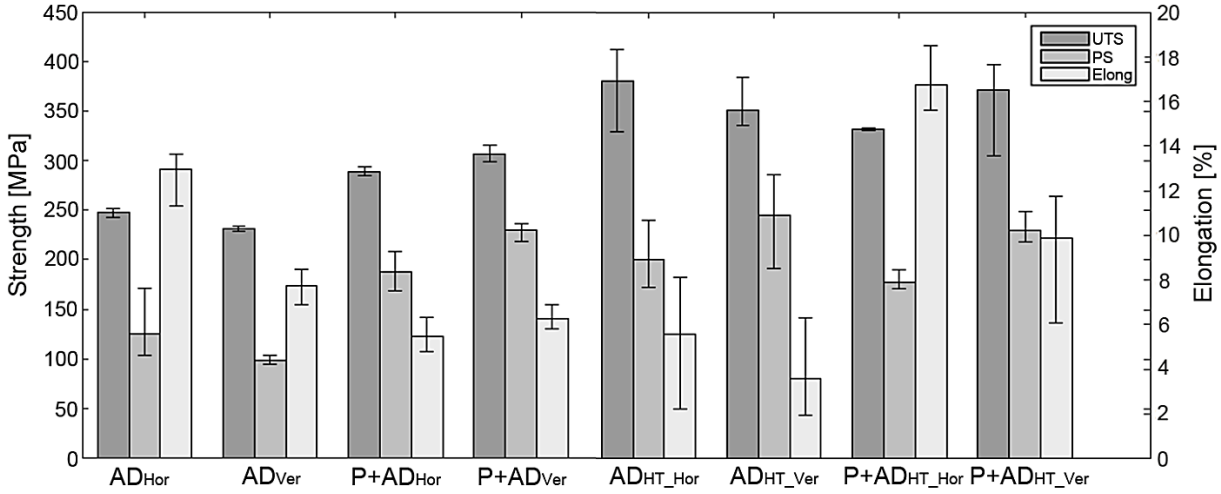

Figure 77 – Tensile test results for specimens not peened and peened with and without heat treatment

4.4. Side Rolling

Cold rolling is already a widely used cold work strategy. The effects of inter-layer rolling in aluminium WAAM have proven to be effective in the reduction or elimination of porosity and increase of mechanical properties [9,10]. However, the application of this process on every layer of deposited material results in low productivity and also reduces significantly the height of deposited beads. To avoid these constraints, the capability of pinch rolling was tested through the application of side rolling on a parallel wall of AA4043.

4.4.1. Effect on Porosity

To access the effect of cold rolling on porosity of cold worked samples, cross sections were examined for different loads, as presented in Figure 78. Once again, a depression zone near the surface can be distinguished due to plastic deformation. It can be seen that there is a porosity-free region under the area of application of the corner of the roller, which suggests that only in this zone enough plastic deformation was applied to affect porosity. The values of deformation and depth of porosity free zone vary greatly with the applied load, as presented in Table 13.

Figure 78 presents a narrow and deep porosity free zone near the edge of the roller. This observation implies that only in the corner of the flat roller, enough strain was induced to eliminate porosity. As explained in Section 4.3.1, the porosity annihilation is highly dependable on the applied strain during cold work. Only for a compressive strain of 50% or higher, the elimination of porosity occurs. Neves et al. [78] reported a strain distribution for cold-forged parts. A much higher strain was recorded for the

region that was in the contact with the edge of the plunger compared to region that was in contact with the central part of the tool. Most likely, a similar situation is occurring during the application of the flat roller in the WAAM deposited wall. Only the corners of this tool apply enough compressive strain for the annihilation of porosity and in the rest of the material the strain is more evenly distributed and material uniformly compressed without significant effect on porosity. Also, the deformation and depth of porosity free zone increase with increasing the load. Similar results were obtained with the application of interlayer rolling in AA2319 [9,10].

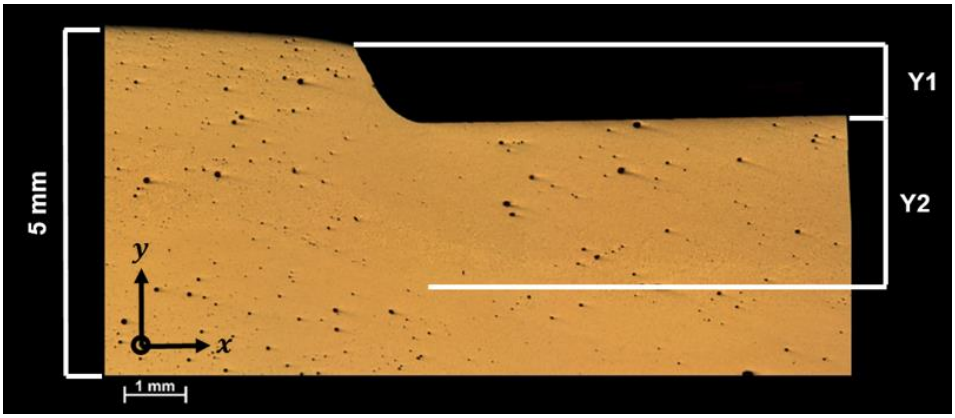

Figure 78 – Representation of deformation and depth of porosity free zone for cold rolling with 150kN

Table 13 – Depth of deformation and porosity free zone values for cold rolling with 75 kN and 150 kN loads

Load [kN]	Deformation (Y1) [mm]	Depth of porosity free zone (Y2) [mm]
75	0.24	1.11
150	1.32	2.60

4.4.2. Effect in Microstructure

To analyse the effect of rolling on microstructure, etched cross sections were studied for both loads, as presented in Figure 79. Note that as presented in Section 4.3.2, microstructure AA40043 alloy is highly dependable on the heating and cooling rate. Thus, it varies from layer to layer and between different beads in parallel deposition. In Figure 79 (a) and (b), the microstructure for the applied load of 75 kN is presented. The corner image show a superficial refinement of grains caused by the flat roller. However, the subsequent image, presents high porosity and an incoherent grain structure, which is characteristic for the arc based deposition of AA4043. Figure 79 (c) and (d) presents the microstructure for the applied load of 150 kN. The results are very similar to the previous case. However, on the image of the corner, the microstructure shows squashed grains, which proves that the increase in rolling load increases plastic deformation.

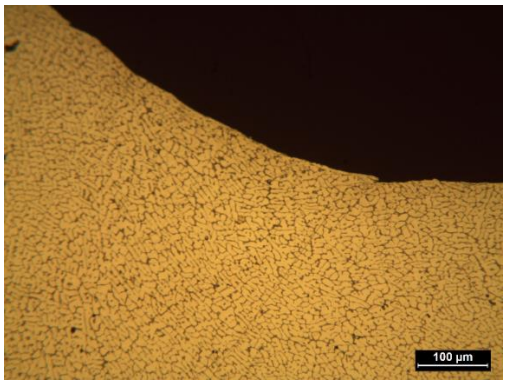

(a) Micrograph of the surface under the edge of the roller with applied load of 75 kN

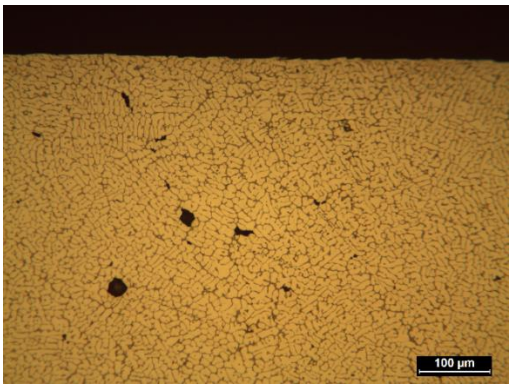

(b) Micrograph of the surface under the central part of the roller with applied load of 75 kN

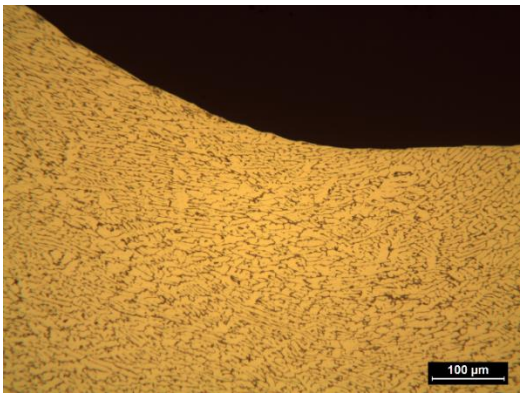

(c) Micrograph of the surface under the edge of the roller with applied load of 150 kN

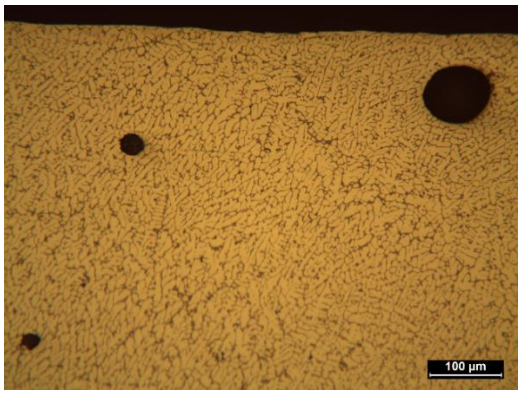

(d) Micrograph of the surface under the central part of the roller with applied load of 150 kN

Figure 79 – Micrographs of corner and surface affected by the rolling for AA4043

4.4.3. Effect on Micro-hardness

Micro-hardness measurements were carried out to access the depth of cold work by side rolling. The bulk average value from the region unaffected by rolling is presented as a reference.

Figure 80 presents the micro-hardness results measured from the surface to a depth of 6mm for the sample side rolled with 75 and 150 kN. The improvement obtained for a load of 75 kN was not considerable. There is scatter of the data for this load and the average micro-hardness is almost the same as the bulk average. However, when the load was increased to 150 kN, an overall increase in hardness was obtained. Comparing with the bulk average results, micro-hardness was increased by approximately 20%. The same trend was found in another work with the application of inter-layer rolling in AA2319 [10].

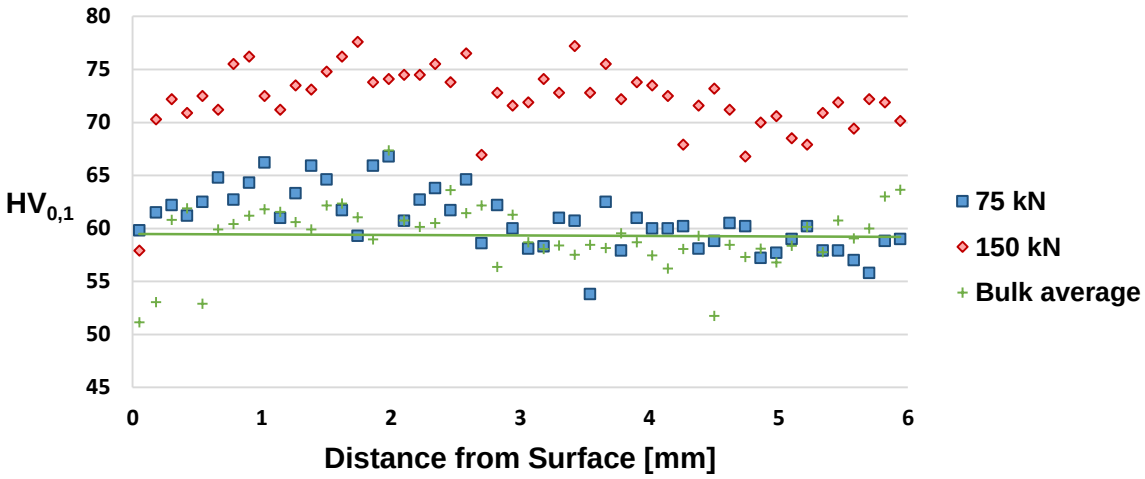

Figure 80 – Micro-hardness measurements for AA 4043 rolled with two different loads

4.5. Comparison between Side Rolling and Machine Hammer Peening

Figure 81 compares the micro-hardness results of side rolled sample with a load of 150kN and MHP with a peening density of 100 hits/mm^2. This comparison reveals a completely different behaviour for each cold work process. The micro-hardness enhancement for peening is only considerable near the surface, whereas side rolling presented a throughout improvement. But the maximum value near the surface is much higher for peening. This suggests that peening applies more concentrated effect, rolling in contrast, applies more uniform but over greater depth change of properties. For this reason, MHP should be applied to walls with approximately 1mm thickness or in cases where only superficial improvement is required. Side rolling does not reach such a high micro-hardness near the surface but it offers homogenous micro-hardness improvement in the examined thickness, which proves its capability for deeper improvement.

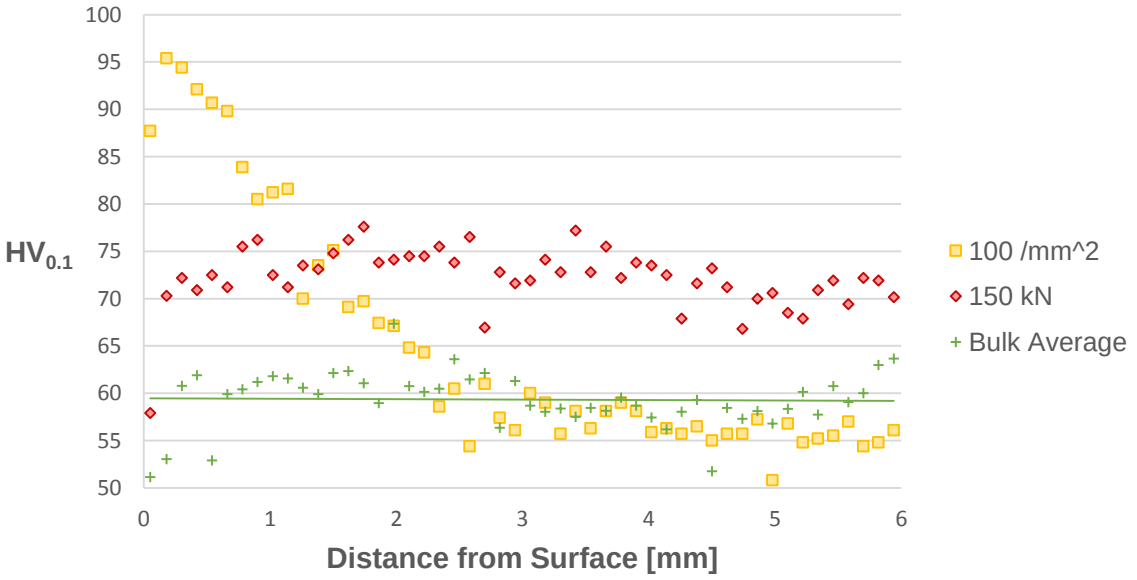

Figure 81 – Comparison of higher micro-hardness between MHP and side rolling for AA4043

4.6. Summary

To determine a suitable tool path to obtain single bead crossings for aluminium, an optimization study was carried out. The importance of temperature (heat input), material and deposition strategy on the dimensions of deposits and defects was accessed. For both CMT-P and CMT-PADV processes (different heat input), crossings with no apparent defects were achieved. A considerably lower effective wall width was obtained for the later process. This can be explained by the lower temperature and higher surface tension of liquid metal with CMT-PADV process, which results in lateral depression of the section where both walls merge together. Consequently, this process was not successfully used for crossings with the opposite angles 2 strategy, but could be applied to curved link intersection, due to higher contact area between both bead surfaces.

The previous findings were used to develop one of the build strategies for the final part, by combining them with parallel deposition, to achieve thicker wall crossings. This was achieved by depositing crossing beads parallelly with a defined distance. Although this method had a continuous heat sink in the intersection of beads, the large number of start and stop points in the final part would increase the likelihood of defects and could increase the material waste. Thus, the alternative option to combine parallel and oscillated walls was also studied. In this strategy, the central feature was deposited using parallel deposition and for the side features oscillated deposition was used. Due to variable heat sink effect in the intersection, the lack of fusion defects can occur, but these can be mitigated by an increase of heat input. Also, the fewer number of start and stops makes this method less prone to defects and, thus, this option was selected to build the final part. In this way, the largest part ever deposited with WAAM was manufactured, exhibiting good quality and dimensional accuracy.

With the aim to further increase the mechanical properties and reduce porosity, two cold work processes were studied: machine hammer peening and side rolling.

When applying machine hammer peening to the side surface of a WAAM aluminium wall, deformation and a porosity free zone was induced. The deformation was almost constant for all samples, with a slight increase in samples where a second and third tool pass was applied. This was attributed to the more evenly distributed compressive strain and consequently more evenly flattened surface. For the as-deposited peened AA4043, an increase in peening density resulted in an increase of depth of porosity free zone. For AA2319, the response of porosity free zone to the peening density was less visible, which can be explained by the non-homogeneous compressive strain in some conditions. When exposing the peened material to solution treatment and natural aging, the depth of porosity free zone increased. As the micro porosity is mainly located in grain boundaries, the relocation of porosity can be explained by the change in microstructure. Although for the as-deposited peened samples a fine and equiaxed grain structure was found, after heat treatment a microstructure instability occurred (abnormal growth generation). By further exposing the material to artificial aging, the reappearance of porosity occurred and consequently the decrease of porosity free zone was observed. MHP also caused an increase in superficial hardness for both alloys. For artificial aged samples, a general increase in hardness was

obtained but with the same values as for without peening, which implies that the peening enhancement is only presented in non-heat treated conditions. Moreover, as-deposited heat treated and peened conditions achieved improved strength, while peened heat treated condition achieved improved elongation and considerable increase in strength. The positive effect of cold work and/or heat treatment on improvement of strength and/or elongation has been shown.

Side rolling was applied to thick WAAM walls in AA4043 with loads of 75 and 150 kN. A deep and narrow porosity free zone directly under the edge of the roller was obtained, which implies that only in this region, enough strain to eliminate porosity was induced. In this same region, a superficial refinement of grains was obtained while the remaining material presents an incoherent grain structure, i.e., not affected by the rolling. Regarding micro-hardness, there was no considerable increase for 75 kN load but when applying 150 kN an overall increase of approximately 20% was obtained.

The micro-hardness results for MHP and side rolling have a completely different behaviour. For peening, a micro-hardness enhancement is only considerable near the peened surface, whereas for side rolling a throughout improvement is obtained. However, the maximum hardness value is much higher for peening, which suggests that a more concentrated effect is applied. In contrast, side rolling applies a more uniform effect that applies greater depth of properties change.

5. Conclusions and Future Work

5.1. Conclusions

During this study, the capability of large scale AM deposition was proven with the manufacturing of a preliminary aerospace structure. Considering the need to improve the mechanical properties of the deposited material, two cold work options were applied and analysed. The following conclusions can be drawn from this work:

- Single bead crossings for aluminium were deposited successfully with different overlaps. To obtain the least possible material wastage, curved links in the crossing intersection were successfully connected with no visible defects using CMT-PA process. By applying the opposite angles 2 strategy, crossing of single beads using CMT-P were successfully manufactured.
- For thick wall crossings, two reliable strategies were developed by combining parallel strategy with single bead crossings, and parallel with oscillated strategies. Due to the lower likelihood of defects, as a result of better control of heat input and lower number of start and stops, the parallel and oscillated strategy was selected for the manufacturing of the preliminary 6-metre long structure, which was successfully deposited.
- It was proven that by applying machine hammer peening to the side of already deposited material, a porosity free zone was obtained for considerably low deformation. It was found that the depth of porosity free zone increases with increasing peening density, i.e., by increasing overlap or by applying multi-pass. However, these results were dependent on the material. For AA2319, this zone increased after solution treatment and natural aging but after applying artificial aging porosity reappeared due to the high temperature exposure.
- For two-sided peening only some porosity was found in the middle section of the as-deposited peened sample and after solution treatment and artificial aging, the porosity seems to have reduced. By applying side rolling, the only porosity free zone was located in the area below the impact point of the corner of the flat roller, caused by the concentration of compressive strain in this area. Thus, peening is more suitable for superficial annihilation of porosity.
- Regarding the microstructure of AA2319, as-deposited peened samples showed fine and equiaxed grains but after heat treatment an abnormal grain growth developed. This was caused by the material flow and high temperature exposure of the compressive strained material. However, for two-sided peened sample the same result was not achieved and a fine microstructure was obtained. For AA4043, the microstructure of the material changed considerably throughout the WAAM deposited material with a slight grain refinement near the peened surface, as was expected. For side rolled samples, microstructure refinement was only slightly improved in the area below the corner and the left area presents high porosity and incoherent grain structure. This is obtained for both loads used.
- An increase of hardness after peening or rolling was found. For as deposited peened samples, an improvement of 50% for AA2319 and 70% AA4043 was obtained, when comparing with the

bulk average. After solution treatment and natural aging, the hardness values increased by 15-20% in the first 1.5 to 2mm from the surface with a sudden decrease to values below the bulk average. This was attributed to the abnormal grain growth and inhomogeneous dispersion of tensile and compressive stresses. After performing artificial aging, a similar trend for peened and non-peened samples values was obtained. For side rolling, an overall hardness improvement of 20% was obtained for the sample with an applied load of 150kN, but for 75kN no significant improvements were achieved. In conclusion, peening is suitable for a superficial hardness improvement, whereas rolling applies an overall increase of hardness.

- It was proven that by applying peening and heat treatment the ratio of strength to elongation can be controlled. The strength improved considerably for as-deposited and heat treated samples as well as peened. The elongation increased considerably for the peened and heat treated conditions.

5.2. Future Work

To improve understanding of the process the following future work is recommended:

- Although a preliminary part was successfully manufactured, the capability of AM has to be further studied with the manufacturing of the actual aerospace rib;
- The possibility of manufacturing thick wall crossings for titanium has been achieved by only applying oscillated strategy. Further studies regarding the possibility to achieving the same for aluminium should be considered;
- Further study to determine the quantity of material wastage and time of deposition in the crossing of single beads and thick walls should be carried out;
- To improve statistical significance of the results obtained for the depth of porosity free zone and deformation some conditions should be replicate;
- Hardness measurements for the double sided peening samples should be carried out to be compared with the presented results and asses, if further improvement was achieved;
- Residual stresses measurements for the peened samples should be performed in order to determine the stress distribution before and after peening. These results are also necessary to determine if the distribution of strain is actually correlated with the lack of porosity;
- Although the depth of porosity free zone is not substantially higher than the remelting of the following layer, a study of inter-layer peening is suggested to test its influence in residual stresses and porosity;
- The effects of cold rolling with an inverted profiled roller on porosity in aluminium WAAM deposition should be carried out. The use of this roller should have a similar reduction in porosity as the one reported in the corner of the flat roller.

6. References

1. S. W. Williams, F. Martina, A. C. Addison, J. Ding, G. Pardal and P. Colegrove, “Wire+ Arc Additive Manufacturing”, Materials Science and Technology, vol. 32, no. 7, pp. 641-647, 2016.

2. F. Martina, “Wire + arc additive manufacturing vs. traditional machining from solid: a cost comparison”, unpublished data of Welding Engineering and Laser Processing Centre, Cranfield University.

3. D. Ding, Z. Pan, D. Cuiuri and H. Li, “Wire-feed additive manufacturing of metal components: technologies, developments and future interests”, International Journal of Advanced Manufacturing Technology, vol. 81, no. 1-4, pp. 465-481, 2015.

4. G. Venturini, F. Montevecchi, A. Scippa and G. Campatelli, “Optimization of WAAM deposition patterns for T-crossing features”, Procedia CIRP, vol. 55, pp. 95-100, 2016. DOI https://doi.org/10.1016/j.procir.2016.08.043

5. J. Ding, F. Martina and S. W. Williams, “Production of large metallic components by additive manufacture – issues and achievements”, 1st Metallic Materials and processes: industrial challenges, Deauville, France, 2015.

6. J. Gu, B. Cong, J. Ding, S. W. Williams and Y. Zhai, “Wire + Arc Additive Manufacturing of Aluminium”, 25th International Solid Freeform Fabrication Symposium, Austin Texas, pp. 451-458, 2014.

7. B. Cong, J. Ding and S. W. Williams, “Effect of arc mode in cold metal transfer process on porosity of additively manufactured Al-6.3%Cu alloy”, vol. 76, no. 9-12, pp. 1593-1606, 2014.

8. J. H. Devletian and W. E. Wood, “Factors Affecting Porosity in Aluminium Welds – A Review”, Welding Research Council, Bulletin, pp. 1-18, 1983.

9. J. Gu, J. Ding, S. W. Williams, H. Gu, J. Bai, Y. Zhai and P. Ma, “The strengthening effect of inter-layer cold working and post-deposition heat treatment on the additively manufactured Al–6.3Cu alloy”, Materials Science and Engineering: A, vol. 651, pp. 18-26, 2016.

10. J. Gu, J. Ding, S. W. Williams, H. Gu, J. Bai, P. Ma and Y. Zhai, “The effect of inter-layer cold working and post-deposition heat treatment on porosity in additively manufactured aluminum alloys”, Journal of Materials Processing Technology, vol. 230, pp. 26-34, 2016.

11. P. A. Colegrove, J. Donoghue, F. Martina, J. Gu, P. Prangnell and J. Hönnige, “Application of bulk deformation methods for microstructural and material property improvement and residual stress and distortion control in additively manufactured components”, Scripta Materialia, 2016.

12. M. Malaki and H. Ding, “A review of ultrasonic peening treatment”, Materials and Design, vol. 87, pp. 1072-1086, 2015.

13. P. J. Withers, “Residual stress and its role in failure”, Reports on Progress in Physics, vol. 70, no. 12, pp. 2211-2204, 2007.

14. H. Toda, T. Yamaguchi, M. Nakazawa, Y. Aoki, K. Uesugi, Y. Suzuki and M. Kobayashi, “Four-Dimensional Annihilation Behaviors of Micro Pores during Surface Cold Working”, Materials transactions, vol. 51, no. 7, pp. 1288-1295, 2010.

15. Webpage – http://chemicalengineeringdata.blogspot.pt/ – Chemical Engineering, 2010.

16. ASTM. ASTM F 2792-10 standard terminology for additive manufacturing technologies.

17. G. N. Levy, R. Schindel and J.P. Kruth, “Rapid manufacturing and rapid tooling with layer manufacturing (LM) technologies, state of the art and future perspectives”, CIRPAnn Manuf Technol, vol. 52, pp. 589–609, 2003.

18. Y. Bandari, S. W. Williams, J. Ding and F. Martina, “Additive manufacture of large structures: robotic or CNC systems?”, 26th International Solid Freeform Fabrication Symposium, Austin Texas, 2015.

19. F. Martina, “Investigation of methods to manipulate geometry, microstructure and mechanical properties in titanium large scale Wire+ Arc Additive Manufacturing”, PhD Thesis, Cranfield University, School of Applied Sciences, 2014.

20. N. Guo and M. Leu, “Additive manufacturing: technology, applications and research needs”, Frontiers of Mechanical Engineering, vol. 8, no. 3, pp. 215-243, 2013.

21. Webpage – http://waammat.com/ – WAAMMAT official website.

22. Y. Zhang, Y. Chen, P. Li and A. T. Male, “Weld deposition-based rapid prototyping: a preliminary study”, Journal of Materials Processing Technology, vol. 135, no. 2, pp. 347-357, 2003.

23. J. Ding, P. Colegrove, J. Mehnen, S. Ganguly, P. M. S. Almeida and F. Wang, “Thermo-mechanical analysis of Wire and Arc Additive Layer Manufacturing process on large multi-layer parts”, Computational Materials Science,

24. P. Kazanas, P. Deherkar, P. Almeida, H. Lockett and S. Williams, “Fabrication of geometrical features using wire and arc additive manufacture”, Proceedings of the Institution of Mechanical Engineers, Part B: Journal of Engineering Manufacture, vol. 226, no. 6, pp. 1042-1051, 2012.

25. K. P. Karunakaran, S. Suryakumar, V. Pushpa and S. Akula, “Low cost integration of additive and subtractive processes for hybrid layered manufacturing”. Robotics and Computer-Integrated Manufacturing, vol. 26, no. 5, pp. 490-499, 2010.

26. Webpage – http://waammat.com/documents/ – S. W. Williams, “Large Scale Metal Wire + Arc Additive Manufacturing of Structural Engineering Parts”, presentation at 69th IIW Annual Assembly and International Conference – Plenary, 2016.

27. S. Suryakumar, K. P. Karunakaran, A. Bernard, U. Chandrasekhar, N. Raghavender and D. Sharma, “Weld bead modeling and process optimization in hybrid layered manufacturing”, Computer-Aided Design, vol. 43, no. 4, pp. 331-344, 2011.

28. J. Xiong, G. Zhang, J. Hu and L. Wu, “Bead geometry prediction for robotic GMAW-based rapid manufacturing through a neural network and a second-order regression analysis”, Journal of Intelligent Manufacturing, vol. 25, no. 1, pp. 157-163, 2014.

29. Y. Cao, S. Zhu, X. Liang and W. Wang, “Overlapping model of beads and curve fitting of bead section for rapid manufacturing by robotic MAG welding process”, Robotics and Computer-Integrated Manufacturing, vol. 27, no. 3, pp. 641-645, 2011.

30. K. F. Ayarkwa, S. W. Williams and J. Ding, “Investigation of pulse advance cold metal transfer on aluminium wire arc additive manufacturing”, Int. J. Rapid Manufacturing, vol. 5, no. 1, pp. 44-57, 2015.

31. F. Martina, J. Mehnen, S. W. Williams, P. Colegrove, P. and F. Wang, “Investigation of the benefits of plasma deposition for the additive layer manufacture of Ti–6Al–4V”, Journal of Materials Processing Technology, vol. 212, no. 6, pp. 1377-1386, 2012.

32. B. Cong, Z. Qi, B. Qi, H. Sun, G. Zhao and J. Ding, “A Comparative Study of Additively Manufactured Thin Wall and Block Structure with Al-6.3%Cu Alloy Using Cold Metal Transfer Process”, Applied Sciences, vol. 7, no. 3, pp. 275, 2017.

33. J. Mehnen, J. Ding, H. Lockett and P. Kazanas, “Design study for wire and arc additive manufacture”, International Journal of Product Development 20, vol. 19, no. 1-3, pp. 2-20, 2014.

34. P. A. Colegrove, A. R. McAndrew, J. Ding, F. Martina, P. Kurzynski and S. Williams, “System Architectures for Large Scale Wire + Arc Additive Manufacture”, 10th International Conference on Trends in Welding Research, Japan, 2016.

35. J. Xiong, G. Zhang, H. Gao and L. Wu, “Modeling of bead section profile and overlapping beads with experimental validation for robotic GMAW-based rapid manufacturing”, Robotics and Computer-Integrated Manufacturing, vol. 29, no. 2, pp. 417-423, 2013.

36. D. Ding, Z. Pan, D. Cuiuri and H. Li, “A multi-bead overlapping model for robotic wire and arc additive manufacturing (WAAM)”, Robotics and Computer-Integrated Manufacturing, vol. 31, pp. 101-110, 2015.

37. H. Wang and R. Kovacevic “A Novel Welding-Based Solid Freeform Fabrication Technology for Aluminum Alloy”, 84th Annual AWS Convention, Detroit, Mich, 2003.

38. E. A. Starke and J. T. Staley, “Application of modern aluminum alloys to aircraft”, Progress in Aerospace Sciences, vol. 32, no. 2-3, pp. 131-172, 1996.

39. J. Gu, J. Ding, S.W. Williams and Y. Zhai, “High performance aluminium properties for space applications using Wire + Arc Additive Manufacturing”, 1st Metallic Materials and processes: industrial challenges, Deauville, France, 2015.

40. P. N. Anyalebechi, “Hydrogen-induced gas porosity formation in Al–4.5 wt% Cu–1.4 wt% Mg alloy”, Journal of Materials Science, vol. 48, no. 15, pp. 5342-5353, 2013.

41. H. Wang, W. Jiang, J. Ouyang and R. Kovacevic, “Rapid prototyping of 4043 Al-alloy parts by VP-GTAW”, Journal of Materials Processing Technology, vol. 148, no. 1, pp. 93-102, 2004.

42. P. D. Lee and J.D. Hunt, “Hydrogen porosity in directionally solidified aluminium–copper alloys: a mathematical model”, Acta materialia, vol. 49, no. 8, pp. 1383-1398, 2001.

43. A. Russell and K. L. Lee, “Structure-property relations in nonferrous metals”, John Wiley & Sons, 2005.

44. K. Pal and S. K. Pal, “Effect of pulse parameters on weld quality in pulsed gas metal arc welding: a review”, Journal of Materials Engineering and Performance, vol. 20, no. 6, pp. 918-931, 2011.

45. R. R. Ambriz and D. Jaramillo, ”Mechanical behavior of precipitation hardened aluminum alloys welds”, Light Metal Alloys Applications, InTech, 2014.

46. F. Matsuda, H. Nakagawa, K. Nakata and R. Ayani, ”Effect of electromagnetic stirring on weld solidification structure of aluminum alloys (Report I): investigation on gta weld metal of thin sheet”, Transactions of JWRI, vol. 7, no. 1, pp. 111-127, 1978.

47. P. N. Anyalebechi, “Analysis of the effects of alloying elements on hydrogen solubility in liquid aluminum alloys”, Scripta metallurgica et materialia, vol. 33, no. 8, pp. 1209-1216, 1995.

48. H. Sehitoglu, T. Foglesong and H. J. Maier, “Precipitate effects on the mechanical behavior of aluminum copper alloys: Part I. Experiments”, Metallurgical and Materials Transactions A, vol. 36, no. 3, pp. 749-761, 2005.

49. Webpage - http://www.fronius.com/cps/rde/xchg/fronius_usa - CMT: Cold Metal Transfer MIG/MAG dip-transfer process for automated applications.

50. Webpage - http://www.fronius.com/cps/rde/xchg/fronius_usa - The CMT weld process: The technology.

51. Webpage - http://www.fronius.com/cps/rde/xchg/fronius_usa - CMT: Cold Metal Transfer MIG/MAG dip-transfer arc process.

52. C. G. Pickin and K. Young, “Evaluation of cold metal transfer (CMT) process for welding aluminium alloy”, Science and Technology of Welding and Joining, vol. 11, no. 5, pp. 583-585, 2006, DOI http://dx.doi.org/10.1179/174329306X120886.

53. C. G. Pickin, S. W. Williams and M. Lunt, “Characterisation of the cold metal transfer (CMT) process and its application for low dilution cladding”, Journal of Materials Processing Technology, vol. 211, no. 3, pp. 496-502, 2011.

54. C. E. Albino, “Desenvolvimento de um procedimento automatizado de soldagem para revestimento de tubos de caldeira via MIG/MAG CMT, utilizando Inconel 625 como metal de adição”, Msc. Thesis, Universidade Federal de Santa Catarina, Florianópolis, 2014.

55. J. Cho, J. J. Lee and S. H. Bae, “Heat input analysis of variable polarity arc welding of aluminum”, The International Journal of Advanced Manufacturing Technology, vol. 81, no. 5-8, pp. 1273-1280, 2015.

56. D. D. Harwig, J. E. Dierksheide, D. Yapp and S. Blackman, “Arc behavior and melting rate in the VP-GMAW process”, Welding journal, vol. 85, no. 3, pp. 52-62, 2006.

57. J. L. Gu, J. L. Ding, B. Q. Cong, J. Bai, H. M. Gu, S. W. Williams and Y. C. Zhai, “The Influence of Wire Properties on the Quality and Performance of Wire+ Arc Additive Manufactured Aluminium Parts”, Advanced Materials Research, vol. 1081, pp. 210-214, 2015.

58. H. E. Coules, G. C. M. Horne, S. Kabra, P. Colegrove and D. J. Smith, “Three-dimensional mapping of the residual stress field in a locally-rolled aluminium alloy specimen”, Journal of Manufacturing Processes, vol. 26, pp. 240-251, 2017.

59. X. Zhou, H. Zhang, G. Wang, X. Bai, Y. Fu and J. Zhao, “Simulation of microstructure evolution during hybrid deposition and micro-rolling process”, Journal of Materials Science, vol. 51, no. 14, pp. 6735-6749, 2016.

60. J.R. Hönnige, S. Williams, M.J. Roy, P. Colegrove, S. Ganguly, “Residual Stress Characterization and Control in the Additive Manufacture of Large Scale Metal Structures”, 10th Int. Conf. Residual Stress., Sydney, 2016.

61. C. Lechner, F. Bleicher, C. Habersohn, C. Bauer and S. Goessinger, “The use of machine hammer peening technology for smoothening and structuring of surfaces”, Proceedings of the 23rd International DAAAM Symposium, DAAAM International, Vienna, pp. 331-336, 2016.

62. F. Bleicher, C. Lechner, C. Habersohn, E. Kozeschnik, B Adjassoho and H. Kaminski, “Mechanism of surface modification using machine hammer peening technology”, CIRP annals-manufacturing technology, vol. 61, no. 1, pp. 375-378, 2012.

63. D. Kirk, “Estimate Compressed Layer Depth by Using Almen Peening Intensity”, The shot peener, 2014.

64. T. Chen, H. John, J. Xu, Q. Lu, J. Hawk and X. Liu, “Influence of surface modifications on pitting corrosion behavior of nickel-base alloy 718. Part 2: Effect of aging treatment”, Corrosion Science, vol. 78, pp. 151-161, 2014.

65. DIN EN 573-3. Aluminium and aluminium alloys – Chemical composition and form of wrought products – Part 3: Chemical composition and form of products.

66. Webpage – http://www.kwm-tools.de/index.php?id=40 – KWM tools gmbh official webpage.

67. P. A. Colegrove, H. E. Coules, H. E., J. Fairman, F. Martina, T. Kashoob, H. Mamash and D. L. Cozzolino, “Microstructure and residual stress improvement in wire and arc additively manufactured parts through high-pressure rolling”, Journal of Materials Processing Technology, vol. 213, no. 10, pp. 1782-1791, 2013.

68. D. Radaj, “Heat effects of welding: temperature field, residual stress, distortion”, Springer Science & Business Media, 2012.

69. Unpublished data of Welding Engineering and Laser Processing Centre, Cranfield University.

70. H. Toda, K. Minami, K. Koyama, K. Ichitani, M. Kobayashi, K. Uesugi and Y. Suzuki, “Healing behavior of preexisting hydrogen micropores in aluminum alloys during plastic deformation”, Acta Materialia, vol. 57, no. 15, pp. 4391-4403, 2009.

71. H. Toda, T. Hidaka, M. Kobayashi, K. Uesugi, A. Takeuchi and K. Horikawa, “Growth behavior of hydrogen micropores in aluminum alloys during high-temperature exposure”, Acta Materialia, vol. 57, no. 7, pp. 2277-2290, 2009.

72. T. Chen, H. John, J. Xu, Q. Lu, J. Hawk and X. Liu, “Influence of surface modifications on pitting corrosion behavior of nickel-base alloy 718. Part 1: Effect of machine hammer peening”, Corrosion Science, vol. 77, pp. 230-245, 2013.

73. I. Charit and R. S. Mishra, “Abnormal grain growth in friction stir processed alloys” Scripta materialia, vol. 58, no. 55, pp. 367-371, 2008.

74. C. Huang and S. Kou, “Partially melted zone in aluminum welds—planar and celluar solidification”, Welding Journal, vol. 80, no. 2, pp. 46-53, 2001.

75. P. Peyre, R. Fabbro, P. Merrien and H. P. Lieurade, “Laser shock processing of aluminium alloys. Application to high cycle fatigue behavior”, Materials Science and Engineering: A, vol. 210, no. 1-2, pp. 102-113, 1996.

76. G. M. Pharr, T. Y. Tsui, A. Bolshakov and W. C. Oliver, “Effects of residual stress on the measurement of hardness and elastic modulus using nanoindentation”, MRS Online Proceedings Library Archive, vol. 338, 1994.

77. J. Liu, W. X. Gou, W. Liu, W and Z. F. Yue, “Effect of hammer peening on fatigue life of aluminum alloy 2A12-T4”, Materials & Design, vol. 30, no. 6, pp. 1944-1949, 2009.

78. F. O. Neves, T. L. L. Oliviera, D. U. Braga and A. S. C. D. Silva, “Influence of heat treatment on residual stress in cold-forged parts”, Advances in Materials Science and Engineering, 2014.

7. Appendix

Appendix A – Technical Drawing of preliminary 6-metre long part

7. Appendices

Annex A

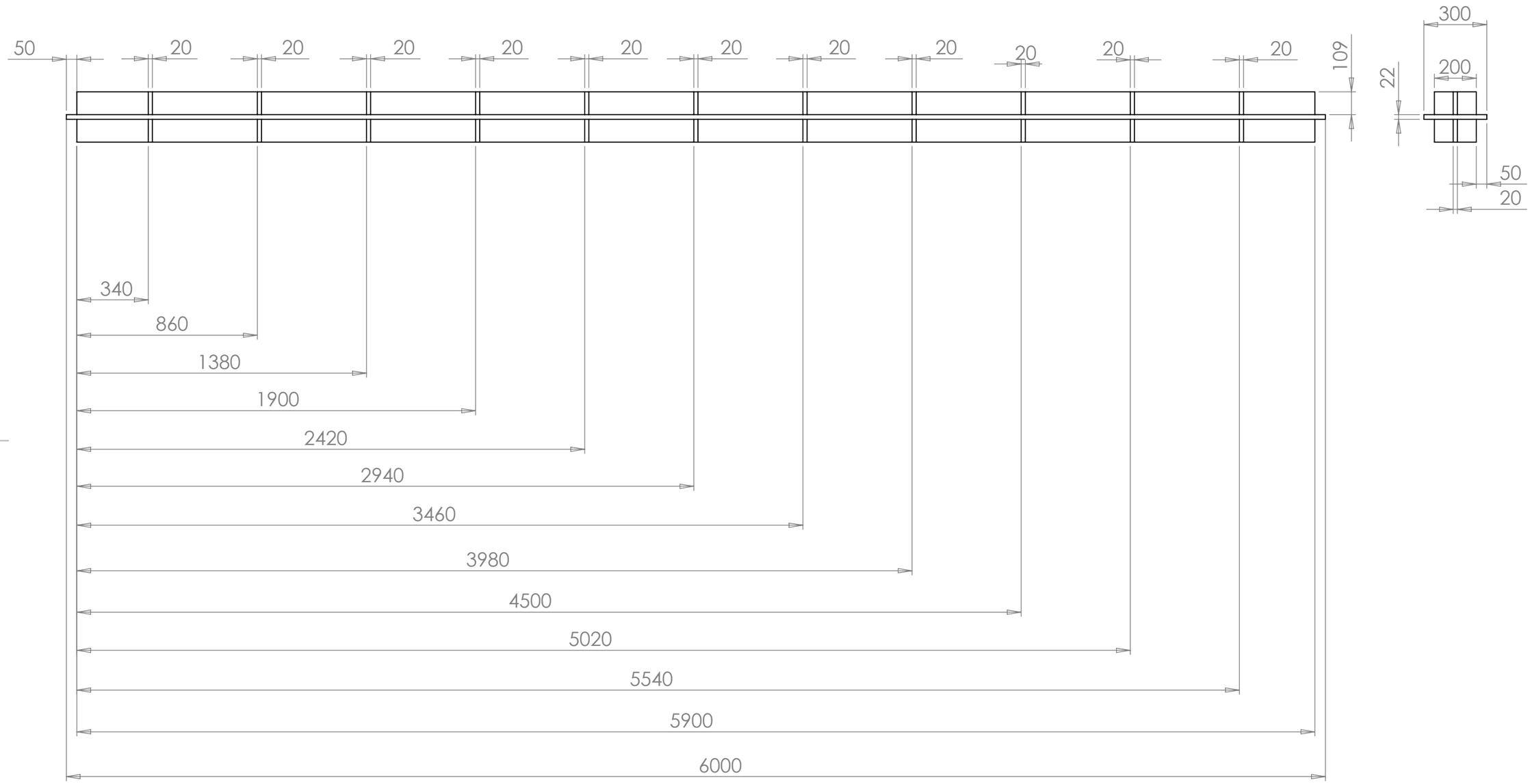

TÉCNICO LISBOA

Preliminary 6-metre long aerospace structure

Name: Leonor Machado Santos Carvalho Neto
Number: 69596

A3

SCALE:1:50

May 2017